

UC Berkeley

UC Berkeley Electronic Theses and Dissertations

Title

Mechanisms of Size Control in Pipid Frogs

Permalink

<https://escholarship.org/uc/item/241047r7>

Author

Miller, Kelly

Publication Date

2020

Peer reviewed|Thesis/dissertation

Mechanisms of Size Control in Pipid Frogs

by

Kelly E. Miller

A dissertation submitted in partial satisfaction of the

requirements for the degree of

Doctor of Philosophy

in

Molecular and Cell Biology

in the

Graduate Division

of the

University of California, Berkeley

Committee in charge:

Professor Rebecca Heald, Chair

Professor Richard Harland

Professor Daniel Rohksar

Professor David Wake

Spring 2020

Mechanisms of Size Control in Pipid Frogs

Copyright 2020
by
Kelly E. Miller

Abstract

Mechanisms of Size Control in Pipid Frogs

by

Kelly E. Miller

Doctor of Philosophy in Molecular and Cell Biology

University of California, Berkeley

Professor Rebecca Heald, Chair

Size is a fundamental feature of biology that affects physiology at all levels, from the organism to organs and tissues to cells and subcellular structures. How size is determined at these different levels, and how biological structures scale to fit together and function properly are important open questions. Historically, amphibian systems have been extremely valuable to describe scaling phenomena, as they occupy some of the extremes in biological size and are amenable to manipulations that alter genome and cell size. More recently, the application of biochemical, biophysical, and embryological techniques to amphibians has provided insight into the molecular mechanisms underlying scaling of subcellular structures to cell size, as well as how perturbation of normal size scaling impacts other aspects of cell and organism physiology. This thesis is comprised of three projects which examine mechanisms of size scaling in Pipid frogs at the subcellular, cellular, and organismal levels. We find that molecular mechanisms for spindle size scaling in eggs of the small frog *Hymenochirus boettgeri* are not conserved with those of *Xenopus* species. Instead, a novel mechanism operates involving post-translational modification of microtubule depolymerizing motor protein kif2a to modulate spindle size. We also characterize size scaling in viable *Xenopus laevis*/*Xenopus tropicalis* hybrids and use this system to establish a novel screening method for candidate genes involved in size control. Finally, we characterize size scaling in the rare dodecaploid *Xenopus longipes* to examine how genome size impacts cell size and other traits such as developmental rate. The well-documented correlation between genome size and cell size is conserved in somatic cells but not in early development, which proceeds more slowly in *Xenopus longipes* than in *Xenopus laevis*, thus highlighting an important correlation between genome size and developmental rate.

Acknowledgements

I would like to thank: Adam Session and Sofia Medina Ruiz for assistance with *H. boettgeri* and *X. longipes* transcriptome assemblies, Austin Mudd for kif2a and katanin sequences in *Xenopus borealis*, Tae Joon Kwon for RNA-seq advice and assembly, my committee members Rebecca Heald, Richard Harland, David Wake, and Dan Rohksar for valuable guidance and input into this project, students Rebecca Lamothe, Mike Fitzsimmons, Sophie Kawada, and Scott Aposhian for dedicated assistance with the experiments presented, and all past and current members of the Heald laboratory for stimulating scientific discussions, technical advice, mentorship and friendship.

Additionally, I would like to thank the NSF GRFP as well as NIH MIRA grant R35 GM118183 and the Flora Lamson Hewlett Chair for funding.

Endless love and kisses to the loves of my life who own my heart and soul and make it all worth it: Cole, Mike, and Eliza (in no particular order)

Dedication

This work is dedicated to Rebecca Heald, for dedicated guidance, mentorship, and advice on these projects and in life throughout the years. I will never forget learning about the spindle from you for the first time, igniting a passion in me I didn't know I had. If not for you, I wouldn't be a scientist, author, teacher, professional, or a "frog whisperer". The lab will always be a place dear to my heart, and you a member of my family. As you say- from that I will never graduate. Thank you for being a true role model, inspiration, and the wind beneath my wings.

Contents

1	Introduction	1
1.1	Historical scaling observations made in amphibians lead to molecular questions	1
1.2	Frog species exhibit extremes in body and genome size	3
1.3	<i>Xenopus</i> species reveal molecular mechanisms of intracellular scaling	3
1.4	Volume-dependent size scaling of organelles in <i>Xenopus</i> egg and embryo extracts	4
1.5	Sensing the cell surface area to volume ratio coordinately mediates spindle and nuclear scaling in vivo	5
1.6	Interspecies comparison of Pipid frogs provides molecular insight into scaling and architecture of the meiotic spindle	6
2	Regulation of meiotic spindle size in the small frog <i>Hymenochirus boettgeri</i>	8
2.1	Introduction	8
2.2	Results	9
2.3	Discussion	21
2.4	Methods	22
2.5	Supplemental figures	28
3	<i>Xenopus</i> hybrids provide insight into cell and organism size control	30
3.1	Introduction	30
3.2	Results	31
3.3	Discussion	39
3.4	Methods	40
3.5	Supplemental figure	46
4	Investigating size scaling in the dodecaploid <i>Xenopus longipes</i>	47
4.1	Introduction	47
4.2	Results	47
4.3	Discussion	57
4.4	Methods	59
5	Conclusions	62
6	References	64

Chapter 1

Introduction

Absolute and relative size of biological entities varies widely at all levels above the atomic/molecular. A fundamental question in biology is how organisms control size, from the dimensions of an organism down to its component cells and subcellular structures. How does scaling occur so that everything fits and functions properly? What mechanisms operate to build subcellular structures, cells, and organisms with a diverse range of sizes optimized for function?

1.1 Historical scaling observations made in amphibians lead to molecular questions

It has long been observed that genome size correlates strongly and linearly with cell size [1–3]. This principle was first noted in organisms including plants and arthropods, in which increases in genome copy number (ploidy) led to increased cell size, sometimes accompanied by an increase in organism size [4–6]. Amphibians present a unique opportunity to study these phenomena in vertebrates, as deviations in ploidy without immediate organism lethality occur spontaneously in nature and can be induced experimentally. Additionally, compared to other model organisms, amphibians lay abundant quantities of large eggs and produce embryos that can easily be manipulated. Some of the earliest known studies in vertebrate size scaling were performed by cell biologist and embryologist Gerhard Fankhauser in the 1930s-1940s using the small newt *Triturus viridescens*, which naturally produces haploid and triploid individuals under certain environmental conditions. By replicating these conditions in the lab, Fankhauser was able to generate embryos of different ploidies and monitor the effects of genome content on cell and organism size. He found that haploid embryos possessed smaller cells and nuclei than diploid embryos, had short and stunted body lengths, and died by metamorphosis [7]. In contrast, triploid embryos were viable and possessed larger cells and nuclei, with a similar or only slightly increased body size relative to diploids [8]. In the 1950s-60s, similar methods applied to *Xenopus* embryos revealed comparable trends [9,10]. Remarkably, Fankhauser noted that cell number was altered in triploids, so that embryonic tissues had fewer cells than diploids, but organ size remained constant in terms of total cell mass [11]. A similar compensatory mechanism for maintenance of organ size was also observed in triploid *Xenopus* embryos that contain cells ~1.5x normal size. In this system, tactile sense organs in the lateral line system grew normally and attained normal size through a decrease in cell number [12]. Based on these

studies, it was hypothesized that one limitation on body size arises from functional constraints on tissues, which are under homeostatic pressure to maintain their characteristic sizes to preserve proper organ function.

By the 1970s and 1980s, it was noted that the linear relationship between genome size and cell size was conserved among many different species of urodeles [13] and anurans [14], with an inverse correlation between amphibian cell size and cell number [15]. At the cellular level, other studies suggested a direct relationship between amphibian genome size and duration of meiotic and mitotic cell cycles [2,16,17] and an inverse relationship between cell size and metabolic rate [18–20], thus suggesting possible molecular links between genome size, cell size, and whole organism physiology. Taken together, these observations predicted that amphibians with large genome and cell sizes would exhibit lower metabolic rates, slower growth rates, and possess relatively fewer cells. They also suggested that, if whole-body metabolic rate could be considered as the sum of the individual metabolic rates of its component cells, then an individual composed of smaller cells should have a higher metabolic rate than a similarly-sized individual comprised of larger cells.

These early observations not only established experimental frameworks for testing the effects of ploidy alteration on vertebrate size and physiology, but also outlined the fundamental principle that while genome and cell size are clearly linked, the connection between cell size and cell or whole-body metabolic rates is more complex and likely subject to regulation by other factors in addition to genome size [21]. The issue is confounded by the fact that organism size rarely scales with cell size. For instance, despite their tremendous genome and cell sizes, *Necturus* salamanders do not grow to be very large [22]. Some of the world's smallest reported salamander species from the genus *Thorius* contain relatively large genomes at 25 pg DNA/haploid nucleus, but are characterized by tiny body lengths of less than 2 cm [23,24]. Thus, abrupt changes in ploidy induced experimentally usually do not have dramatic effects on organism size. Rather, variation in organism size on evolutionary time scales is thought to be driven by habitat specialization in which larger or smaller animals are better adapted to distinct environmental conditions [25].

What are the molecular mechanisms that operate to alter size and scaling relationships? A number of studies in a variety of other systems including yeast, *Drosophila*, and cultured mammalian cells have identified a plethora of signaling pathways and molecular factors that influence cell size [26–29]. However, the size control mechanisms that operate in vivo, for example in response to changes in DNA content across species or within an individual organism, remain very poorly understood, particularly in vertebrate systems. As discussed below, anuran systems spanning a

wide range of size parameters provide a unique opportunity to explore the molecular basis of different scaling behaviors. Experiments described in Chapters 3 and 4 set out to characterize live anuran systems more specifically for size control studies.

1.2 Frog species exhibit extremes in body and genome size

Anurans are the largest amphibian clade of 7204 extant species, [30]. They exhibit extreme ranges of size from the tiny frog *Paedophryne amauensis*, the smallest known vertebrate at 7 mm long weighing 0.02 grams [31], to the 33 cm, 3250 gram Goliath frog (*Conraua goliath*) [32]. Intriguingly, they exhibit large variability in genome size among vertebrates, with genome sizes occupying both ends of the size spectrum. In contrast to mammalian species that exhibit relatively low variation in DNA content (1-4 pg/haploid nucleus) [33], anuran genome sizes vary from 0.95-13.4 pg DNA/nucleus [24]. even among species belonging to the same genus [14]. *Xenopus tropicalis* for instance contains ~1.7 pg/nucleus while *Xenopus longipes* contains ~8 pg/nucleus [34]. Among anurans, the wide variation in genome content may be attributed to interspecific hybridization and whole genome duplication leading to polyploidization, common in frogs and a driver of their evolution and speciation [35]. Independent of whether the size or number of chromosomes differs across species, somatic cell size correlates linearly with genome size, for example in amphibian neuronal cells [36] and erythrocytes [15]. In contrast to somatic cells, amphibian egg sizes do not necessarily scale with genome size, nor do cells in cleaving embryos. Anuran eggs are quite large and variable, ranging from ~0.7 mm in the small Pipid frog *Hymenochirus boettgeri* to ~6.5 mm in the Peruvian frog *Gastrotheca antoniiichoai* [37].

1.3 *Xenopus* species reveal molecular mechanisms of intracellular scaling

Perhaps the best known family of frogs utilized most commonly in laboratory settings today are the Pipid frogs, a group of tongueless aquatic frogs including the *Xenopus* species, such as *Xenopus laevis* and *tropicalis*. *Xenopus* eggs and embryos possess unique biological features which pose interesting questions about size scaling of subcellular structures. During early development, cleavage divisions without intervening growth phases split the fertilized *Xenopus* zygote from one large cell to thousands of smaller ones without any net growth of the embryo itself. The size of subcellular structures must therefore scale concomitantly with the size of the cells themselves to best adapt their function. But how is this accomplished? Is it via compositional changes in cellular components as development proceeds or via a physical mechanism such as changing cell volume or shape? Furthermore, how

specifically do subcellular structures modify their organization in order to best adapt to changes in cell size?

Answers to these questions have recently emerged owing largely to in vitro experiments in frog egg extracts focusing on the nucleus and the spindle, the dynamic microtubule-based apparatus responsible for faithful segregation of sister chromatids during cell division. Cytoplasmic extracts from metaphase-arrested *Xenopus* eggs were historically used to elucidate fundamental principles of cell cycle control and meiotic spindle assembly [38]. This system provides large volumes of concentrated cytoplasm which can be arrested in specific stages of the cell cycle. With the addition of sperm nuclei as a source of DNA, cell-cycle specific structures such as meiotic spindles [39][40] and interphase nuclei [41] can be formed in vitro, and processes such as DNA replication [42], chromosome condensation [43] and segregation [44–46] monitored. In a similar manner, large amounts of synchronized *Xenopus* embryos can be generated through in vitro fertilization, and cytoplasmic “embryo extracts” generated from specific developmental stages [47].

1.4 Volume-dependent size scaling of organelles in *Xenopus* egg and embryo extracts

Using *Xenopus* extract systems, a number of studies over the past decade have revealed that both physical and biochemical mechanisms operate in concert to adapt the size of subcellular structures to cell size during development, and that size control operates primarily through differences in the amount or composition of the cytoplasm [48]. With respect to cell geometry, cell size has been directly linked to organelle size through cytoplasmic volume, which has been suggested to be a universal regulator of organelle growth [49–51]. This theory is supported by experiments encapsulating *Xenopus* egg extracts inside microfluidic droplets to form cell-like compartments of different dimensions [52,53]. Meiotic spindle size was observed to decrease in droplets of decreasing volume at a specific size threshold, similar to what occurs during early cleavage divisions in embryogenesis. Interestingly, spindle size did not differ in spherical droplets compared to compressed droplets of equal volume but differing droplet diameter, indicating that the scaling trend was dependent on cell volume rather than shape [52]. In similar experiments examining the effects of confinement on nuclear size, increasing the concentration of sperm per unit volume of *X. laevis* egg extract was sufficient to shrink the resulting interphase nuclei [54]. Additionally, confinement of pre-assembled nuclei in engineered microchannels of decreasing size was sufficient to shrink nuclei as channel size was reduced. As with meiotic spindles, this trend was not due to physical confinement or boundary sensing of nuclei, since altering the volume, but not the aspect ratio of the channel, affected nuclear size. Taken together,

these results suggest that cytoplasmic volume plays an important role in regulating the size of subcellular structures independent of a cell boundary.

In addition to volume-dependent mechanisms, specific biochemical mechanisms due to changes in cytoplasmic composition have also been shown to regulate the size of subcellular structures during development. In both cleaving *Xenopus* embryos and egg extracts encapsulated in droplets, spindle length has been observed to scale linearly with cytoplasmic volume at a threshold size, above which spindle size reaches a maximum that is uncoupled from volume [52], [67]. However, spindles and nuclei in extracts prepared from stage 8 (~4000 cell) *X. laevis* embryos were smaller than spindles from stage 3 (4 cell) embryos, even when encapsulated in similar volumes [52,55]. Similar trends are noted in later-stage embryo extracts. Therefore, cytoplasmic factors also influence intracellular scaling [56]. One mechanism is thought to derive from limiting components as cell or compartment volume decreases, reducing the maternal supplies necessary for organelle assembly, such as the concentration of tubulin required to form a spindle of a specific size [50]. With respect to nuclear size scaling, the histone chaperone nucleoplasmin (Npm2) was recently identified by fractionation of *Xenopus* egg extracts as a key effector. Cytoplasmic levels of Npm2 decrease throughout development and microinjection of Npm2 into stage 10 embryos was sufficient to increase nuclear size [66]. Therefore, factors that become limiting as cell volumes decrease contribute to subcellular scaling[53–57],

1.5 Sensing the cell surface area to volume ratio coordinately mediates spindle and nuclear scaling in vivo

While limiting amounts of cytoplasmic components provide a simple physical explanation for spindle and nuclear scaling, the underlying molecular mechanisms have proven to be more complex. A major player has emerged as the nuclear transport receptor importin α , which by binding to cargoes and regulating their localization and/or activity can modulate both nuclear and spindle size [47] [55]. Interestingly, as early development proceeds in the cleaving *Xenopus* embryo, an increasing fraction of maternal importin α was found to be associated with the plasma membrane [47]. The resulting decrease in cytoplasmic importin α correlated with decreased import of cargoes known to mediate nuclear growth, such as lamin B3 [55], [57]. A similar importin α -based mechanism that modulates spindle size during development was also discovered. Importin α binds and inhibits kif2a, a microtubule depolymerizing motor protein of the Kinesin-13 family, via kif2a's nuclear localization sequence (NLS). These observations led to a model in which progressive titration of importin α to the plasma membrane as cell size decreases reduces inhibition of kif2a in the cytoplasm, allowing it to bind

and depolymerize spindle microtubules and decrease spindle size [47], [57]. These findings suggested that in addition to cell volume, cell surface area is a second physical parameter that could function to regulate subcellular scaling.

1.6 Interspecies comparison of Pipid frogs provides molecular insight into scaling and architecture of the meiotic spindle

In addition to revealing mechanisms that contribute to the subcellular scaling that occurs during embryogenesis, in vitro systems have also been applied to study scaling across frog species with eggs and genomes of different sizes (Figure 1.1). Interestingly, the spindles of even closely related species differ not only in size but also in architecture and morphology. ~35 μm long meiotic spindles in *X. laevis* egg extracts possess a high microtubule density in the spindle center, with bundled microtubule arrays extending continuously from pole to pole. In contrast, smaller ~22 μm long spindles in *X. tropicalis* egg extracts have higher microtubule density at the spindle poles and more prominent astral microtubule arrays with a significant lack of microtubule density in the spindle midzone [58,59]. The size difference is not due to the difference in the DNA content of each species spindle, as using *X. laevis* sperm nuclei as a DNA source in *X. tropicalis* extract or vice versa only exerted a minimal effect on spindle size [48]. Therefore, differences in cytoplasm components such as microtubule-associated proteins were proposed to modulate spindle size. Computational modeling of microtubule dynamics within the spindle predicted that spindle length could be determined by a balance of forces within the spindle that contribute to bipolarity, such as the microtubule-based motor proteins Eg5 and dynein that function to slide microtubules relative to one another, as well as the modulation of spindle microtubule lifetimes controlled by factors that regulate microtubule depolymerization [60,61]. Interestingly, mixing of *X. laevis* and *X. tropicalis* extracts revealed dose-dependent effects on spindle size and morphology indicating that cytoplasmic factors are sufficient to scale subcellular structures, and that the extract provided a unique approach to identify them [48].

Using this interspecies system, it was determined that the differing sizes and architectures of the *X. laevis* and *X. tropicalis* spindles were largely due to differences in microtubule stability and forces within the spindle, as the computational models predicted. Microtubule severing rates were higher in *X. tropicalis* egg extracts compared to *X. laevis* due to increased activity of the microtubule severing enzyme katanin, a AAA-ATPase that destabilizes microtubules by severing them along their length, as well as by promoting kinesin-13 driven depolymerization of newly exposed microtubule ends [62,63]. The increased activity of *X.*

tropicalis katanin was found to be due to loss of an inhibitory Aurora B kinase phosphorylation site in its catalytic p60 subunit, a serine residue at amino acid position 131, which is present in *X. laevis*. Adding a recombinant version of katanin harboring a mutation of this serine to alanine increased severing activity and decreased spindle size in *X. laevis* egg extracts [58]. A second spindle scaling factor was identified as TPX2, a microtubule-associated protein that modulates microtubule nucleation and organization [64]. The concentration of TPX2 is ~3-fold higher in *X. tropicalis* extracts compared to *X. laevis*. By increasing recruitment of the Eg5 motor to spindle poles, TPX2 was shown to locally increase microtubule density and parallel bundling, further reducing spindle size in *X. tropicalis* relative to *X. laevis* [59]. Interestingly, analysis of a third *Xenopus* species, *Xenopus borealis*, revealed meiotic spindles that possess morphological and molecular features of both *X. laevis* and *X. tropicalis*, resulting in a spindle size and architecture intermediate between the other two species [65].

Interspecies studies in *Xenopus* egg extracts have thus allowed for identification of precise molecular scaling mechanisms of subcellular structures. However, these studies have narrowly focused on species within the *Xenopus* genus only. How conserved are these scaling mechanisms among different species? And are there evolutionary constraints on what mechanisms a particular species can utilize? The following chapter explores answers to these questions in detail.

Chapter 2


Regulation of meiotic spindle size in the small frog *Hymenochirus boettgeri*

The following chapter contains material from a publication on which I am the first author [66]. This article is distributed under the terms of the Creative Commons Attribution License (CC BY 4.0), which permits unrestricted use and redistribution provided that the original author and source are credited.

2. 1 Introduction

Xenopus frog species possess a variety of egg and meiotic spindle sizes, and differences in activities or levels of microtubule-associated proteins in the egg cytoplasm between *Xenopus laevis* and *Xenopus tropicalis* have been shown to account for spindle scaling [48]. Increased activity of the microtubule severing protein katanin scales the *X. tropicalis* spindle smaller compared to *X. laevis* [67], as do elevated levels of TPX2, a protein that enriches the cross-linking kinesin-5 motor Eg5 at spindle poles [59]. However, it is unknown whether these same mechanisms operate in other frog species over a diverse range of sizes. To this end, we utilized the tiny, distantly related Pipid frog *Hymenochirus boettgeri*, which to date has been poorly studied relative to its *Xenopus* counterparts and is best known in the pet trade. The *Hymenochirus* and *Xenopus* genera diverged over 110 MYA [68,69]. The body weight of *H. boettgeri* averages only 2 grams- about 1/15th the average weight of *X. tropicalis*, and 1/45th that of the larger *X. laevis* (Fig 2.1). In this work, we find that egg extracts from *H. boettgeri* form meiotic spindles similar in size to *X. tropicalis*, but that TPX2 and katanin-mediated scaling is not conserved. Instead, the microtubule depolymerizing motor protein kif2a functions to modulate spindle size. *H. boettgeri* kif2a possesses an activating phosphorylation site that is absent from *X. laevis*. Comparison of katanin and kif2a phosphorylation sites across a variety of species revealed strong evolutionary conservation, with *X. laevis* and *X. tropicalis* possessing distinct and unique alterations.

Figure 2.1



Species	Avg female body mass (g)/ length (cm)	DNA content (pg/haploid nucleus)	Chromosome #	Avg egg diameter (mm)
<i>H. boettgeri</i>	2/3	2.35	2n=24	0.7
<i>X. tropicalis</i>	30/5	1.8	2n=20	0.8
<i>X. borealis</i>	65/7	3.6	4n=36	1.2
<i>X. laevis</i>	90/10	3.2	4n=36	1.4
<i>X. longipes</i>	12/4	8	12n=108	1.2

Figure 2.1: Morphometrics and genome content of Pipid frogs. Pipid frogs display a diverse range of egg, body, and genome sizes, from the large allotetraploid *Xenopus laevis* and *Xenopus borealis* to the tiny diploid *Hymenochirus boettgeri*. Despite the large genome of the dodecaploid *Xenopus longipes*, egg and body size are relatively small.

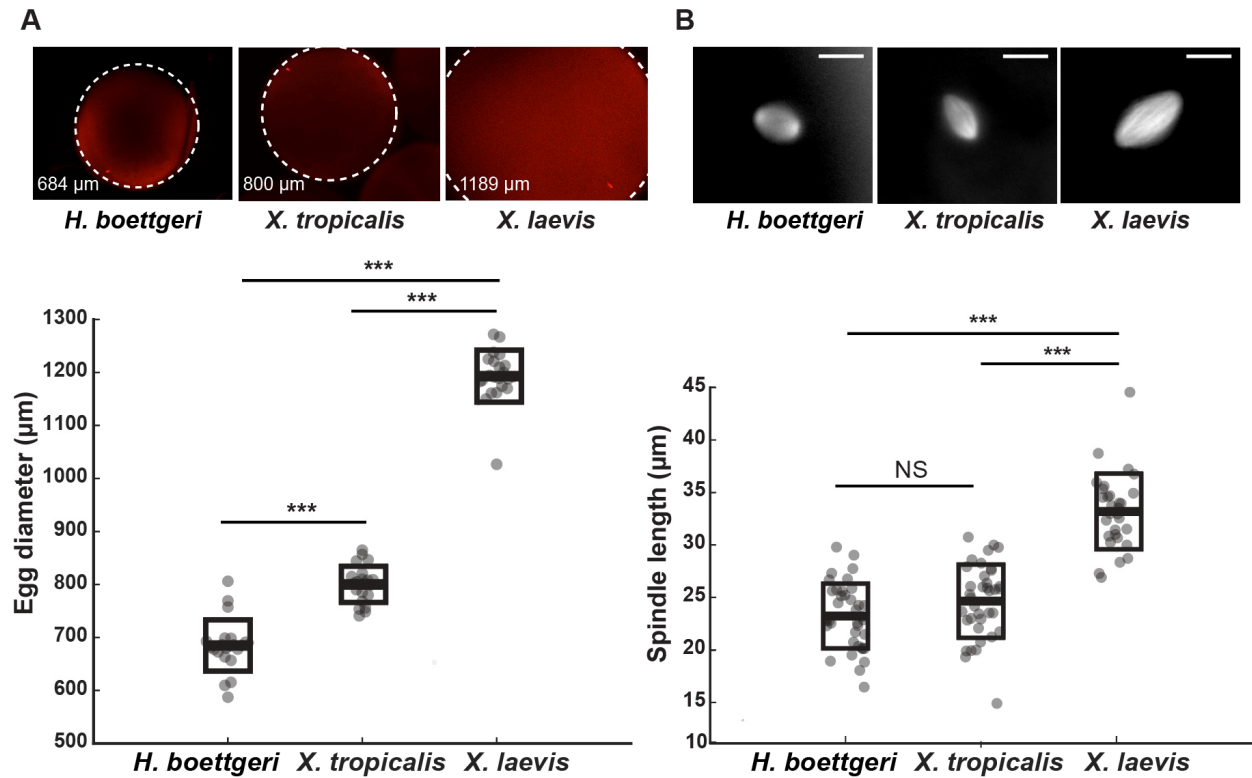
2.2 Results

H. boettgeri egg extracts recapitulate spindle assembly in vitro

H. boettgeri eggs average ~684 μm in diameter, compared to *X. tropicalis* at 800 μm , and *X. laevis* at 1189 μm , corresponding to an overall ~5-fold difference in volume (Fig 2.1). Interestingly, although *H. boettgeri* eggs are significantly smaller than those of *X. tropicalis*, spindle lengths are similar in both species, with averages of 23 and 24 μm , respectively (Fig 2.2 A,B). To determine whether mechanisms of spindle size control previously identified in *Xenopus* are conserved in *H. boettgeri*, we developed an egg extract system similar to that of *Xenopus* that is subject to cell cycle control and amenable to biochemical manipulation. Although extract preparation was challenging due to the small size of the eggs and required the ovulation of at least 8-12 frogs per extract, the system robustly recapitulated events of the cell cycle such as meiotic spindle assembly (Fig 2.2C) and formation of interphase nuclei

(unpublished data). The architecture of spindle microtubules in *H. boettgeri* eggs and extracts appeared slightly different from that of the *Xenopus* species, with increased microtubule density at the poles relative to the central spindle (Fig 2.2B, 2.2C). Spindles formed in *H. boettgeri* extracts were statistically similar in length to meiotic spindles in the egg, indicating that extract conditions faithfully reproduced in vivo spindle size (Fig 2.2 D).

Figure 2.2



Continued on next page

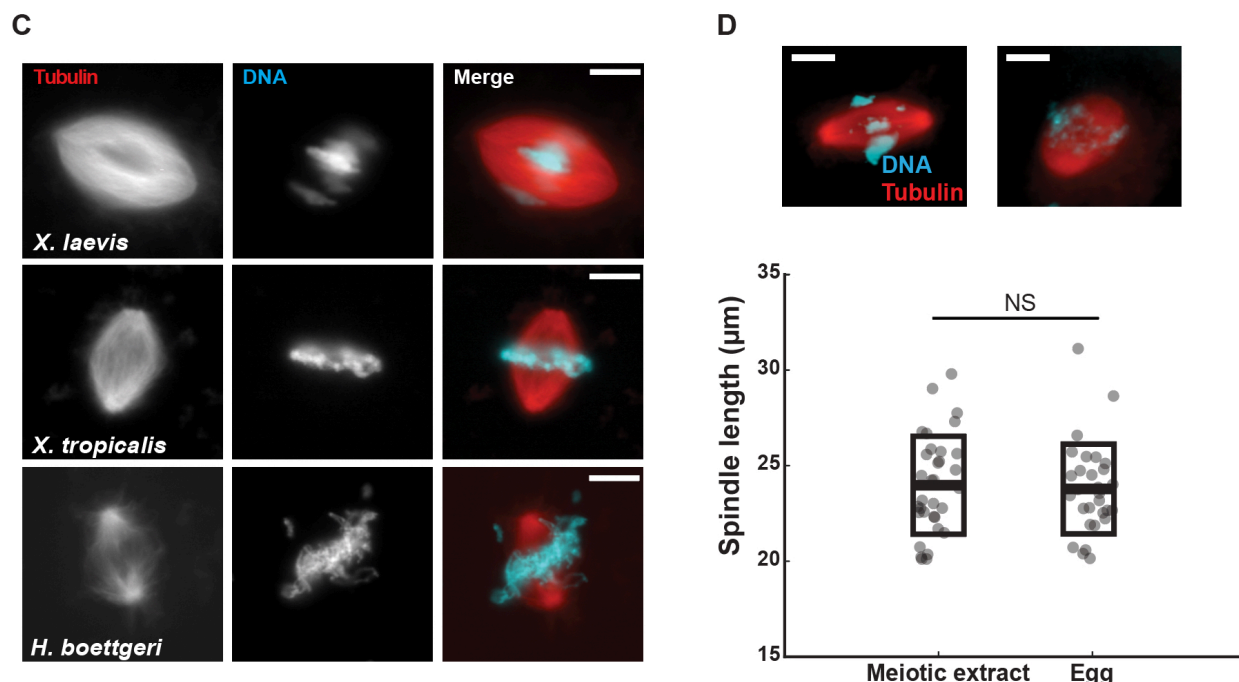


Figure 2.2: Comparison of meiotic spindle length in Pipid frog species

A. Immunofluorescence images and egg diameter quantification of fixed eggs of each frog species. Box plot shows all individual egg diameters. $n \geq 20$ egg diameters measured for each species. B. Comparison of meiotic spindle length of *X. laevis*, *X. tropicalis*, and *H. boettgeri*, measured by immunofluorescence in fixed eggs. $n > 30$ spindles for each species. Box plot shows all individual spindle lengths. C. Representative images of spindles assembled in *X. laevis*, *X. tropicalis*, and *H. boettgeri* egg extracts. D. Spindle length measured in either fixed *H. boettgeri* eggs in vivo or *H. boettgeri* egg extracts in vitro. $n = 30$ egg spindles, $n = 38$ extract spindles from 3 separate *H. boettgeri* extracts. Box plot shows all individual spindle lengths. $p = 0.426$. For all box plots, thick line inside box = average length, upper and lower box boundaries = \pm std dev. $***p < 0.0001$, NS = not significant. All scale bars = $10 \mu\text{m}$.

Spindle size scaling in *H. boettgeri* egg extracts

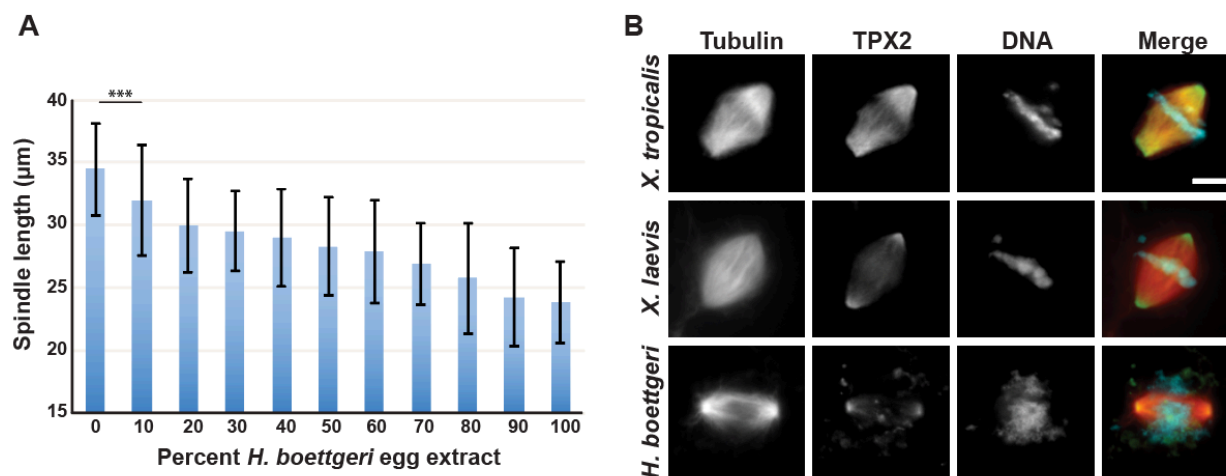
Addition of *H. boettgeri* egg extracts to *X. laevis* egg extracts reduced spindle length in a dose-dependent manner (Fig 2.3A), suggesting that not only are egg extracts from two entirely different frog genera compatible enough to assemble spindles, but also that cytoplasmic factors are responsible for controlling spindle size.

To determine whether mechanisms of spindle size control previously identified in *Xenopus* are conserved in *H. boettgeri*, we examined TPX2 and katanin as candidate spindle scaling factors. In *X. tropicalis* egg extracts, TPX2 is present at 2-3-fold higher levels than in *X. laevis* egg extracts and is highly enriched on spindle microtubules. Increased TPX2-mediated recruitment of Eg5 is thought to increase parallel microtubule

cross-linking at spindle poles, thereby decreasing spindle length [59]. In comparison, TPX2 did not localize as intensely to spindle microtubules in *X. laevis* and *H. boettgeri* egg extracts (Fig 2.3B). By immunoblot TPX2 levels in *H. boettgeri* egg extracts were similar to those in *X. laevis* (Fig 2.3C) and Eg5 was not enriched at spindle poles as observed in *X. tropicalis* egg extracts ([59], unpublished data), indicating that TPX2 does not function to reduce meiotic spindle size in *H. boettgeri*.

A second spindle scaling mechanism operating in *Xenopus* is altered microtubule depolymerization rates, which were shown to be higher in *X. tropicalis* egg extracts due to differential regulation of the microtubule severing enzyme katanin. Katanin concentrates at spindle poles in *X. tropicalis* where it is thought to promote depolymerization by severing microtubules along their length, as well as by promoting kinesin-13 driven depolymerization of newly exposed microtubule ends [47,63]. The *X. laevis* homolog of katanin contains a serine residue at amino acid 131 of its catalytic p60 subunit, which is phosphorylated and inhibited by Aurora B kinase. In contrast, the *X. tropicalis* homolog of p60 katanin possesses a glycine residue at this position, thereby blocking phosphorylation and increasing microtubule severing rates [67]. Interestingly, although the *H. boettgeri* homolog of p60 katanin is 88% identical to that of *X. tropicalis* and 89% identical to *X. laevis*, (Supplemental Figs 2.5), it possesses the predicted Aurora B phosphorylation site at serine 131 (Fig 2.3D), and microtubule severing rates in *H. boettgeri* egg extracts were qualitatively similar to those in *X. laevis* (Fig 2.3E). Therefore, it is unlikely that katanin is responsible for the reduced spindle size in *H. boettgeri* egg extracts.

Figure 2.3



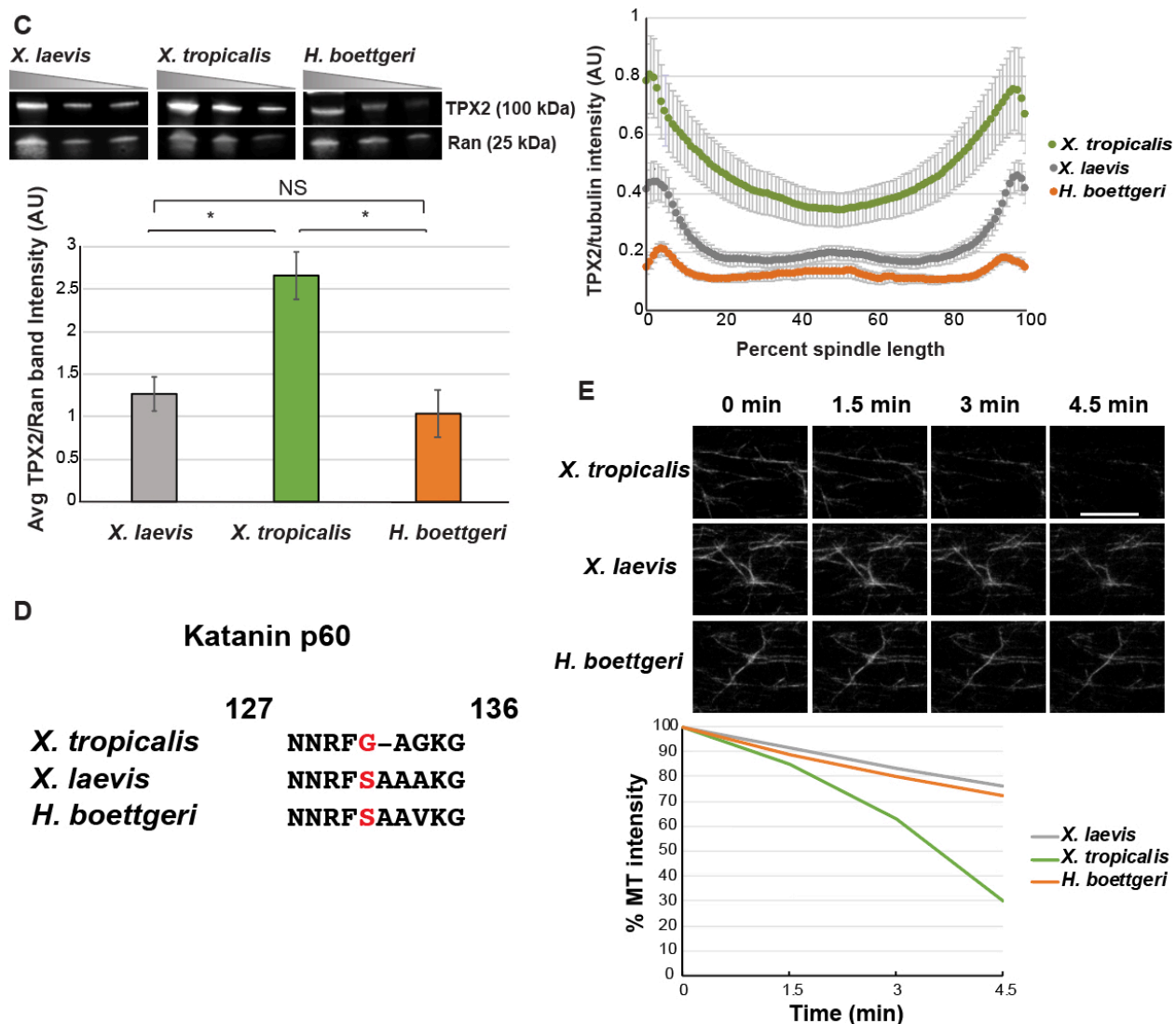


Figure 2.3: Cytoplasmic factors scale spindle length in *H. boettgeri* egg extracts through a mechanism distinct from that of *Xenopus* species

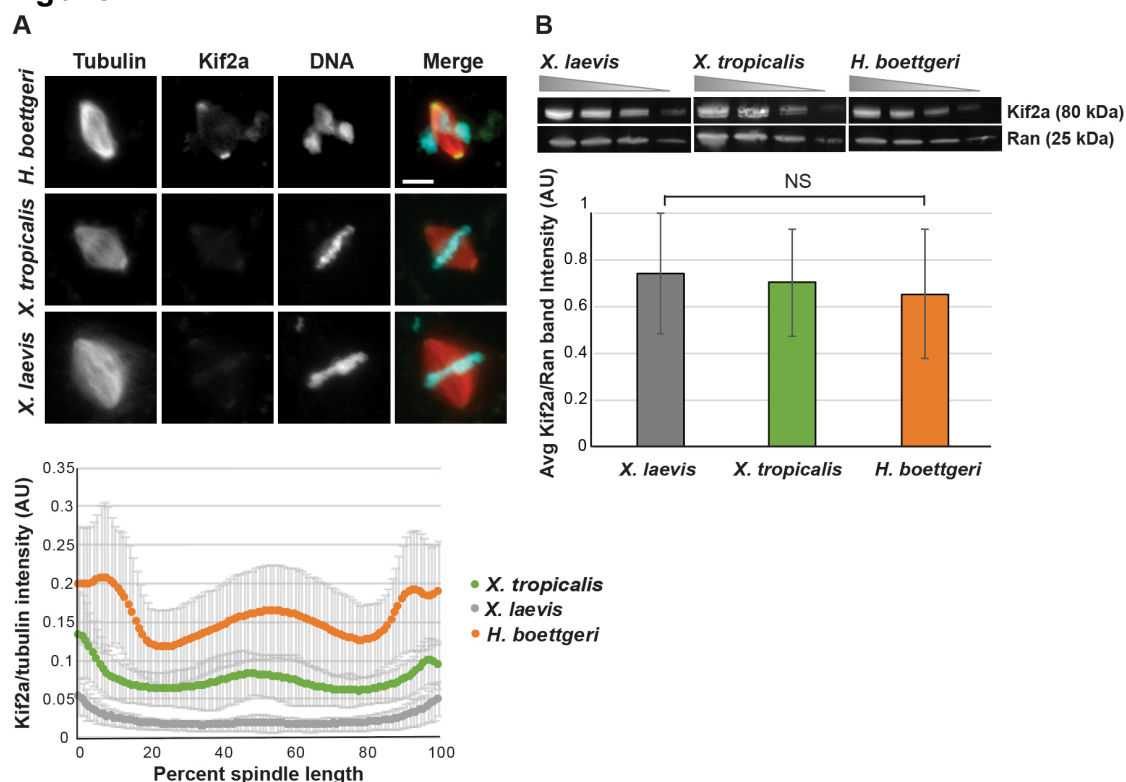
A. Quantification of spindle length in *X. laevis* extract mixed with increasing amounts of *H. boettgeri* extract. $n > 25$ spindles each condition from 3 separate mixing experiments using 3 separate *X. laevis* egg extracts and 3 separate *H. boettgeri* extracts. Error bars = \pm std dev. There was a significant decrease in spindle length at 10% *H. boettgeri* egg extract added, $***p = 0.0059$. B. Top Panel: Representative immunofluorescence images of TPX2-stained spindles in *X. laevis*, *X. tropicalis*, and *H. boettgeri* egg extracts. Bottom Panel: Line scan quantification of the average ratio of TPX2 to tubulin fluorescence intensity across the spindle length in each species egg extract. $n > 50$ spindles each extract from at least 3 extracts per species. Error bars = \pm std dev. AU = arbitrary units. C. Top Panel: Western blot of *X. laevis*, *X. tropicalis*, and *H. boettgeri* extracts, probed for TPX2. Bottom Panel: Quantification of 3 separate blots for each species. Band intensities were normalized to the integrated density of the corresponding Ran loading control. AU = arbitrary units. D. Alignment of sequences

around serine 131 in *X. laevis*, *X. tropicalis*, and *H. boettgeri* katanin p60. E. Top Panel: Representative images of fluorescently-labeled microtubule severing over time in each species egg extract. Bottom Panel: Quantification of integrated fluorescence intensity of representative images shown over time in each species egg extract. Similar effects were observed in $n \geq 3$ egg extracts per species; one representative assay is quantified here. All scale bars= 10 μm .

Serine 252 of kif2a modulates spindle size in *H. boettgeri*

Kif2a, a microtubule depolymerizing motor protein of the kinesin 13 family, was previously identified as a spindle scaling factor that operates during early *X. laevis* development, when rapid cell cleavages give rise to smaller and smaller cells [47]. We therefore investigated a potential role for kif2a in spindle size scaling in *H. boettgeri*. Kif2a antibodies stained *H. boettgeri* spindles more intensely compared to *X. laevis* and *X. tropicalis* (Fig 2.4A), although levels of kif2a were similar in egg extracts of all three species (Fig 2.4B). Whereas inhibition of kif2a in *X. laevis* eggs and early embryos was not observed to affect spindle length ([47] and unpublished data), addition of an inhibitory anti-kif2a antibody to *H. boettgeri* egg extracts caused an increase in spindle size as well as spindle microtubule density (Fig 2.4C). These observations indicated a role for kif2a as a scaling factor in an interspecies rather than a developmental context.

Figure 2.4



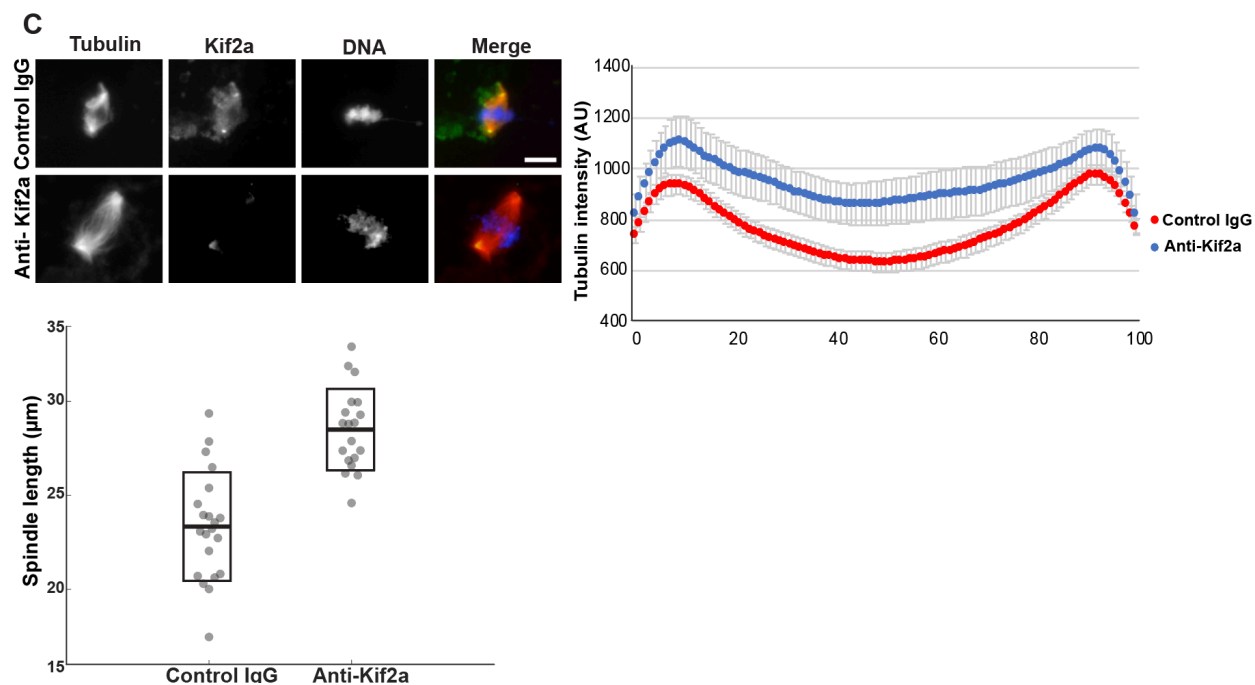


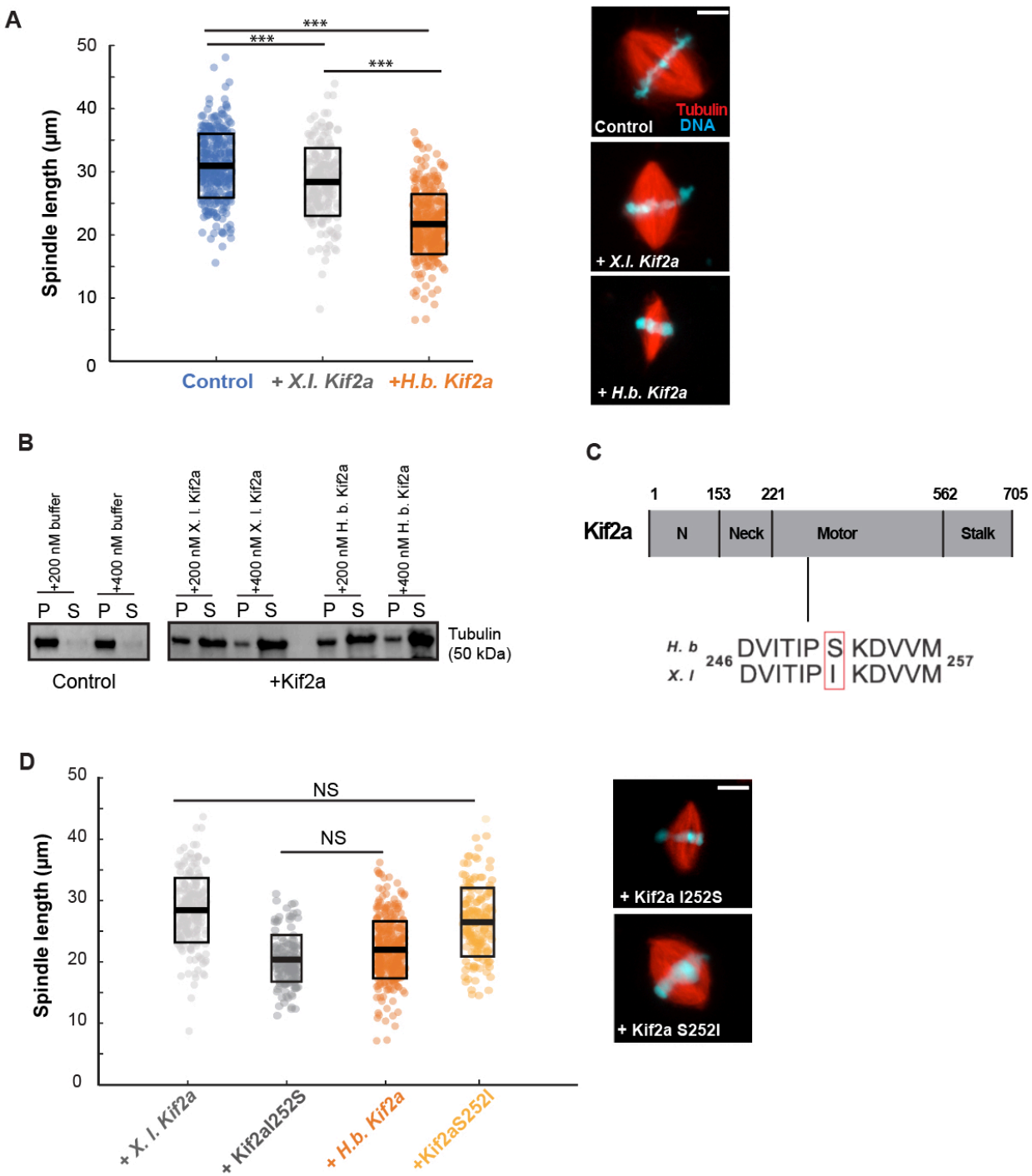
Figure 2.4: Kif2a is enriched on spindles in *H. boettgeri* egg extracts, and inhibition of kif2a increases spindle length. Top Panel: Representative immunofluorescence images of kif2a-stained spindles in *X. laevis*, *X. tropicalis*, and *H. boettgeri* egg extracts. Bottom Panel: Line scan quantification of the average ratio of kif2a to tubulin fluorescence intensity across the spindle length in each species egg extract. $n > 50$ spindles each extract from at least 3 extracts per species. Error bars = \pm std dev. B. Top Right Panel: Western blot of *X. laevis*, *X. tropicalis*, and *H. boettgeri* extracts, probed for kif2a. Bottom Panel: Quantification of 3 separate blots for each species. Band intensities were normalized to the integrated density of the corresponding Ran loading control. AU=arbitrary units. C. Top Left Panel: Representative spindle images in *H. boettgeri* egg extracts upon addition of a kif2a antibody or control IgG. Top Right Panel: Line scan quantification of the average tubulin fluorescence intensity along the long axis of spindles in control- and kif2a-inhibited *H. boettgeri* egg extracts. AU=arbitrary units. Error bars = \pm std dev. Bottom Left Panel: Quantification of spindle length in kif2a inhibited *H. boettgeri* egg extracts. $n \geq 19$ spindles each from 2 extracts. Thick line inside box = average length, upper and lower box boundaries = \pm std dev. Kif2a antibody or control IgG were added to a final concentration of 0.7 mg/ml. Scale bars = 10 μ m.

To determine whether the *H. boettgeri* homolog of kif2a contributed to spindle length scaling, we added purified recombinant kif2a proteins to *X. laevis* egg extracts. Whereas addition of *H. boettgeri* kif2a decreased spindle length by $\sim 25\%$, addition of an equal amount of *X. laevis* kif2a had

a much lesser effect (Fig 2.5A). The kif2a protein is comprised of a conserved central catalytic domain flanked by N and C terminal regions that mediate dimerization and subcellular targeting [70,71]. Sequence alignment of the *H. boettgeri* and *X. laevis* kif2a homologs revealed 93.6% identity (Supplemental Figs 2.5). To test whether minor sequence variations contributed directly to differences in microtubule depolymerization by the kif2a homologs, we compared activity of the recombinant proteins in a microtubule pelleting assay (Fig 2.5B). *H. boettgeri* and *X. laevis* kif2a possessed very similar activities in shifting tubulin subunits to the supernatant, implicating a post-translational modification in their differential activity regulating spindle length.

Close inspection of kif2a sequences revealed a potential regulatory site at serine 252 within the catalytic domain of *H. boettgeri* kif2a. In human cells this residue was previously implicated as a site phosphorylated by Polo-like-kinase 1 (Plk1), a kinase shown to activate the microtubule depolymerizing activity of kif2a [72]. However, the *X. laevis* kif2a homolog contains an isoleucine residue at position 252 (I252), which cannot be phosphorylated (Fig 2.5C, Supplemental Figs 2.5). Addition of a mutant version of the *X. laevis* kif2a containing a serine residue at this site (Kif2a I252S) to *X. laevis* egg extracts caused a dramatic reduction in spindle length, similar to that observed when an equal concentration of recombinant wild type *H. boettgeri* kif2a was added (Fig 2.5D). A similar effect was observed when a phosphomimetic mutant version of the *X. laevis* kif2a containing a glutamic acid residue at this site (Kif2a I252E) was added to extracts. Interestingly, this mutant did not show increased intensity at spindle poles compared to wild type *X. laevis* kif2a, indicating that increased kif2a activity rather than concentration leads to the reduction in spindle length (Fig 2.5E,F). Conversely, addition of *H. boettgeri* kif2a in which the serine was substituted with an isoleucine at position 252 (Kif2a S252I) reduced spindle length to a lesser degree, which was similar to the activity of wild type *X. laevis* kif2a (Fig 2.5D). These results identify kif2a phosphorylation and activation as the likely mechanism scaling spindles smaller in *H. boettgeri* compared to *X. laevis*. Interestingly, the phosphomimetic version of kif2a did not possess greater microtubule depolymerizing activity towards pure microtubules than the wild-type version, suggesting that phosphorylation of serine 252 on its own is not sufficient to activate kif2a (data not shown). Future experiments will address whether other modifications or interacting factors act to modulate kif2a activity in vivo.

Figure 2.5



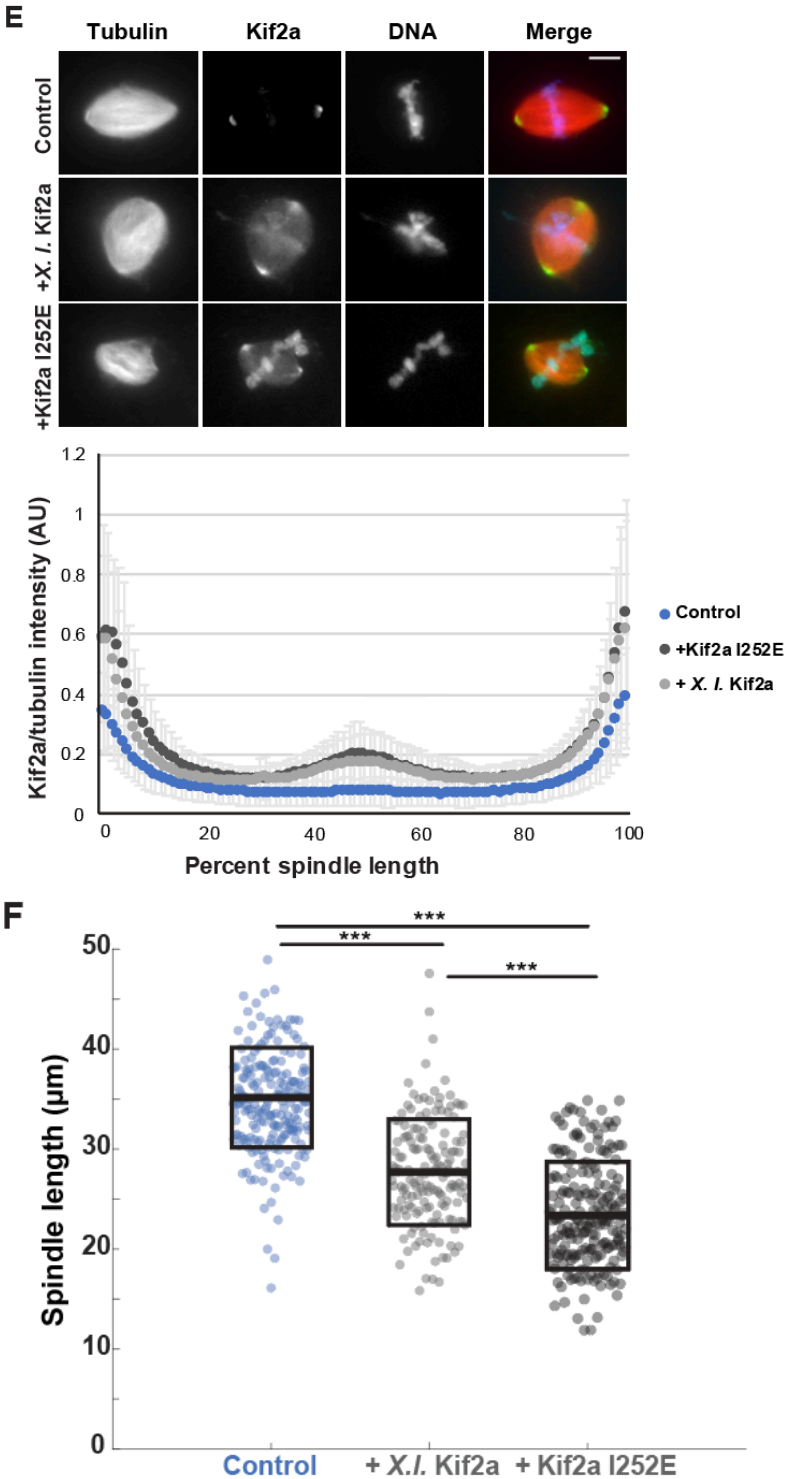


Figure 2.5: Serine 252 of kif2a regulates its activity A. Left Panel: Spindle length in *X. laevis* egg extracts with 0.5 μM exogenous recombinant *X. laevis* or *H. boettgeri* proteins added. Right Panel: Representative images of spindles in (A). $n \geq 137$ spindles from 3 separate extracts. B. Top Panel: Increasing amounts of recombinant *X. laevis* or

H. boettgeri kif2a proteins were added to taxol-stabilized microtubules and microtubules sedimented through a sucrose cushion. Amounts of soluble tubulin in the supernatant (S) and pellet (P) were quantified by SDS-PAGE and Coomassie staining. Bottom Panel: Ratio of pellet to supernatant gel band intensities in the microtubule sedimentation assay with 200 nM *H. boettgeri* or *X. laevis* kif2a added. Bands from 3 separate gels quantified, $p=0.2768$. NS= Not Significant. Error bars= +/- std dev. C. Schematic of kif2a domain organization and sequence alignment of the area around amino acid 252 in *H. boettgeri* (*H.b.*), and *X. laevis* (*X.l.*). D. Left Panel: Spindle length in *X. laevis* egg extracts with 0.5 μ M exogenous recombinant wildtype *X. laevis*, *H. boettgeri*, and mutant Kif2a I252S or Kif2a S252I proteins added. Right Panel: Representative images of spindles in (D). $n \geq 138$ spindles from 3 separate extracts. E. Top panel: Representative images of spindles in *X. laevis* egg extracts with 0.5 μ M recombinant wild type *X. laevis* or an *X. laevis* phosphomimetic mutant (Kif2a I252E) added. Bottom panel: Line scan quantification of the average ratio of kif2a to tubulin fluorescence intensity across the spindle length of spindles described above. F. Spindle length quantification of experiments described in (E). $n \geq 161$ spindles from 3 separate extracts. All box plots show all individual spindle lengths. Thick line inside box= average length, upper and lower box boundaries= +/- std dev. *** $p < 0.0001$, NS=Not Significant. Scale bars=10 μ m.

Conserved constellations of spindle scaling factors operate across species

Taken together, our results suggest that mechanisms of interspecies spindle scaling identified in *Xenopus* are not conserved at the level of the genus in the more distantly related frog *Hymenochirus boettgeri*. However, commonalities exist among spindle scaling mechanisms across frog species that involve microtubule destabilizing factors and their regulation by mitotic kinases. To examine the evolutionary conservation of spindle scaling activities by microtubule depolymerizing factors, we compared the regulatory phosphorylation sites of kif2a and katanin across a variety of species (Fig 2.6, see Supplemental Figs 2.5 for full sequences).

Figure 2.6

A

Kif2a

246257

<i>Xenopus laevis</i>	DVITIP I KDVVM
<i>Xenopus tropicalis</i>	DVITIPSKDVVM
<i>Xenopus borealis</i>	DVITIPSKDVVM
<i>Xenopus longipes</i>	DVITIPSKDVVM
<i>Hymenochirus boettgeri</i>	DVITIPSKDVVM
<i>Rana pipiens</i>	DVITIPSKDVVM
<i>Nanorana parkeri</i>	DVITIPSKDVVM
<i>Danio rerio</i>	DVITIPSKDVVM
<i>Anolis carolinensis</i>	DVITIPSKDVVM
<i>Gallus gallus</i>	DVITIPSKDVVM
<i>Mus musculus</i>	DVITIPSKDVVM
<i>Homo sapiens</i>	DVITIPSKDVVM

B

Katanin p60

124138

<i>Xenopus laevis</i>	KSHNNRFSAAAKGPN
<i>Xenopus tropicalis</i>	KSHNNRF G A-GKGP
<i>Xenopus borealis</i>	KSHNNRFSAAAKGPN
<i>Xenopus longipes</i>	KSHNNRFSAAAKGPN
<i>Hymenochirus boettgeri</i>	RAQNNRLSAAVRGPI
<i>Rana pipiens</i>	RVQNNRISAAVRGPN
<i>Nanorana parkeri</i>	RVHNNRISAAVRGPN
<i>Danio rerio</i>	RGHNNRISAAVRGPH
<i>Anolis carolinensis</i>	KVQNNRASAAPRVPN
<i>Gallus gallus</i>	RGHNNRISAAVRGPH
<i>Mus musculus</i>	KPHSNRPSTVVRA-H
<i>Homo sapiens</i>	KSHGNRPSTTVRVHR

Figure 2.6: Phylogenetic prediction of spindle size scaling mechanisms by comparing microtubule depolymerizing proteins across species. A. Sequence alignment of kif2a in vertebrates around amino acid 252. B. Sequence alignment of katanin in vertebrates around amino acid 131.

Interestingly, all species examined except for *X. laevis* contained the activating serine at residue 252 of kif2a, suggesting that reduced activity of kif2a is unique to *X. laevis*. Moreover, only *X. tropicalis* katanin possessed the inhibitory serine at position 131. These observations suggest that spindle size control mechanisms are overall evolutionarily conserved, but that some species are “outliers” that possess distinct mechanisms setting meiotic spindle length.

2.3 Discussion

Our study reveals that distinct mechanisms operate across frog species to set meiotic spindle length. Whereas high levels of TPX2 and the absence of an inhibitory phosphorylation site on katanin scales the *X. tropicalis* spindle smaller than that of *X. laevis*, an activating phosphorylation site on *H. boettgeri* kif2a appears to be crucial for setting meiotic spindle size in this tiny species.

Thus, to date, three meiotic spindle scaling factors including TPX2, katanin, and kif2a have been identified. Previous computational simulations evaluating the microtubule dynamic parameters that set meiotic spindle length indicated that the activity of depolymerizers such as kif2a or microtubule severing enzymes such as katanin could operate primarily at microtubule minus ends, which are enriched at spindle poles [61]. Although our study implicates kif2a phosphorylation in regulating its activity, differences in localization may also play a role. In addition to modulating spindle length, variation among spindle factors and their regulators likely contributes to differences in spindle architecture across species [65].

Interestingly, with respect to phosphoregulatory sites on katanin and kif2a, there is not a clear correlation between their presence or absence and spindle size. For example, *Xenopus borealis*, which is similar to *X. laevis* in terms of genome and egg size, forms meiotic spindles of similar length to *X. laevis*, yet possesses both the inhibitory phosphorylation site of *X. laevis* katanin and the activating phosphorylation site found in *X. tropicalis* and *H. boettgeri* kif2a (Fig 2.6, [65]). This suggests that other factors or regulatory mechanisms operate, which could differentially set the activity of mitotic kinases Aurora B and Polo, or affect the small GTPase Ran, which functions through importins to regulate a number of spindle assembly factors. Observed differences in meiotic spindle morphology and microtubule distribution along the length of the spindle of multiple frog species, as well as sensitivity to Ran disruption, highlight many possible variations in spindle architecture and assembly mechanisms. Furthermore, other factors such as the microtubule

polymerase XMAP215 and microtubule cross-linking motors have also been shown to regulate spindle length [73],[74]. Future studies will shed light on how the collective activities and regulation of a suite of factors can generate spindles with distinct architectures and sizes.

An important open question is the importance of spindle size for chromosome segregation. Experiments decreasing mitotic spindle length through manipulation of *kif2a* in *X. laevis* embryos caused defects in metaphase spindle alignment, but spindle orientation defects were corrected in anaphase and cleavage divisions were not disrupted [47], suggesting that astral microtubule growth rather than metaphase spindle length plays a crucial role. Of note, while *X. laevis*, *X. tropicalis*, and *H. boettgeri* scale in size at the level of the organism, egg, and genome, the *H. boettgeri* meiotic spindle size is very similar to that of *X. tropicalis*. Furthermore, a comparison of meiotic spindle morphometrics across many species did not reveal a strong correlation between egg size and spindle length, which possesses a narrow range compared to mitotic spindle size [75]. One possibility is that there is a lower limit to meiotic spindle size in amphibian eggs, and has this been reached in frogs as small as *X. tropicalis* and *H. boettgeri*. Manipulation of meiotic spindle size in vivo will be required to address this question.

Why have rare variations in spindle scaling factor sequences evolved in *X. laevis* *katanin* and *X. tropicalis* *kif2a*? Did these changes provide a fitness advantage, or did other changes compensate for them? It is interesting that the *X. borealis* *kif2a* sequence resembles that of the ancestral, *X. tropicalis*-like species prior to polyploidization, while the sequence in *X. laevis*, which is much more closely related to *X. borealis*, has diverged. Yet uncharacterized changes in spindle size control mechanisms in *X. borealis* may accommodate the increase in genome size in this species. Surveying sequence and expression levels of spindle size control factors over a diverse range of amphibian species promises to reveal whether additional mechanisms have evolved together with changes in ploidy to mediate spindle scaling.

2.4 Methods

Whole mount immunofluorescence of *X. laevis*, *X. tropicalis*, and *H. boettgeri* eggs

Dejellied eggs were fixed for one hour using MAD fixative (2 parts methanol [Thermo Fisher Scientific], 2 parts acetone [ThermoFisher Scientific], 1 part DMSO [Sigma]). After fixation, eggs were dehydrated in methanol and stored at -20°C. Eggs were then processed as previously

described [76] with modifications. Following gradual rehydration in 0.5X SSC (1X SSC: 150 mM NaCl, 15 mM Na citrate, pH 7.0), eggs were bleached with 1-2% H₂O₂ (ThermoFisher Scientific) in 0.5X SSC containing 5% formamide (Sigma) for 2-3 h under light, then washed in PBT (137 mM NaCl, 2.7 mM KCl, 10 mM Na₂HPO₄, 0.1% Triton X-100 [Thermo Fisher Scientific]) and 2 mg/mL bovine serum albumin (BSA). Eggs were blocked in PBT supplemented with 10% goat serum (Gibco – Thermo Fisher Scientific) and 5% DMSO for 1-3 h and incubated overnight at 4°C in PBT supplemented with 10% goat serum and primary antibodies. The following antibodies were used to label tubulin and DNA, respectively: 1:500 mouse anti-beta tubulin (E7; Developmental Studies Hybridoma Bank), and 1:500 rabbit anti-histone H3 (ab1791; Abcam). Eggs were then washed 4×2 hours in PBT and incubated overnight in PBT supplemented with 1:500 goat anti-mouse or goat anti-rabbit secondary antibodies coupled either to Alexa Fluor 488 or 568 (Invitrogen – ThermoFisher Scientific). Eggs were then washed 4×2 hours in PBT and gradually dehydrated in methanol. Eggs were cleared in Murray's clearing medium (2 parts Benzyl Benzoate, 1 part Benzyl Alcohol; Sigma). Cleared eggs were then mounted on a microscope slide, squashed under a coverslip, and imaged by epifluorescence microscopy.

***Xenopus* egg extract preparation**

Xenopus laevis and *Xenopus tropicalis* egg extracts were prepared as previously described [48,77]. Briefly, eggs in metaphase of meiosis II were collected, dejellied and fractionated by centrifugation. The cytoplasmic layer was isolated, supplemented with 10 mg/mL each of the protease inhibitors leupeptin, pepstatin and chymostatin (LPC), 20 mM cytochalasin D, and a creatine phosphate and ATP energy regeneration mix, and stored on ice (*X. laevis*) or at room temp (*X. tropicalis*) for up to 6 hours. Typical spindle reactions contained 25 µL CSF extract, *X. laevis* or *X. tropicalis* sperm at a final concentration of 500 nuclei per µl, and rhodamine-labeled porcine brain tubulin at a final concentration of 50 µg/ml.

***H. boettgeri* egg extract preparation**

Methods for working with *H. boettgeri* were generally based on those described in [78,79]. 8-12 *H. boettgeri* females were injected in the dorsal lymph sac with 200 units HCG (Sigma, in a limited volume of 100 µL) 16 hours before egg collection. Frogs were housed overnight at room temperature in distilled deionized water (ddW). Eggs were dejellied using a solution of 2% cysteine and 0.1% bovine serum albumin (BSA) in ddW adjusted to pH 7.8. Eggs were then washed extensively in CSF-XB buffer (5 mM EGTA, 100 mM KCl, 3 mM MgCl₂, 0.1 mM CaCl₂, 50 mM sucrose, and 10 mM HEPES pH 7.7) plus protease inhibitors (leupeptin, pepstatin, and chymostatin, 10 µg/ml each) and cytochalasin D (20 µg/ml), then packed by centrifugation in a 1.5 -ml microfuge tube at 1000×g for 1 min

followed by $2000\times g$ for 10 s. All buffer was removed, and eggs were crushed by centrifugation at $17,000\times g$ for 15 min in a swinging bucket rotor (Sorvall HB-6, Thermo Fisher Scientific). Concentrated cytoplasm was removed from the tube and immediately placed at room temperature. Additional protease inhibitors, cytochlasin D, and energy mix were added as for *Xenopus* egg extracts. Typical spindle reactions contained 25 μL CSF extract, *H. boettgeri* sperm at a final concentration of 500 nuclei per μL , and rhodamine-labeled porcine brain tubulin at a final concentration of 50 $\mu\text{g}/\text{ml}$.

Immunofluorescence of spindles in egg extracts

Spindle reactions were processed as described in [77]. Briefly, 25 μL egg extract reactions were fixed by addition to 1 ml of dilution buffer (80 mM Pipes, 1 mM MgCl_2 , 1 mM EGTA, 30% glycerol, 0.5% Triton X-100, and 2.5% formaldehyde). After incubating for 10 min at 23°C , samples were spun onto coverslips through a 5-ml cushion (BRB80 + 40% glycerol) at 10,200 rpm for 15 min using a swinging bucket rotor (Sorvall HB-6). Coverslips were postfixed for 5 min in 100% methanol, rinsed with PBS-0.1%NP40, blocked with PBS-1% BSA for 45 min, and incubated with primary antibody against TPX2 (diluted 1: 2500 in PBS-1% BSA) or kif2a (diluted 1: 5,000 in PBS-1% BSA) overnight in a humidified container at 4°C . Coverslips were rinsed 3x with PBS-0.1%NP40, then incubated for 45 min at room temp with secondary antibody (Invitrogen; Goat anti-rabbit or mouse anti-human IGG conjugated to Alexa Fluor 488, used at a 1:1000 dilution). Coverslips were then stained with 5 $\mu\text{g}/\text{ml}$ Hoechst 33258 (Sigma), and mounted on microscope slides using Vectashield (Vector Laboratories).

Microscopy, image processing, and spindle measurement

Images were obtained on a fluorescence microscope (BX51; Olympus) with TRITC, DAPI, and FITC filters (Chroma Technology Corp.) and a 20 or 40x objective (0.75 NA; UPlanFI N; Olympus) controlled by $\mu\text{Manager}$ software (<http://www.micro-manager.org/>) with an Orca-ER cooled charge-coupled device camera (Hamamatsu Photonics). Spindle length was measured using pole-to-pole distance with the line tool in Fiji [80]. Fluorescence intensity line scans were generated using an automated Java ImageJ plugin developed by X. Zhou (<https://github.com/XiaoMutt/AiSpindle>) [81].

Western blots

Egg extract protein concentrations were measured by Bradford assay (Biorad). Decreasing volumes of *X. laevis*, *X. tropicalis*, or *H. boettgeri* egg extracts (corresponding to 50, 25, and 12.5 μg total protein per lane) were separated by SDS-PAGE and wet transferred to nitrocellulose membrane (BioRad). Blots were blocked with PBS-0.1%Tween+ 5% milk for 45 min, probed with primary antibodies diluted in PBS-0.1%Tween+

5% milk overnight at 4°C, rinsed 3x over a 10 minute period at room temp with PBS-0.1%Tween, then probed with secondary antibodies diluted in PBS-0.1%Tween (Rockland Immunochemicals ; goat anti-rabbit DyLight 800, goat anti-human DyLight 800, or donkey anti-mouse DyLight 680, all used at a 1:10,000 dilution). Blots were scanned on an Odyssey Infrared Imaging System (LI-COR Biosciences). Band intensities were quantified using Fiji.

Antibody inhibition of Kif2a in *H. boettgeri* egg extracts

An antibody raised against an N-terminal sequence of human kif2a (Novus Biologicals) was added to *H. boettgeri* egg extracts at a final concentration of 0.7 mg/ml. Rabbit IGG was added to control reactions at a final concentration of 0.7 mg/ml. Egg extract reactions were then fixed and sedimented onto coverslips as described for immunofluorescence above.

RNA Isolation and Sequencing

To isolate RNA, *H. boettgeri* eggs and embryos at stage 14 were homogenized mechanically in TRIzol® (Thermo Fisher Scientific) using a 30-gauge needle and processed according to manufacturer instructions. After resuspension in nuclease-free H₂O, RNAs were isolated using a RNeasy kit (Qiagen Inc.) according to manufacturer instructions. Libraries were prepared using the manufacturer's non-standard specific RNA-seq library protocol with poly-A capturing mRNA enrichment method (Illumina, CA, USA). The paired-end 2 × 100 bp reads were generated by the QB3 Functional Genomics Laboratory at the University of California, Berkeley using Illumina HiSeq 2000.

***H. boettgeri* transcriptome assembly**

H. boettgeri RNAseq reads from each library were assembled using Trinity [82] with default parameters for a denovo assembly. The complete transcriptome was aligned to *X. tropicalis* v9 proteome via BLASTX [83]. For each *X. tropicalis* protein, the highest scoring (based on BLAST bit score), transcript that aligned across the full-length (90% of the CDS) was chosen as the representative homolog for *H. boettgeri*. The raw RNA-seq data and initial Trinity assemblies were deposited at NCBI under BioProject PRJNA306175 [35].

Vertebrate sequence alignments

Vertebrate sequences for katanin and kif2a were aligned using Dialign-TX [84]. *X. tropicalis* and *X. laevis* cDNA and peptide sequences were obtained from Xenbase (version 9 genomes). Human, chicken, and lizard peptides were obtained from Ensembl (version 96; [85]). *Nanorana parkeri*

sequences were obtained from Sun et al [86]. *Rana pipiens* sequences were obtained from Christenson et al. [87]. *X. borealis* cDNA sequences were kindly provided by Austin Mudd (UC Berkeley).

Cloning of *H. boettgeri* kif2a

Total RNA was isolated from *H. boettgeri* eggs as described above in “RNA isolation and sequencing,” and cDNA was synthesized from RNA using the SuperScript III First Strand Synthesis system (Thermo Fisher Scientific) according to the manufacturer’s instructions. The *H. boettgeri* kif2a sequence was then PCR-amplified from the cDNA using the following primer sequences (written 5’-3’):

FWD: ATGGCCGTC AATAGCTTTG

REV: TTAAAGAGC ACGTGGCCTTT

The amplified sequence was then subcloned into a pMal-c5x vector (New England BioLabs) using In-Fusion cloning (Takara). The construct was then amplified using XL1-Blue competent *E. coli* (Agilent).

Expression and purification of recombinant kif2a

Recombinant N-terminally MBP-tagged full length *X. laevis* and *H. boettgeri* kif2a and point mutants (all in a pMal- c5x vector from New England BioLabs, *X. laevis* construct is further described in [47]) was expressed in One Shot BL21 Star *E. coli* (Thermo Fisher Scientific) overnight with shaking at 16°C in the presence of 1 mM IPTG. Purification of *X. laevis* kif2a was originally described in [47] and purification of *H. boettgeri* kif2a and point mutants proceeded similarly. Bacteria were pelleted and lysed in Kif2a Purification Buffer containing 20 mM Hepes, 250mM NaCl, 1 mM DTT, pH7.2. To reduce viscosity of lysate and to limit proteolysis, Lysonase Bioprocessing Reagent (EMD Millipore) and Complete EDTA-free Protease Inhibitor Tablets (Roche) were added to the lysis buffer according to the manufacturer’s instructions. Bacteria were lysed using sonication, then the clarified lysate incubated with amylose resin (New England Biolabs) for 40 min with rotation at 4°C. The amylose resin was then thoroughly rinsed with Kif2a Purification Buffer and the recombinant kif2a eluted with Kif2a Purification Buffer + 10 mM maltose. The most concentrated fractions were pooled and then buffer-exchanged into Kif2a Purification Buffer using Amicon Ultra Centrifugal filters, 15 ml, 30K MWCO (EMD Millipore) according to the manufacturer’s instructions.

Time lapse microtubule depolymerization assay in frog egg extracts

Microtubules were polymerized from unlabeled + Alexa488-labeled porcine brain tubulin at a ratio of 20:1 unlabeled:labeled tubulin using taxol (Paclitaxel, Sigma) as described [88]. Flow cells were constructed with an 18 × 18 glass coverslip and double-sided Scotch tape for a volume of ~10 µl. A mutant rigor kinesin [89] in KAB (20 mM HEPES pH 7.5, 25 mM K-glutamate, 2 mM MgCl₂, 1 mg/ml BSA, 10% glycerol, 0.02% Triton X-100) with 1 mM ATP [90] was incubated in the flow cell. The cell

was washed with KAB, incubated with microtubules in KAB with ATP, and washed with BRB80 (80 mM PIPES [pH 6.8], 1 mM MgCl₂, 1 mM EGTA). Finally, 18–20 µl of crude egg extract was flowed in and immediately imaged at 15 s intervals with a 60× oil objective. Percent microtubule intensity was quantified by measuring the total integrated fluorescence intensity of each image per unit time using Fiji software.

Microtubule sedimentation assay using recombinant kif2a

5 µM Taxol-stabilized microtubules were generated as described in [88]. Microtubules were then incubated at room temp for 20 min with 200–400 nM recombinant *X. laevis* or *H. boettgeri* kif2a + 1.5 mM MgATP, or 200–400 nM Kif2a Purification Buffer (control) containing 20 mM Hepes, 250mM NaCl, 1 mM DTT, pH7.2. Total reaction volume was 25 µl. Reactions were layered onto 200 µl of a 40% sucrose/1× BRB80 cushion and sedimented at 23°C at 40,000 rpm for 20 min in a TL-100 rotor. Samples were taken of the supernatant (30 µl), the supernatant aspirated, the interface between the supernatant and the cushion washed with 100 µl dH₂O, the cushion aspirated and the pellet resuspended in 30 µl Laemmli sample buffer. Samples were then run on a 4–20% SDS-PAGE gradient gel (Biorad) and stained with Coomassie Blue.

Antibodies

Anti-TPX2: A rabbit polyclonal antibody against a 242 amino acid sequence in the N-terminus of *X. laevis* TPX2 was raised by Covance and affinity purified from total serum on a HiTrap N-hydroxysuccinimide-activated HP column (GE Healthcare) coupled with recombinant full length *X. laevis* TPX2. Antibodies were eluted with Gentle Ag/Ab Elution Buffer (Thermo Fisher Scientific) and dialyzed into 50 mM Hepes. The 242 amino acid sequence is highly conserved between *X. laevis* and *X. tropicalis* (87% identical) and *X. laevis* and *H. boettgeri* (86% identical), and was used at a 1:5,000 dilution for Western blot, and a 1:5,000 dilution for immunofluorescence.

Anti-kif2a: A rabbit polyclonal antibody raised against an N-terminal sequence of human kif2a (Novus Biologicals; 91% identical to *X. laevis* and *H. boettgeri* kif2a, 93% identical to *X. tropicalis* kif2a). Used at a 1:10,000 dilution for Western blot, and a 1:5,000 dilution for immunofluorescence.

Anti-Ran: A mouse polyclonal antibody (BD Biosciences) raised against amino acids 7–171 of human Ran. Within this region the *X. laevis*, *X. tropicalis*, and *H. boettgeri* sequences are identical. Used at a 1:2,000 dilution for Western blot.

Anti-beta-tubulin: A mouse monoclonal antibody (E7; Developmental Studies Hybridoma Bank, Iowa City, IA) raised against full length chlamydomonas tubulin. Used at a 1:500 dilution for whole-mount immunofluorescence.

Anti-histone H3: A rabbit polyclonal antibody (ab1791; Abcam) raised against amino acids 100-136 of human histone H3. Used at a 1:500 dilution for whole-mount immunofluorescence.

Anti-katanin: A rabbit polyclonal antibody raised against full length p60 subunit of *X. tropicalis* katanin [58]. Used at a 1:1000 dilution for Western blot.

2.5 Supplemental Figures

p60 katanin alignment in *Xenopus laevis*, *Xenopus tropicalis*, and *H. boettgeri*

H.boettgeri	MSLLMISENVKLAREYALLGNYDSAMVYYQGVLDQMNKYLYSVKDTFLHQKWOQVWQEI	60
X.laevis	MSLLMISENVKLAREYALLGNYDSAMVYYQGVLDQMNKYLYSVKDTFLQQKWQVWQEI	60
X.tropicalis	MSLLMISENVKLAREYALLGNYDSAMVYYQGVLDQMNKYLYSVKDTFLQQKWQVWQEI	60
	*****:*****	
H.boettgeri	VEAKHVKDIMSTLESFKLDSSPVKAAQHDFPTHGDEVWVSLPVAERRPSGPRKRQSIQC	120
X.laevis	MECKHVKDIMSTLEGFKLDSSPVKTTQHEFP SHDGEVWVSLPVPVERRPSGPRKRQSVQC	120
X.tropicalis	MEAKHVKDIMSTLEGFKLDNSPVKTTQHEFPAHDGEVWVSLPVPVERRPSGPRKRQSVQC	120
	:*.*****.***.***:.*:***:*****.*****.*	
H.boettgeri	NDIRAQNRLSAAVKGPIPHVSR-----NSNKSSGDVSETE	156
X.laevis	NDNKSHNNRFSAAAKGNLPSARNANNVKMKPVRAREKKDALIK----NKSSADVSETE	175
X.tropicalis	NDNKSHNNRFGA-GKGNLPSKNTNNVKMKPVRAREKKDTFLKVKDEKNSSVDVSETE	179
	** :.:***:.* *** ::	**** *****
H.boettgeri	VKKFDGTGYDKDLVEALERDIISQNPNIWDDIADLEEAKKLLKEAVVLPWMPEFFKGI	216
X.laevis	VKRFDGSGYDKDLIEALERDIISQNPNIWDDIADLEEAKKLLKEAVVLPWMPEFFKGI	235
X.tropicalis	VKKFDGTGYDKDLIEALERDIISQNPNIWDDIADLEEAKKLLKEAVVLPWMPEFFKGI	239
	** :.***:*****:*****:*****:*****:*****:*****	
H.boettgeri	RRPWKGLVMVGGPGTGKTLAKAVATECKTTFNFVSSSTLTSKYRGESEKLVRLLFEMAR	276
X.laevis	RRPWKGLVMVGGPGTGKTLAKAVATECKTTFNFISSTLTSKYRGESEKLVRLLFEMAR	295
X.tropicalis	RRPWKGLVMVGGPGTGKTLAKAVATECKTTFNFISSTLTSKYRGESEKLVRLLFEMAR	299
	*****:*****:*****:*****:*****:*****:*****:*****	
H.boettgeri	YYAPTTIFIDEIDSICSRRTSEEHEASRRVKAELLVQMDGVGGASENDDPSKMVMVLAA	336
X.laevis	FYAPTTIFIDEIDSICSRRTSEEHEASRRVKAELLVQMDGVGGASENDDPSKMVMVLAA	355
X.tropicalis	FYAPTTIFIDEIDSICSRRTSEEHEASRRVKAELLVQMDGVGGASENDDPSKMVMVLAA	359
	:*****:*****:*****:*****:*****:*****:*****:*****	
H.boettgeri	TNFPWDIDEALRRRLEKRIYIPLPSAKGREELLRISLKELELADDVNIETIAENMDGYSG	396
X.laevis	TNFPWDIDEALRRRLEKRIYIPLPSAKGREELLRINLKELELADDVNIETIAENMDGYSG	415
X.tropicalis	TNFPWDIDEALRRRLEKRIYIPLPSAKGREELLRINLKELELADDVNIETIAENMDGYSG	419
	*****:*****.*****.*****.*****	
H.boettgeri	ADITNVCRDASLMAMRRRIEGLTPEIRNLSRDDMHMPTTMEDFEMALKKVKSVSALDI	456
X.laevis	ADITNVCRDASLMAMRRRIEGLTPEIRNLSRDDMHMPTTMEDFEMALKKVKSVSASDI	475
X.tropicalis	ADITNVCRDASLMAMRRRIEGLTPEIRNLSRDDMHMPTTMEDFEMALKKVKSVSASDI	479
	*****:*****:*****:***** *	
H.boettgeri	EKYEKWIEEFGSC	469
X.laevis	EKYEKWIEEFGSC	488
X.tropicalis	EKYEKWIEEFGSC	492

Kif2a alignment in *Xenopus laevis*, *Xenopus tropicalis*, and *H. boettgeri*

<i>X. laevis</i>	-MAGSFGKIHIIGVYVES--SFGRIHQAMVTSLNEDSESI TVEWIENGDTKGKEIDLESIF	57
<i>X. tropicalis</i>	-MAGSFGKIHIIGIYVEIKRSDGRIHQAMVTSLNEDSESI TVEWIENGDTKGKEIDLESIF	59
<i>H. boettgeri</i>	MAVNSFGKIQIGIYVEIKRSDGRIHQAMVTSLNEDSESI TVEWIENGDTKGKEIDLESIF . . *****: ** : *** * *****	60
<i>X. laevis</i>	SLNHDLAPDEEIDPGPEMPPPPAPTTKVNKIVKNRRTVAPVKNETPAKDNRVAAVGSARA	117
<i>X. tropicalis</i>	SLNPDLAPDEEIDPGPEMPPPPPTTKVNKIVKNRRTVAPVKNETPARDNRVAAVSSARA	119
<i>H. boettgeri</i>	SLNPDLAPDEEIDPGPEMPPPTPTSKVNKIVKNRRTVAPPKNETPARDNRVAAVNSART *** *****: ** : ***** *****: ***** . *** :	120
<i>X. laevis</i>	RPIQPIEQSASRQNGSVSDISPDPQGGKDFGLASRRKSNVCVKEVEKLEKREKRRRLQQQ	177
<i>X. tropicalis</i>	RPSQPIEQSASRQNGSVSDISPDPQGGKDFGPPSRRKSNVCVKEVEKLEKREKRRRLQQQ	179
<i>H. boettgeri</i>	RPSQPPEPPASAPQNGSVSDISPDPQGGKDFGPPSRRKSNVCVKEVEKLEKREKRRRLQQQ ** * * * * ***** *****: *****	180
<i>X. laevis</i>	ELREKKAQDFDATNPNYEIMCMIKDFRGLDYLPLTTSDPIDEHRCVVCVRRKPLNKKET	237
<i>X. tropicalis</i>	ELREKKAQDVDA TNPNYEIMCMIKDFRGLDYLPLTTADTIDEHRCVVCVRRKPLNKKEN	239
<i>H. boettgeri</i>	ELREKRALDVDA TNPNYEIMCMIKDFRGNLDYLPLTTADPIDEHRCVVCVRRKPLNKKET *****: * * . ***** *****: ***** * *****	240
<i>X. laevis</i>	TIKDLDVITIPKDVVMVHEPKQKVDL TRFLENQTFRFDYAFDE TAPNETVYRFTARPLV	297
<i>X. tropicalis</i>	TVKDLDVITIPSKDVVMVHEPKQKVDL TRFLENQTFRFDYAFDE TAPNEMVYRFTARPLV	299
<i>H. boettgeri</i>	TIKDLDVITIPSKDVVMVHEPKQKVDL TRFLENQTFRFDYAFDE TAPNEMVYRFTARPLV * : ***** ***** *****	300
<i>X. laevis</i>	ETIFERGMATCFAYGQTGSGKTHTMGGDFSGKNQDCSKGIYALAARDV FQMLKKPNYKKL	357
<i>X. tropicalis</i>	ETIFERGMATCFAYGQTGSGKTHTMGGDFSGKNQDCSKGIYALAARDV FQMLKKPNYKKL	359
<i>H. boettgeri</i>	ETIFERGMATCFAYGQTGSGKTHTMGGDFSGKNQDCSKGIYALAARDV FQMLKKPNYKKL *****	360
<i>X. laevis</i>	ELQVYATFFEIYSGKVFDDLNRKTKLRVLEDGKQQVQV VGLQEREVKCEDV LKLIIEIGN	417
<i>X. tropicalis</i>	ELQVYATFFEIYSGKVFDDLNRKTKLRVLEDGKQQVQV VGLQEREVKCEDV LKLIIEIGN	419
<i>H. boettgeri</i>	ELQVYATFFEIYSGKVFDDLNRKTKLRVLEDGKQQVQV VGLQEREVKCEDV LKLIIEIGN *****	420
<i>X. laevis</i>	SCRTSGQTSANAHSSRSRAV FQIILRRKKGKMHGKFSLIDLAGNERGADTSSADRQTRLEG	477
<i>X. tropicalis</i>	SCRTSGQTSANAHSSRSRAV FQIILRRKKGKMHGKFSLIDLAGNERGADTSSADRQTRLEG	479
<i>H. boettgeri</i>	SCRTSGQTSANAHSSRSRAV FQIILRRKKGKMHGKFSLIDLAGNERGADTSSADRQTRLEG *****: *** : *****	480
<i>X. laevis</i>	AEINKSLALKECIRALGRNKPHTPFRASKLTQVLRDSFIGENSRTCMIATISPGMASCE	537
<i>X. tropicalis</i>	AEINKSLALKECIRALGRNKPHTPFRASKLTQVLRDSFIGENSRTCMIATISPGMASCE	539
<i>H. boettgeri</i>	AEINKSLALKECIRALGRNKPHTPFRASKLTQVLRDSFIGENSRTCMIATISPGMASCE *****	540
<i>X. laevis</i>	NTLNTRLRYANRVKELDPSRCRRPPHDTSCP----QTSW-----	572
<i>X. tropicalis</i>	NTLNTRLRYANRVKEFGISPSDIPFSQGSRSRDLSPSYEYDDFSPTL TRVKELTVDP SAA	599
<i>H. boettgeri</i>	NTLNTRLRYANRVKELTVDP-----SG *****: .	561
<i>X. laevis</i>	-----MTWKQCGEW--GVAPQRDDLKLLCEQNEEEVSPQLFTTFHEAVSQMVEM	618
<i>X. tropicalis</i>	GDLRPMIHHAPNQLDDVEALWVGSSPQRDDLKLLCEQNEEEVSPQLFTTFHEAVSQMVEM	659
<i>H. boettgeri</i>	GDLRPMIHHAPNQLDDLEELWVGSSPQRDDLKFLCKQNEEEVSPQLFTTFQEA V SQMLEM . * * : *****: ** : ***** *****: *****: **	621
<i>X. laevis</i>	EEQVVEDHRAVFPGTSIRWLEGLKCKLLEMTTEVDYDADSYATQLEAILEKKIDILTEL R	678
<i>X. tropicalis</i>	EEQVVEDHRAV FQE-SIRWLEDE-KV LLEMTTEVDYDADSYATQLEAILEQKIDILTEL R	717
<i>H. boettgeri</i>	EEQLVEDHRAV FQE-SITWHEDE-KALLMMTEVDYDADSYATQLEAMLDQKIYILTEL R ***: ***** ** * . * * ***** *****: ** : * *****	679
<i>X. laevis</i>	DKVKSFRALQEEEHASKQINPKRPRAL	706
<i>X. tropicalis</i>	DKVKSFRALQEEEQASKQINPKRPRAL	745
<i>H. boettgeri</i>	DKVKSFRALQEEEQASKQINPKRPRAL *****	707

Chapter 3

Xenopus Hybrids Provide Insight Into Cell and Organism Size Control

The following chapter contains material from a publication on which I am a co-first author [91]. This article is distributed under the terms of the Creative Commons Attribution License (CC BY 4.0), which permits unrestricted use and redistribution provided that the original author and source are credited.

3.1 Introduction

Cell size correlates strongly and linearly with genome size in a myriad of different organisms [2,33,92] and increases in genome copy number through polyploidy have been shown to increase cell size within tissues or cell types [93,94]. However, the molecular link between genome size and cell size remains an open question. Although increases in ploidy may globally affect gene expression, work in unicellular organisms such as yeast suggests that the maintenance of scaling between genome size and cell size does not simply reflect gene dosage [27,49,95]. Furthermore, the correlation between genome size and cell size is independent of the proportion of the genome that codes for genes [2,21,96]. A number of factors involved in many different processes, such as growth, metabolism and protein synthesis, development, differentiation, and cell cycle regulation can influence cell size in a variety of organisms [26,27]. Many of these genes are conserved and contribute to tissue and organ size in a variety of multicellular organisms, however, how they influence organism size, and how organism size feeds back to organ/tissue/cell size to attain homeostasis remains unclear.

Interestingly, in the related frog species *Xenopus laevis* and *Xenopus tropicalis*, the size of the genome, cells, and component subcellular structures scale with body size [48,55]. Furthermore, the larger allotetraploid *Xenopus laevis* (6.2×10^9 base pairs, $N = 36$ chromosomes, average body length 10 cm) and smaller diploid *Xenopus tropicalis* (3.4×10^9 base pairs, $N = 20$ chromosomes, 4 cm in length) can hybridize. While fertilization of an *X. tropicalis* egg with a *X. laevis* sperm produces an inviable hybrid embryo that dies as a late blastula, fertilization of an *X. laevis* egg with a *X. tropicalis* sperm ($I_e \times t_s$) produces a viable adult frog intermediate in genome size ($N = 28$ chromosomes) and body length between the two species [97]. This viable hybrid thus provides a unique *in*

vivo vertebrate model for investigating biological size control at the organismal, cellular, and subcellular levels.

In this study, we characterized size scaling in viable $I_e \times t_s$ hybrids and used this system to establish a novel screening method for candidate genes involved in size control to identify factors that affect the body size of the frog, as well as the scaling of its component cells and subcellular structures.

3.2 Results

Reduced size in viable $I_e \times t_s$ hybrids

Whereas cross-fertilization of *X. tropicalis* eggs with *X. laevis* sperm produces hybrid embryos that die during zygotic genome activation (ZGA), the reverse cross of *X. laevis* eggs and *X. tropicalis* sperm ($I_e \times t_s$) results in viable hybrid embryos that possess genetic features of both *X. laevis* and *X. tropicalis* parents [81,97–100]. Hybrid embryos progressed through tadpole, froglet, and adult stages (Fig 3.1A, B), although with significant morbidity. Early development in the $I_e \times t_s$ hybrid proceeded normally according to Nieuwkoop and Faber staging [101] until the end of neurulation, and at a similar rate compared to wild type *X. laevis* embryos (Fig 3.1C). However, by the tailbud stage, body length was significantly decreased in $I_e \times t_s$ hybrids (Fig 3.1D). Relative shortening of body length continued, although development remained similar to *X. laevis*, and both hybrid and control animals initiated metamorphosis with the same timing (Fig 3.1E). As soon as metamorphosis was complete, size scaling stopped and the body length of both the $I_e \times t_s$ hybrid and *X. laevis* froglets increased at the same rate, retaining the difference in size (Fig 3.1F). Strikingly, in adult hybrid frogs, both cell and nuclear size of erythrocytes was reduced (Fig 3.1G). Since the hybrid genome (28 chromosomes) is smaller than the *X. laevis* genome (36 chromosomes), these observations are consistent with genome size-dependent scaling at the organism, cellular and subcellular levels.

Figure 3.1

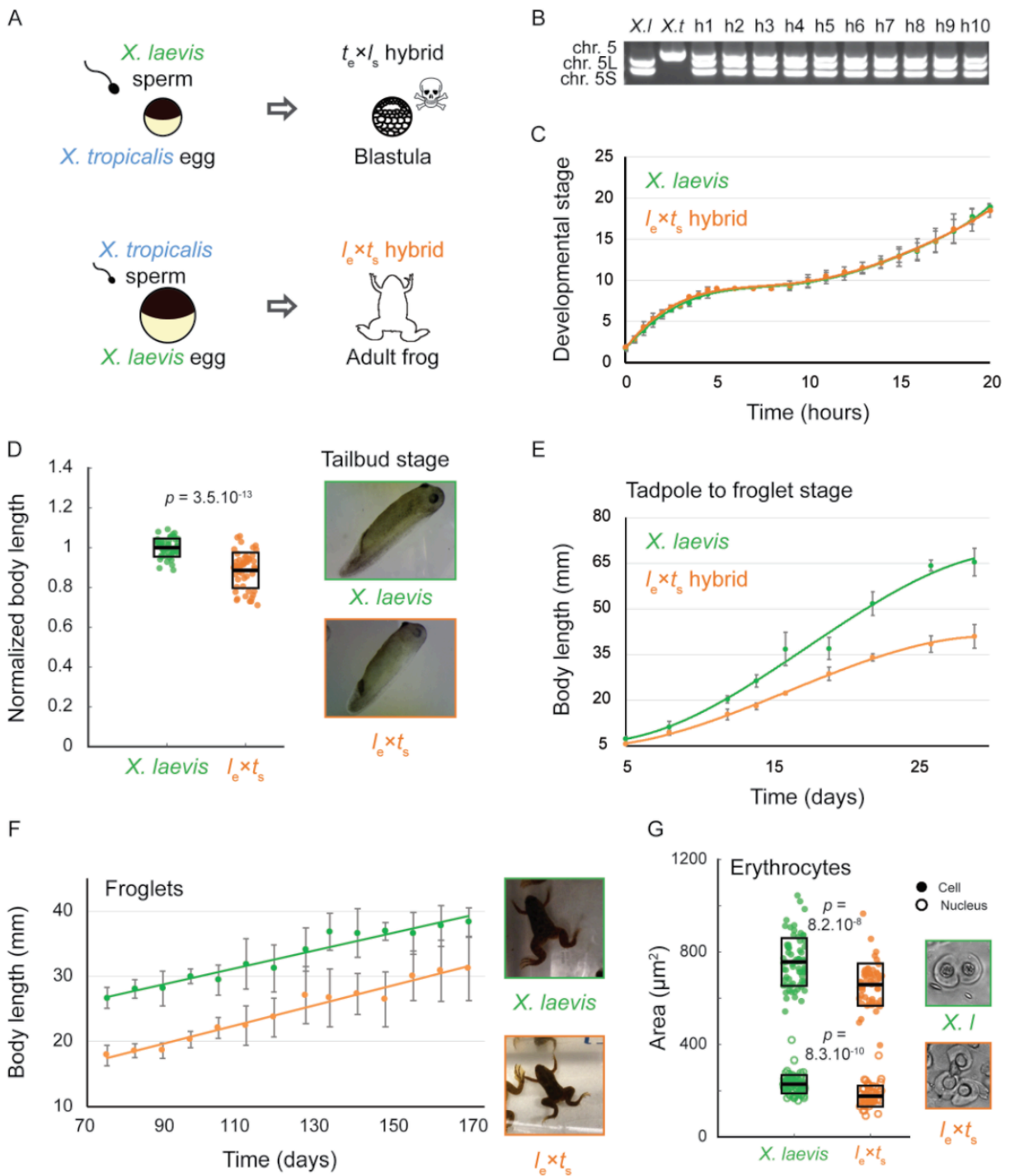


Figure 3.1: Growth and development of *Xenopus* $I_e \times t_s$ viable hybrids.

A. Schematic of developmental outcomes of *Xenopus laevis* and *Xenopus tropicalis* cross-fertilization. **B.** Agarose gel electrophoresis showing PCR amplification of 2 genomic loci in *X. laevis* (*X. l.*, on chromosomes 5L and 5S) and one locus in *X. tropicalis* (*X. t.*, chromosome 5). H1-10 indicates 10 randomly chosen hybrid tadpoles tested, confirming the consistent presence of all 3 subgenomes in hybrids. **C.** Developmental timing in *X. laevis* and $I_e \times t_s$ hybrid embryos. Average is plotted for each time point. Error bars show standard deviation. **D.** Body length of tailbud stage *X. laevis* and $I_e \times t_s$ hybrids. Box plots show all individual body lengths. Thick line inside box = average length, upper and lower box boundaries = +/- standard deviation (SD). P-value was determined by two-tailed heteroscedastic t-test. Representative images of tailbuds at identical scale are shown on the right. **E.** Body length of tadpoles throughout metamorphosis for *X. laevis* and $I_e \times t_s$ hybrids. Average is plotted for each time point. Error bars show standard deviation. **F.** Body length of *X. laevis* and $I_e \times t_s$ hybrid froglets. Average is plotted for each time point. Error bars show standard deviation. Representative images of froglets at identical scale are shown on the right. **G.** Size of erythrocyte cells and nuclei in *X. laevis* and $I_e \times t_s$ hybrid adult frogs. Box plots show all individual cell or nuclear areas. Thick line inside box = average area, upper and lower box boundaries = +/- SD. P-values were determined by two-tailed heteroscedastic t-test. Representative images of erythrocytes at identical scale are shown on the right.

Nuclear to cell size scaling in $I_e \times t_s$ hybrids is more similar to that of *X. laevis* haploids, despite a larger genome size

We wondered whether the scaling observed in hybrid embryos was due to the decrease in genome size, or if the paternal *X. tropicalis* genome also influenced size scaling. To examine the effect of altering genome size alone, we utilized haploid *X. laevis* embryos produced by fertilizing wild type *X. laevis* eggs with irradiated *X. laevis* sperm. While the sperm DNA is inactivated and does not contribute to the genome of the offspring, the sperm centrosome induces embryonic development yielding haploid embryos containing only the N=18 maternal genome [102]. Haploid embryos developed normally to the tailbud stage, and at a similar developmental rate to wild type *X. laevis* embryos (Fig 3.2B). However, by the tailbud stage, body length was significantly reduced in *X. laevis* haploids (Fig 3.2C). Haploid embryos never reach metamorphosis and stop developing as stunted tadpoles [10].

We then evaluated nuclear to cell size scaling relationships before and after ZGA, comparing *X. laevis*, $I_e \times t_s$ hybrids and haploid *X. laevis* embryos (Fig 3.2D-G). Interestingly, no difference in the nuclear to cell size ratio was observed at early stages (6 and 8) among the 3 embryo types (Fig 3.2E). However, we found that, from stage 10, haploid embryos possessed reduced nuclear sizes at similar cell sizes compared to *X. laevis* (Fig 3.2F). Consistent with their intermediate genome size (36 > 28 > 18 chromosomes), the scaling curve of hybrids fell between that of *X. laevis*

and haploids. Strikingly however, by stage 21, nuclear to cell size scaling in hybrids was more similar to that of haploids than to wild type *X. laevis* (Fig 3.2G). Therefore, we hypothesized that upon ZGA, gene expression of the *X. tropicalis* paternal genome, rather than bulk genome size alone, contributes to the reduced size of $I_e \times t_s$ hybrids.

Figure 3.2

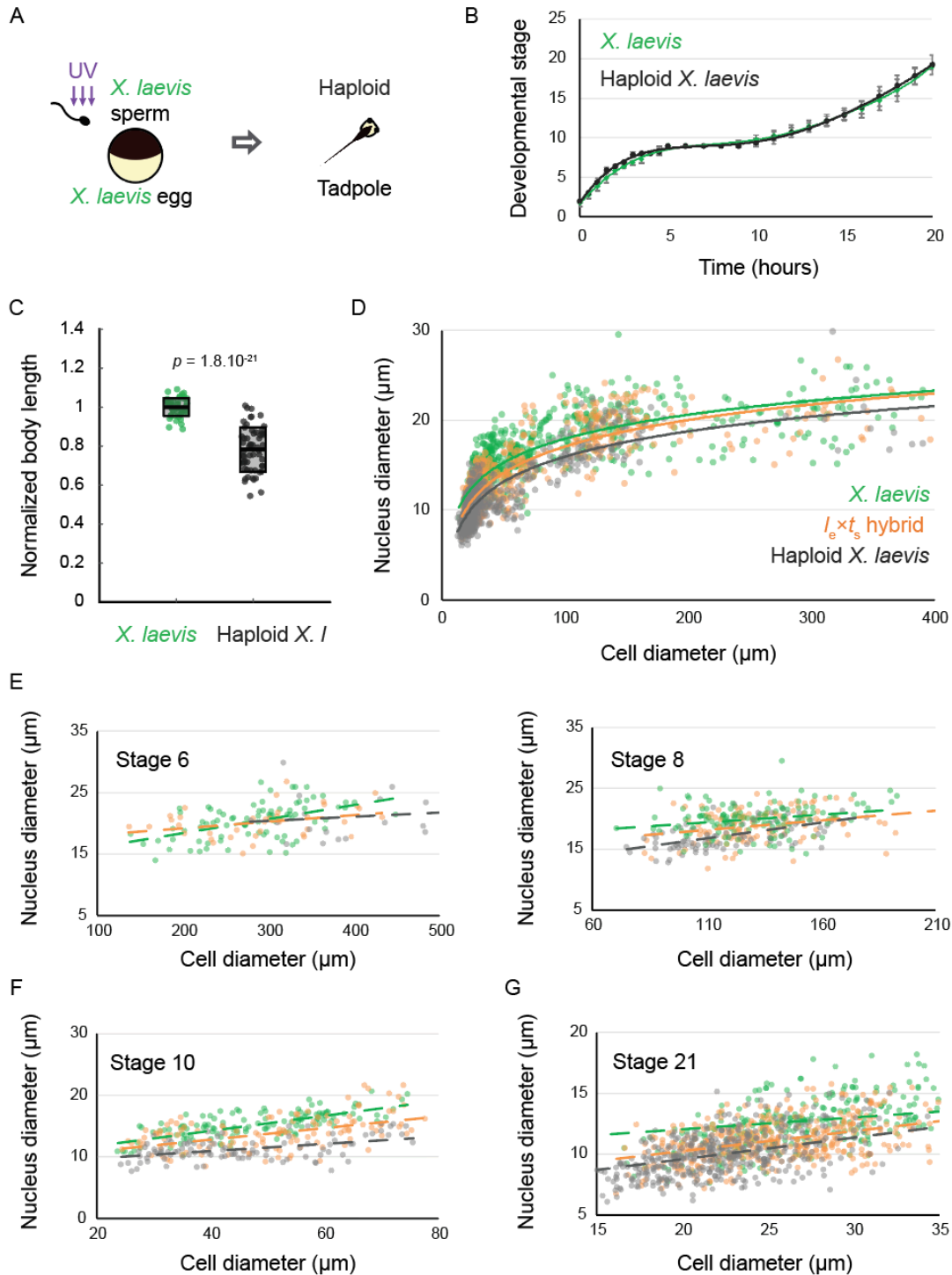


Figure 3.2: Nuclear to cell size relationships pre- and post-zygotic genome activation in $I_e \times t_s$ hybrids compared to *X. laevis* diploids and haploids. A Schematic of generation of haploid *X. laevis* tadpoles via UV irradiation of sperm. **B.** Developmental timing in *X. laevis* and haploid *X. laevis* embryos. Average is plotted for each time point. Error bars show standard deviation. **C.** Body length of tailbud stage *X. laevis* and haploid *X. laevis*. Box plots show all individual body lengths. Thick line inside box = average length, upper and lower box boundaries = +/- SD. P-value was determined by two-tailed heteroscedastic t-test. **D.** Nuclear diameter versus cell diameter in *X. laevis*, *X. laevis* haploid, and $I_e \times t_s$ hybrid embryos. **E.** Nuclear diameter versus cell diameter in *X. laevis*, *X. laevis* haploid, and $I_e \times t_s$ hybrid embryos at developmental stages 6 and 8. **F.** Nuclear diameter versus cell diameter in *X. laevis*, *X. laevis* haploid, and $I_e \times t_s$ hybrid embryos at developmental stage 10. **G.** Nuclear diameter versus cell diameter in *X. laevis*, *X. laevis* haploid, and $I_e \times t_s$ hybrid embryos at developmental stage 21.

Transcriptome analysis identifies 12 *X. tropicalis* transcription factors expressed in hybrids

To identify paternal *X. tropicalis* genes that could contribute to size control in hybrid embryos at ZGA, we performed RNA sequencing and transcriptome analysis of embryos at stage 9. We detected many tropicalis-derived paternally expressed genes in hybrid embryos. Differential expression analysis revealed one maternally expressed *X. laevis* gene that was significantly less abundant in the $I_e \times t_s$ hybrid (Fig 3.3A, Supplemental Fig 3.5), and 41 paternally expressed *X. tropicalis* genes that were significantly more abundant in $I_e \times t_s$ hybrid, compared to *X. laevis* embryos (Fig 3.3B, Supplemental Fig 3.5). Gene ontology (GO) term analysis of differentially expressed paternal genes revealed significant overrepresentation of the molecular function 'DNA binding' (GO:0003677; 4.38 fold enrichment, with a 2.90e-3 false discovery rate), and of the biological process 'transcription, DNA-templated' (GO:0006351; 4.65 fold enrichment, with a 3.93e-04 false discovery rate). Therefore, we concluded that transcriptional regulators with DNA binding functions are significantly enriched in paternally expressed genes in hybrid embryos. To finalize our list of candidates, we used Xenbase [103,104] to validate the transcription factor function of the candidate genes. From this, we set out to screen the following 12 transcription factors, Ers10, Hes7, Mix1, Ventx2, Foxi4, Sox3, Tgif2, Klf17, Sia2, Id3, Not and Oct25, as potential paternal scaling factors.

Figure 3.3

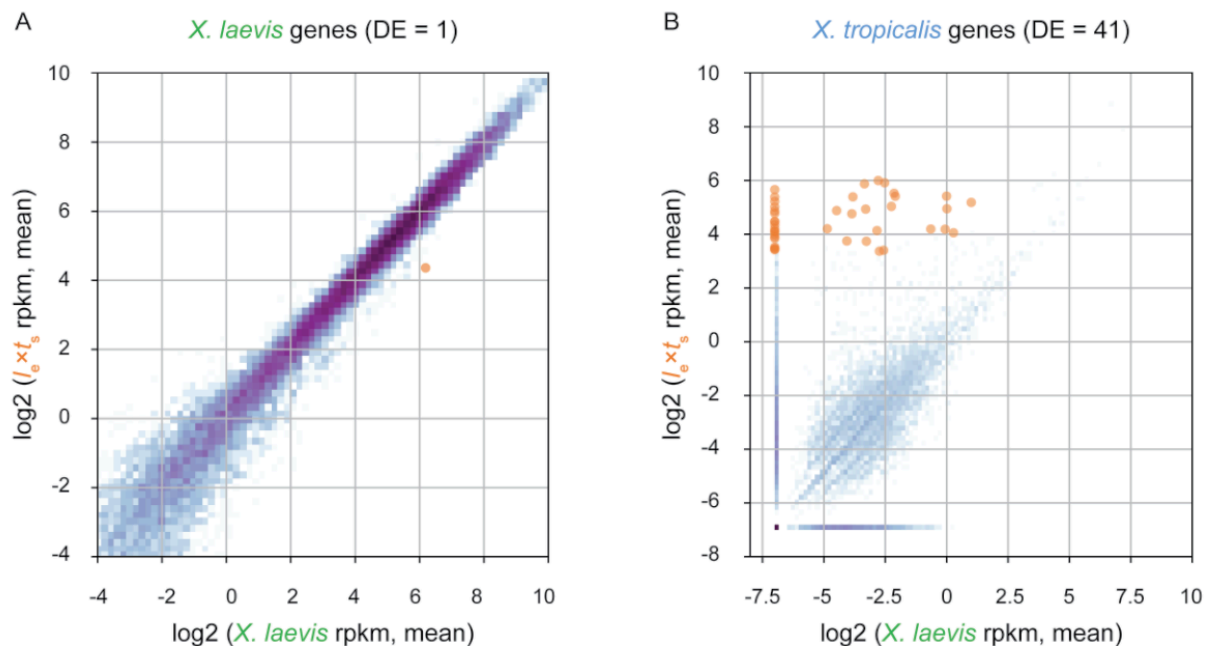


Figure 3.3: Transcriptome analysis of *I_e × t_s* hybrid embryos at the onset of zygotic genome activation. **A.** Differential expression analysis of *X. laevis* maternal genes in stage 9 *I_e × t_s* hybrid vs. *X. laevis* embryos. **B.** Differential expression analysis of *X. tropicalis* paternal genes in stage 9 *I_e × t_s* hybrid vs. *X. laevis* embryos. For both figures, RNA-seq reads are mapped to a database of combined *X. laevis* and *X. tropicalis* transcriptomes and significantly differentially expressed genes (DE; fold-change > 2 and false discovery rate < 0.05) are marked in orange (see Methods for more information).

***X. tropicalis* transcription factors Hes7 and Ventx2 reduce body length in tailbud stage *X. laevis* embryos**

To test whether identified candidate transcription factors were responsible for reducing the size of hybrid embryos, we mimicked overexpression of each transcription factor (as in the *I_e × t_s* hybrid) by microinjecting mRNA encoding each *X. tropicalis* candidate gene into fertilized one-cell *X. laevis* embryos. Cell and nuclear size were assessed in embryos fixed for immunofluorescence around the time of ZGA (10 hours post-fertilization, ~ stage 10) and several hours post ZGA (24 hours post-fertilization, ~ stage 21). Head to tail body length was measured at late tailbud stage, 48 hours post-fertilization (Fig 3.4A). Two candidate transcription factors, Hes7 and Ventx2, significantly reduced overall body length (Fig 3.4B, C). Interestingly, the body length of embryos injected with

Hes7 or Ventx2 was not significantly different from the body length in the $l_e \times t_s$ hybrid ($p = 0.64$ and $p = 0.48$, respectively; two-tailed heteroscedastic

Figure 3.4

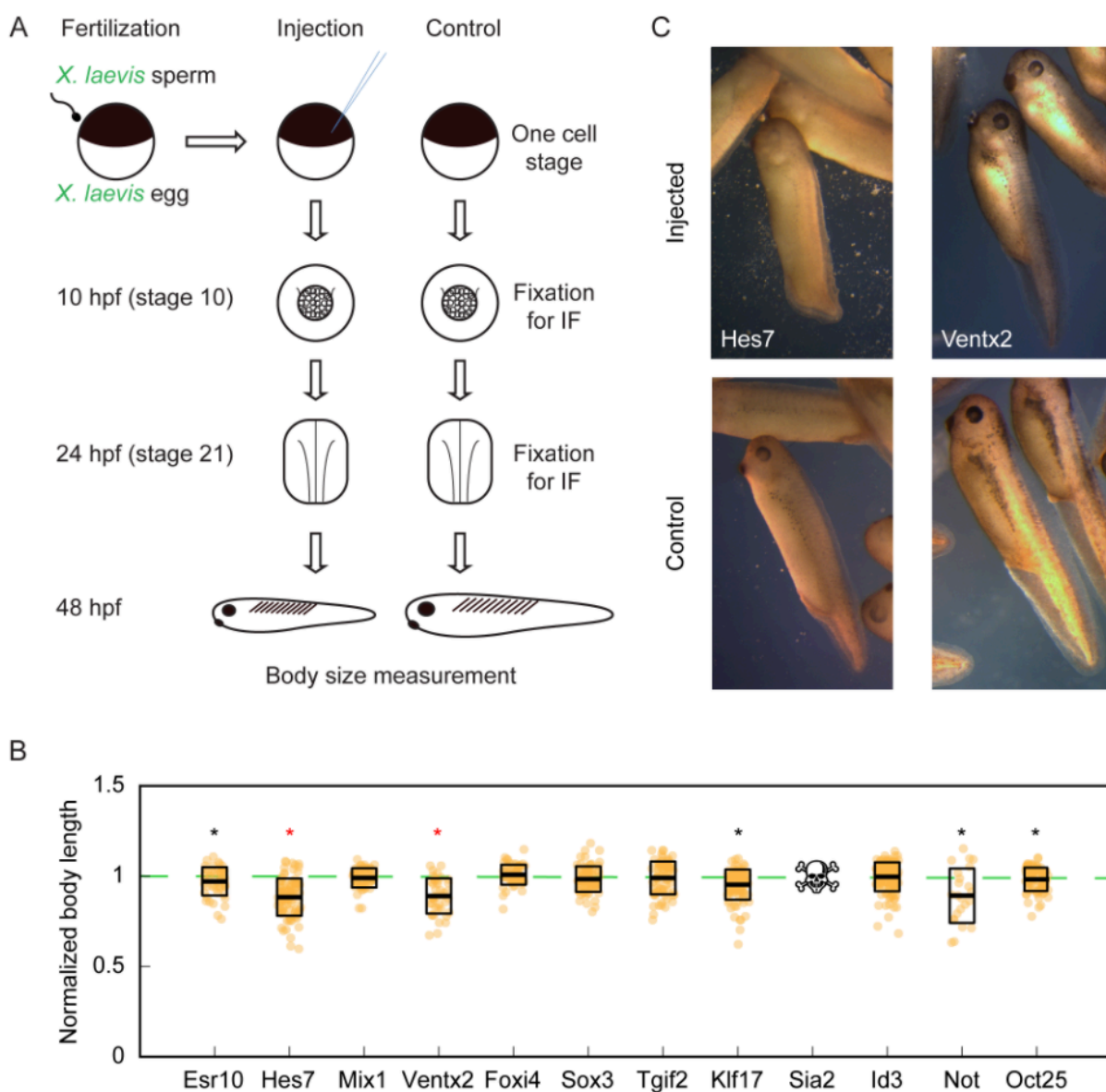
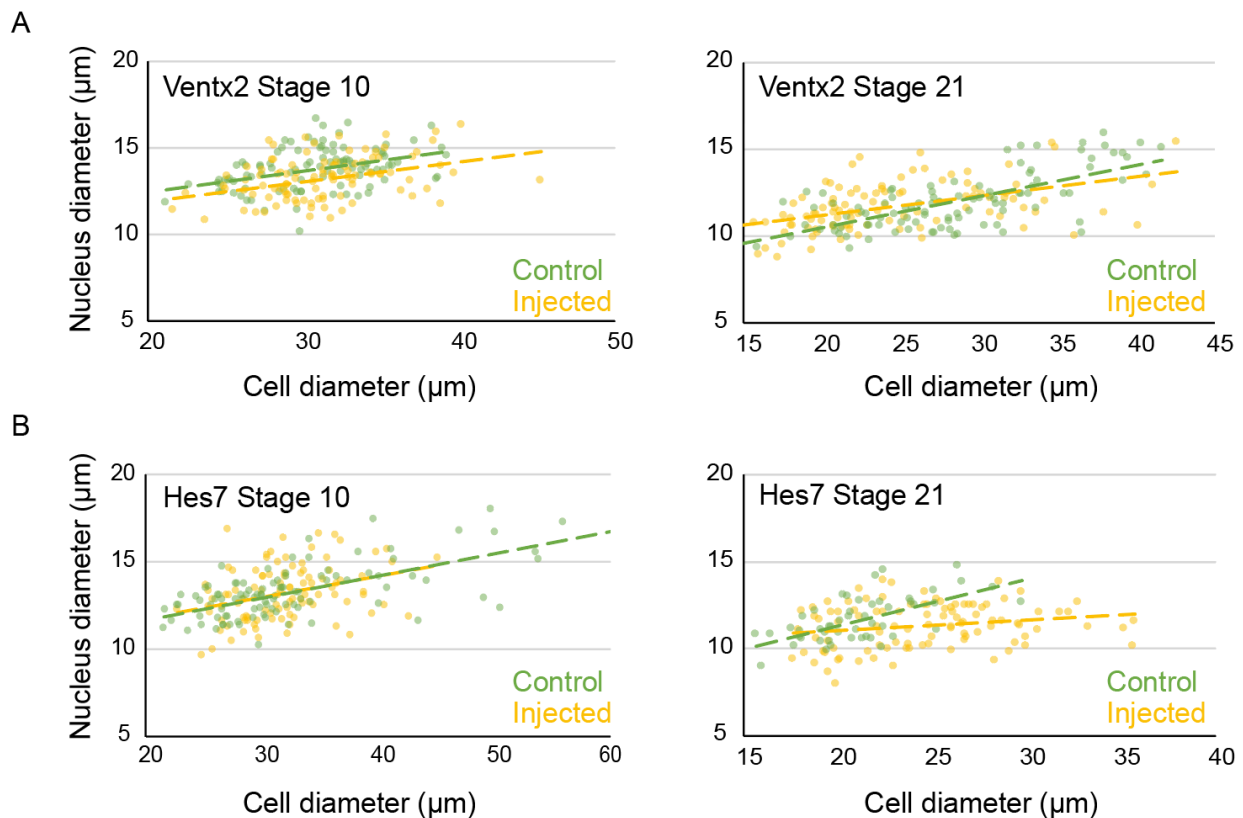


Figure 3.4: Organismal size in *X. laevis* embryos upon overexpression of candidate *X. tropicalis* transcription factors. **A.** Workflow of candidate scaling factor screen. **B.** Body length of tailbud stage injected *X. laevis* embryos. Thick line inside box = average length, upper and lower box boundaries = \pm SD. Stars indicated overall (results of 3 experiments pooled) significance of $p < 0.05$ (two-tailed heteroscedastic t-test). Red coloring indicates significance of each 3 individual technical replicates with $p < 0.05$ (two-

tailed heteroscedastic t-test). Reduced number of measured embryos in Not is due to the fact that, overall, 67.5% of injected-embryos exogastrulated, indicating a developmental defect. **C.** Representative images of injected *X. laevis* embryos 48 hours post-fertilization. Hes7- (left) and Ventx2-injected (right) are shown (top) with corresponding controls (bottom). Images are at identical scale.

t-test). The reduction in body length was however not accompanied by a change in nuclear to cell size scaling relationships as observed in the $l_e \times t_s$ hybrid (Fig 3.5A,B). To test whether co-expression of both genes had an additive or synergistic effect, Hes7 and Ventx2 were co-injected. This caused embryo death (27.39 ± 9.25 % lethality on average) with viable embryos more similar in size distribution to Ventx2 than to Hes7-injected embryos (Fig 3.5C; $p = 0.18$ and $p = 0.04$, respectively, two-tailed heteroscedastic t-test). We also observed significant embryo death in Sia2-injected embryos (to 100% by 48 hours post-fertilization), preventing measurement at tailbud stage, but nuclear to cell size scaling at stage 10 or 21 was not altered as in hybrid embryos (Fig 3.5D). Altogether, while the screen did not reveal factors that significantly affected cell and nuclear size, overexpression of either *X. tropicalis* Hes7 and Ventx2 resulted in a decrease in embryo size that could potentially contribute to organism size scaling in $l_e \times t_s$ hybrids.

Figure 3.5



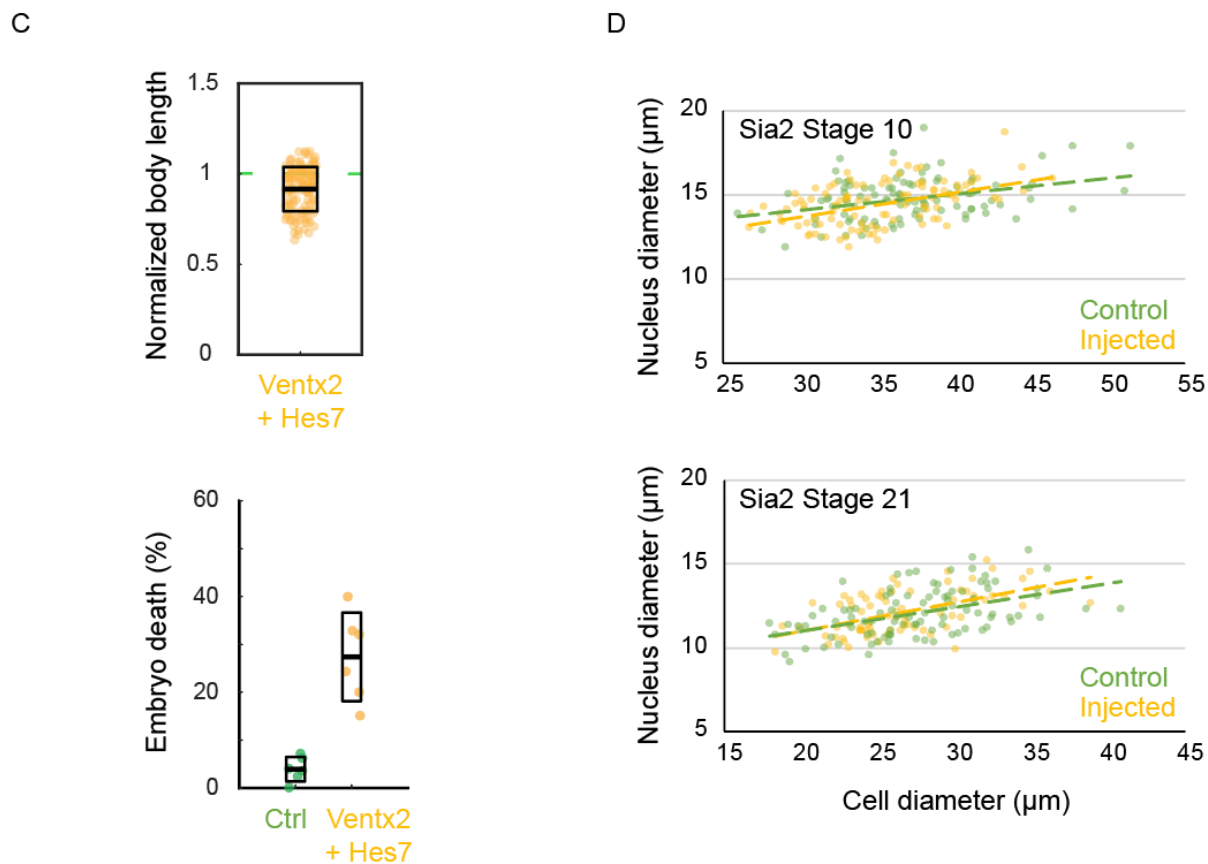


Figure 3.5: Nuclear to cell size relationships post-zygotic genome activation in injected *X. laevis* embryos. **A.** Nuclear diameter versus cell diameter in Ventx2-injected *X. laevis* embryos at stage 10 and 21. **B.** Nuclear diameter versus cell diameter in Hes7-injected *X. laevis* embryos at stage 10 and 21. **C.** Normalized body length of tailbud stage *X. laevis* embryos co-injected with Ventx2 and Hes7 (top). Percent fatality in Ventx2 and Hes7 co-injected embryos (bottom). Embryos were injected with 375 pg mRNA of each factor for a total injection of 750 pg. Thick line inside box = average length, upper and lower box boundaries = \pm SD. **D.** Nuclear diameter versus cell diameter in Sia2 injected *X. laevis* embryos at stages 10 and 21.

3.3 Discussion

Little is known about how organisms scale in size and how size scaling is coordinated at the organismal, cellular, and subcellular levels. Uniquely, between the frogs *X. laevis* and *X. tropicalis*, linear size scaling is observed at the level of the genome, subcellular structures, cell, and organism. The specific factors that influence this phenomenon are unknown.

Generating viable $l_e \times t_s$ hybrids intermediate in genome size, cell size, and body size between *X. laevis* and *X. tropicalis* allowed us to examine whether size scaling in *Xenopus* results from differences in genome size alone, or whether gene expression plays a role. While genome size clearly

correlates with cell and organism size in $l_e \times t_s$ hybrids, other factors likely influence these parameters. Even though the genome size of the $l_e \times t_s$ hybrid is closer to that of a wild type *X. laevis* embryo, the nuclear to cell size scaling curve tracked more closely with that of haploid *X. laevis* embryos. Moreover, changes in nuclear to cell size ratios in $l_e \times t_s$ hybrids began at zygotic genome activation, rather than in the early cleaving embryo, which lacks transcription and growth phases. It is therefore likely that size scaling in hybrids is at least in part a consequence of *X. tropicalis* paternal gene expression rather than from reduced genome size alone.

Two transcription factors from our screen, Ventx2 and Hes7, caused a significant decrease in body length, but did not cause a change in nuclear to cell size scaling as observed in the hybrid. One possible explanation for this result is that both factors are transcriptional repressors known to regulate developmental processes that influence tissue growth, but may not affect cell or subcellular size. For example, Ventx transcription factors have been observed to maintain pluripotency and inhibit cell differentiation during *Xenopus* embryogenesis [105]. Hes7 is essential for regulating somite segmentation in *Xenopus* and mice, and mutation of Hes7 is implicated in miniaturization of dogs [106]. It is also involved in human diseases such as spondylocostal dysostosis, which causes abnormal fusion of the bones of the ribs and spine, leading to a type of dwarfism characterized by a short trunk with normal-length arms and legs [107].

What then precisely regulates cell and subcellular scaling in $l_e \times t_s$ hybrids, and how can gene expression influence these parameters? We propose a model whereby cell size in *Xenopus* is largely dictated by genome size, but can be “fine-tuned” by differential gene expression. Such differential gene expression can also influence organism size, which may be uncoupled from cell size. Our study illustrates an example of both a unique model system and a screening approach to study biological size control and scaling. Future experiments will take advantage of the improving *Xenopus* genome assemblies to identify and screen other candidate genes, particularly those involved in other biological processes such as growth factor signaling and cell proliferation.

3.4 Methods

Generation of viable *Xenopus* $l_e \times t_s$ hybrid embryos

X. laevis females were primed with 100 IU of pregnant mare serum gonadotropin (PMSG, National Hormone and Peptide Program, Torrance, CA) at least 48 h before use and boosted with 500 IU of HCG (Human Chorionic Gonadotropin CG10, Sigma) 14-16 hours before experiments. *X. tropicalis* males were primed with 250 IU of HGC 24 hours before dissection. To obtain testes, *X. tropicalis* males were euthanized by anesthesia through immersion in double-distilled (dd)H₂O containing 0.15% MS222 (tricaine) neutralized with 5 mM sodium bicarbonate before

dissection. Testes were collected in Leibovitz L-15 media (Gibco – Thermo Fisher Scientific, Waltham, MA) supplemented with 10% Fetal Bovine Serum (FBS; Gibco), and stored at room temperature until fertilization. To prepare the sperm solution, one testis was added to 1 mL of ddH₂O in a 1.5 mL microcentrifuge tube, and homogenized using scissors and a pestle. *X. laevis* females were squeezed gently to deposit eggs onto petri dishes coated with 1.5% agarose in 1/10X MMR. Any liquid in the petri dishes was removed and the eggs were fertilized with 1 mL of sperm solution per dish. Fertilized embryos were swirled in the solution to form a monolayer on the bottom of the petri dish and incubated for 10 min with the dish slanted to ensure submersion of eggs. Dishes were then flooded with 1/10X MMR, swirled and incubated for 10 min. To remove egg jelly coats, the 1/10X MMR was completely exchanged for freshly prepared Dejelling Solution (2% L-cysteine in ddH₂O-NaOH, pH 7.8). After dejelling, eggs were washed extensively (>4X) with 1/10X MMR before incubation at 23°C. At Nieuwkoop and Faber stage 2-3, fertilized embryos were sorted and placed in fresh 1/10X MMR in new petri dishes coated with 1.5% agarose in 1/10X MMR.

Confirmation of presence of both *X. laevis* and *X. tropicalis* genomes in $I_e \times t_s$ hybrids

Genomic DNA was extracted from $I_e \times t_s$ hybrid embryos by incubating overnight in lysis buffer (50 mM Tris-HCl, 5 mM EDTA, 100 mM NaCl, 0.5% SDS) containing 250 µg/mL Proteinase K (Roche, Basel, Switzerland). DNA was isolated using Phenol-Chloroform extraction and ethanol precipitation. The genomic DNA was used as a PCR template for a single pair of primers that amplify a specific locus that differs ~100bp in size between all 3 (sub)genomes. In *X. tropicalis*, the locus is on chromosome 5 and PCR product size is 510 bp. In *X. laevis*, one locus is on chromosome 5L for which PCR product size is 408 bp and another one is on chromosome 5S for which PCR product size is 305 bp. The sequences of the primer pair are fwd G T A C T C T T C C C C A G C T T G C T G and rev G C C T G T A T G G C T C C T A G G T T T T C.

Generation of wild type *X. laevis* embryos for microinjection

Ovulations, euthanasias, dissections, and fertilizations were carried out as described above for $I_e \times t_s$ hybrids above, with the following modifications: *X. laevis* males were primed by injecting 500 IU of HCG 24 hours before dissection. Dissected testes were collected in 1X Modified Ringer (MR) (100 mM NaCl, 1.8 mM KCl, 1 mM MgCl₂, 5 mM HEPES-NaOH pH 7.6 in ddH₂O), and stored at room temp for short periods, or at 4°C for up to 5 days. To make sperm solution, 1/3-1/2 of a testis was added to 1 mL of ddH₂O in a 1.5 mL microcentrifuge tube.

Generation of haploid *X. laevis* embryos

Euthanasia of males and dissection/collection of testes proceeded as described for *X. laevis* males above. 1/3-1/2 of a testis was added to 1.1

mL of ddH₂O in a 1.5 mL microcentrifuge tube and homogenized with scissors and a pestle. The tube was briefly centrifuged using a benchtop microcentrifuge for several seconds to pellet large pieces of tissue. One mL of supernatant was removed, avoiding pieces of tissue, and transferred to a non-coated glass petri dish. The open dish was placed into a UV-Crosslinker (Stratalinker, Stratagene) and the sperm solution irradiated twice using 30,000 microjoules. The solution was swirled between the two irradiations. The irradiated sperm solution was then retrieved and used for fertilization by depositing at least 0.5 mL solution on top of freshly squeezed *X. laevis* eggs in a petri dish coated with 1.5% agarose in 1/10x MMR. Fertilization, dejelly, and embryo storage then proceeded as described for $l_e \times t_s$ hybrid embryos above.

Embryo video imaging

Imaging dishes were prepared using a homemade PDMS mold designed to print a pattern of 1 mm large wells in agarose that allowed us to image 4 embryos simultaneously within the 3×4 mm camera field of view for each type of embryo. Embryos were imaged from stage 2. *X. laevis* and $l_e \times t_s$ hybrid or haploid videos were taken simultaneously using two AmScope MD200 USB cameras, (AmScope, Irvine, CA) each mounted on an AmScope SE305R stereoscope. Time lapse movies were acquired at a frequency of 1 frame every 10 s for 20 h and saved as Motion JPEG using a MATLAB (The MathWorks, Inc., Natick, MA) script. Movie post-processing (cropping, concatenation, resizing, addition of scale bar) was done using MATLAB and Fiji [108]. All MATLAB scripts written for this study are available upon request. Two of the scripts used here were obtained through the MATLAB Central File Exchange: “videoMultiCrop” and “concatVideo2D” by Nikolay S.

Imaging and measurement of tailbud, tadpole and frog body size

Tailbud stage embryos were placed in an ice-cold agarose-coated imaging chamber and imaged at 12x magnification using a Wild Heerbrugg M7A StereoZoom microscope coupled to a Leica MC170HD camera and Leica LAS X software. Tadpoles were imaged by placing in a petri dish filled with a limited amount of water to prevent depth-biased measurements. Images were taken with an iphone camera, including a ruler in the field of view. Tadpole measurements were stopped when the tail began to recede at the end of metamorphosis. Froglets were placed in a transparent-bottom container placed on a ruler and fill with a minimal amount of water, and imaged with an iphone camera. Images were analyzed and length measured head to tail for tadpoles, or head to cloaca for froglets. Length measurements were done using the line tool in Fiji.

Erythrocyte preparation and measurements

A small drop of blood was collected from the frog foot with a sterile needle, and the drop was smeared on a slide. The smear was then fixed with

methanol and stained with Giemsa stain (Sigma GS). Cells were imaged in brightfield using micromanager software [109] with an Olympus BX51 microscope equipped with an ORCA-II camera (Hamamatsu Photonics, Hamamatsu city, Japan).

RNA isolation and sequencing

To isolate RNA, embryos at stage 9 were homogenized mechanically in TRIzol® (Thermo Fisher Scientific, Waltham, MA) using up to a 30-gauge needle and processed according to manufacturer instructions. After resuspension in nuclease-free H₂O, RNAs were cleaned using a RNeasy kit (Qiagen Inc.) according to manufacturer instructions. Libraries were prepared using manufacturer's non-standard specific RNA-seq library protocol with poly-A capturing mRNA enrichment method (Illumina, CA, USA). The paired-end 2 x 100 bp reads were generated by the Genome Sequencing and Analysis Facility (GSAF) at the University of Texas at Austin using Illumina HiSeq 2000. Transcriptome data generated in this study are available from NCBI Gene Expression Omnibus (Series record GSE118382).

Gene Expression Analysis

We mapped RNA-seq reads to the database of combined *X. laevis* and *X. tropicalis* transcriptome (available at <http://genome.taejoonlab.org/pub/xenopus/annotation/>; WorldCup_201407 version), using Bowtie1 (version 1.0). To prevent misalignment to other species, we applied stringent criteria, allowing no mismatches (-v 0), and ignoring a read mapped more than one target (-m 1). We estimated relative transcript abundance with 'transcripts per million reads (TPM)' calculated by RSEM (version 1.2.19), and differential expression analysis was conducted using edgeR (version 3.36.1), with greater than two-fold changes and false discovery rate (FDR) less than 0.05 cutoff to determine the significance.

Gene Ontology Analysis

We conducted Gene Ontology analysis with Panther DB (version 13.1). For statistical analysis for overrepresented terms, we used Fischer's exact test and FDR adjustment, and applied FDR less than 0.05 as a significance cutoff. To validate our list of candidates, we searched Xenbase (<http://www.xenbase.org/>) using the gene name as the query.

Cloning and mRNA synthesis of candidate transcription factors

Total RNA was isolated from *X. tropicalis* embryos as described above in "RNA isolation and sequencing", and cDNA was synthesized from RNA using the SuperScript III First Strand Synthesis system (Invitrogen- Thermo Fisher Scientific, Waltham, MA) according to manufacturer instructions. Transcription factor sequences were then PCR-amplified from the cDNA

using the following primer sequences (all are written 5'-3') concatenated with ~30 bp plasmid-homologous sequences:

Esr10, fwd ATGGCTCCTTACAGCGCTAC, rev TTCTCTGGAGACCCTGGAAC;
 Sox3, fwd ATGTATAGCATGTTGGACAC, rev CTGTACCGCTCACTCACATA;
 Foxi4.2, fwd ATGAACCCAGTCCAGCAACC, rev CTTTGTACCAGGGAAGGTAC;
 Hes7.1, fwd ATGAAGGGAGCGAGTGAAGT, rev AGACCTGGAGACCTTGGGTA;
 Mix1, fwd ATGGACTCATTAGCCAACA, rev TCTGTGTGCTCCTCCACCTT;
 Tgif2, fwd ATGATGAATTCGACTTTTGA, rev TCACGACAAGCACCCCAAT;
 Ventx2.1, fwd ATGAACACAAGGACTACTAC, rev TTGGGCAGCCTCTGGCCTAC;
 Klf17, fwd ATGAGTGTGGCTTTCTCAAC, rev CATGTGTCTCTTCATGTGCAG;
 Not, fwd ATGTTACACAGCCCTGTCTTTC, rev CAGTTCAACATCCACATCATC;
 Oct25 fwd ATGTACAGCCAACAGCCCTTC, rev ACCAATATGGCCGCCCATGG;
 Sia2 fwd ATGACTTGTGACTCTGAGCTTG, rev GCCCCACATATCCGGATATTG;
 Id3 fwd ATGAAAGCCATCAGCCCAGTG, rev GTGGCAGACACTGGCGTCCC. These amplified sequences were then subcloned using Gibson assembly (New England Biolabs, Ipswich, MA) into a PCS2 expression vector obtained at the 2013 Advanced Imaging in *Xenopus* Workshop from the Wallingford lab (UT Austin, USA). mRNAs were synthesized from these expression constructs using mMessage mMachine SP6 Transcription Kit (Ambion – Thermo Fisher Scientific, Waltham, MA) following the manufacturer protocol. The mRNAs were then purified using Phenol-Chloroform extraction, resuspended in ddH₂O, aliquoted and stored at -80°C.

Microinjection of candidate transcription factors into *Xenopus* embryos

Stage 1 (one-cell) embryos about 30 minutes post-fertilization were transferred into a mesh-bottom dish containing 1/9X MMR 3% Ficoll for microinjection. Injections were done using a Picospritzer III microinjection system (Parker, Hollis, NH) equipped with a MM-3 micromanipulator (Narishige, Amityville, NY). To mimic overexpression of each transcription factor, each embryo was injected with 750 picograms of mRNA, a dose we determined was large enough to see phenotypes, but was not associated with embryo toxicity. Injected embryos were transferred to a new dish coated with 1.5% agarose in 1/10x MMR, and incubated at 23°C in 1/9X MMR 3% Ficoll for at least 6 hours. The embryos were then transferred to fresh 1/10x MMR in a new agarose-coated dish, and incubated at 23°C with buffer changes into fresh 1/10x MMR several times daily until ready for fixation or imaging.

Embryo whole mount immunofluorescence

Embryos at the desired developmental stage were fixed for one hour using MAD fixative (2 parts methanol [Thermo Fisher Scientific, Waltham, MA], 2 parts acetone [Thermo Fisher Scientific, Waltham, MA]), 1 part DMSO [Sigma]). After fixation, embryos were dehydrated in methanol and stored at -20°C. Embryos were then processed as previously described [76] with modifications. Following gradual rehydration in 0.5X SSC (1X SSC: 150 mM

NaCl, 15 mM Na citrate, pH 7.0), embryos were bleached with 1-2% H₂O₂ (Thermo Fisher Scientific, Waltham, MA) in 0.5X SSC containing 5% formamide (Sigma) for 2-3 h under light, then washed in PBT (137 mM NaCl, 2.7 mM KCl, 10 mM Na₂HPO₄, 0.1% Triton X-100 [Thermo Fisher Scientific, Waltham, MA]) and 2 mg/mL bovine serum albumin (BSA). Embryos were blocked in PBT supplemented with 10% goat serum (Gibco – Thermo Fisher Scientific, Waltham, MA) and 5% DMSO for 1-3 h and incubated overnight at 4°C in PBT supplemented with 10% goat serum and primary antibodies. The following antibodies were used to label tubulin and DNA, respectively: 1:500 mouse anti-beta tubulin (E7; Developmental Studies Hybridoma Bank, Iowa City, IA), and 1:500 rabbit anti-histone H3 (ab1791; Abcam, Cambridge, MA). Embryos were then washed 4 × 2 h in PBT and incubated overnight in PBT supplemented with 1:500 goat anti-mouse or goat anti-rabbit secondary antibodies coupled either to Alexa Fluor 488 or 568 (Invitrogen – Thermo Fisher Scientific, Waltham, MA). Embryos were then washed 4 × 2 h in PBT and gradually dehydrated in methanol. Embryos were cleared in Murray's clearing medium (2 parts of Benzyl Benzoate, 1 part of Benzyl Alcohol).

Confocal imaging and measurement of embryos, cells and nuclei after whole mount immunofluorescence

Embryos were placed in a chamber made using a flat nylon washer (Grainger, Lake Forest, IL) attached with nail polish (Sally Hansen, New York, NY) to a slide, filled with Murray's clearing medium, and covered by a coverslip (Beckman Coulter, Brea, CA) for confocal microscopy. Confocal microscopy was performed on a Zeiss LSM 780 NLO Axio Examiner running the Zeiss Zen Software. Embryos were imaged using a Plan-Apochromat 20x/1.0 water objective and laser power of 12%, on multiple 1024x1024 pixel plans spaced 0.68 µm apart in Z.

Nuclear area was measured in Fiji using the ellipse tool. From this, we calculated the diameter of a circle of the same area, a value that we could directly compare the cell size determined through the measurement of the cell diameter at the nucleus central plane.

3.5 Supplemental figure

Significantly differentially expressed transcripts in *lexts* hybrid, compared to *X. laevis* embryos

Gene	log2FC	FDR	LELS1.tpm	LELS3.tpm	LETS1.tpm	LETS3.tpm
XT.not Tan201204_XENTRc2cell2_000022495	7.916	3.04E-12	0.15	0.13	83.5	44.27
XT.klf17 Tan201204_XENTRc1st11b_000019039	8.077	7.53E-11	0.1	0.09	83.7	33.64
XT.hes7 Tan201204_XENTRc2cell4_000032522	7.048	6.02E-09	0	0.44	63.58	28.3
XT.unnamed Xetrov14052619m	7.681	2.04E-08	0.26	0.07	102.51	18.1
XT.unnamed UG52_57415490	8.653	2.04E-08	0	0	80.96	20.16
XT.foxi4 Tan201204_XENTRc2st16_000018807	8.212	6.47E-08	0	0	52.6	21.83
XT.id3 Tan201204_XENTRc1st11b_000040212	8.375	1.62E-07	0	0	65.81	17.58
XT.esr10 ENSXETT00000048128	6.632	1.70E-07	0	0.41	43.7	21.81
XT.oct25 Tan201204_XENTRc1st11a_000011853	7.115	2.11E-07	0.13	0.06	38.45	22.64
XT.znf350 Xetrov14052642m	7.791	2.72E-07	0.13	0	68.14	15.71
XT.cxcr4 Tan201204_XENTRc2st41_000016478	7.18	4.17E-07	0.12	0	33.21	21.02
XT.znf470 Xetrov14052647m	6.906	6.41E-07	0.35	0.1	72.11	13
XT.znf665 xb201405_189442274	7.497	1.12E-05	0.07	0	47.77	11.03
XT.znf157 Xetrov14052644m	7.773	1.12E-05	0	0	42.92	11.91
XT.znf350 Xetrov14047686m	8.008	1.20E-05	0	0	55.05	9.55
XT.tdgf1 Tan201204_XENTRc2st10_000033441	4.765	1.51E-05	0.8	1.19	42.33	19.38
XT.sox3 Tan201204_XENTRc2cell8_000012412	4.083	1.83E-05	1.8	2.18	45.17	27.41
XT.venb2 Tan201204_XENTRc1st10_000025509	7.469	2.33E-05	0	0	30.96	13.41
XT.eef1a1o Tan201204_XENTRc2st08_000016232	5.243	2.39E-05	0.59	1.39	72.35	13.01
XT.sia2 Xetrov14048884m	7.2	5.64E-05	0	0	16.07	20.73
XT.gs17 Xetrov14041408m	6.087	1.04E-04	0	0.26	21.52	13.58
XT.znf33a xb201405_77622785	7.858	2.22E-04	0	0	53.46	4.71
XT.unnamed Tan201204_XENTRc2st09_000036647	6.996	2.65E-04	0	0	14.05	17.85
XT.znf33a ENSXETT00000016145	6.921	6.06E-04	0	0.05	29.03	7.77
XT.znf665 Xetrov14052632m	7.467	8.82E-04	0	0	39.67	4.64
XT.gdf3 Tan201204_XENTRc2st11_000021873	7.348	9.48E-04	0	0	35.6	5.17
XT.unnamed xb201405_165970537	7.105	1.15E-03	0	0	27.45	6.99
XT.unnamed Xetrov14052628m	7.099	1.43E-03	0	0	27.47	6.82
XT.srsf7 ENSXETT00000040586	4.585	1.77E-03	0.61	0.65	26.51	10.03
XT.tgif2 Xetrov14040166m	6.847	3.03E-03	0	0	21.72	7.03
XT.zcchc3 xb201405_82653391	6.903	5.56E-03	0	0	24.74	5.15
XT.unnamed Xetrov14052643m	6.526	7.81E-03	0	0	15.99	6.97
XT.nodal3 xb201405_29788235	6.479	8.06E-03	0	0	14.66	7.56
XT.ddit4 Tan201204_XENTRc1st19b_000041812	4.069	8.06E-03	0.26	1.64	26.2	10.15
XT.znf33b Xetrov14052622m	6.246	8.27E-03	0	0.1	21.61	5.26
XT.unnamed Xetrov14028100m	5.912	9.43E-03	0.19	0	21.75	4.91
XT.ins Tan201204_XENTRc1st11b_000043530	5.206	9.43E-03	0	0.32	12.75	8.36
XT.srsf5 Tan201204_XENTRc2st10_000021734	3.63	1.59E-02	0.71	1.7	24.32	8.85
XT.venb2 Tan201204_XENTRc2st11_000020250	6.451	1.61E-02	0	0	15.4	6.39
XT.mix1 Tan201204_XENTRc2st13a_000018488	6.429	2.38E-02	0	0	16.63	4.81
XT.rasi11b Tan201204_XENTRc1st09_000021259	5.271	3.28E-02	0.1	0.18	15.83	4.78
XL.not TeperekTkacz201202_000158550	-1.84	4.44E-02	77.55	68.07	28.81	12.29

Chapter 4

Investigating size scaling in the dodecaploid *Xenopus longipes*

4.1 Introduction

As we have seen previously, genome size correlates with somatic cell size (Chapter 3, [2,3,33]) and molecular size scaling mechanisms differ among even closely related Pipid frogs (Chapter 1, [59,65–67]). But how does genome size influence scaling mechanisms? Furthermore, what are the functional consequences of extreme genome size on growth and development?

Taking a similar comparative approach, we characterized *Xenopus longipes*, a rare dodecaploid *Xenopus*, at the cellular level and throughout development, to begin to answer these questions. *X. longipes*, or the Lake Oku clawed frog, is a critically endangered *Xenopus* species found in Lake Oku, a small crater lake in Cameroon, Africa, which has only recently begun to be bred in captivity [110]. Based on measurements done in comparison to *Xenopus ruwensoriensis* which has a similarly sized genome, the *X. longipes* genome contains 8 pg of DNA per haploid nucleus, one of the largest *Xenopus* genomes, and has an estimated $12n=108n$ chromosomes [111].

We found that as expected, somatic cells size scales linearly with genome size in *X. longipes* compared to other Pipid frog species. However, during early development, cell, spindle and nuclear size do not scale with genome size, since cell size is determined by the size of the egg and the number of reductive cell divisions. Interestingly, we found that development of *X. longipes* may proceed more slowly than that of *X. laevis* starting at neurulation, an effect that continues through metamorphosis.

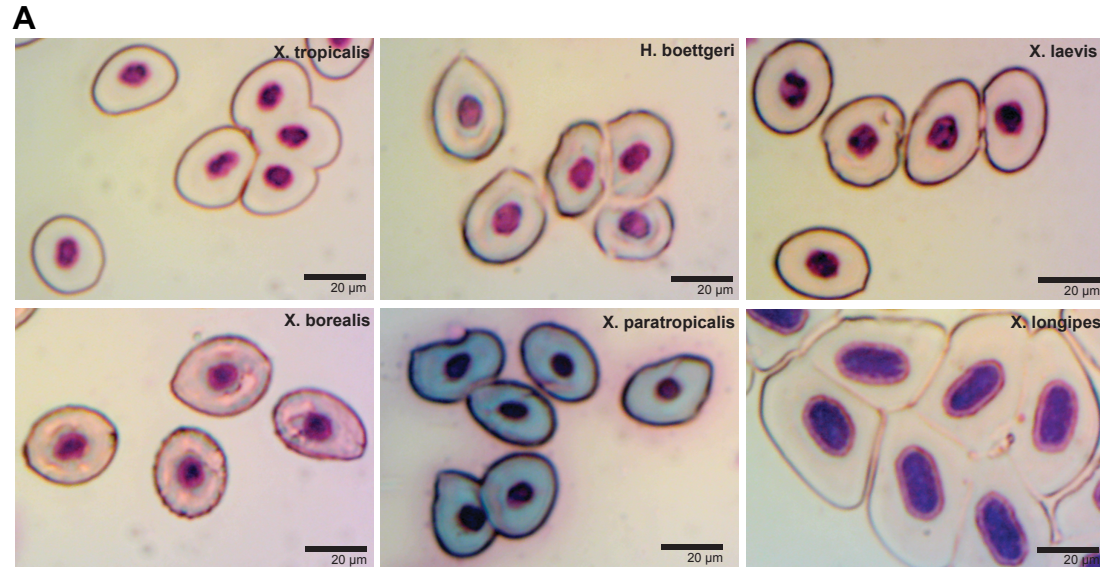
While this work is unpublished and does not yet tell a complete story, we hope it can be used as a foundation for future work.

4.2 Results

In 2016, we obtained several wild-caught *X. longipes* from California Academy of Sciences, which we successfully mated to generate embryos for analysis and to establish our own colony (see Methods). We found that

cell size in Pipid erythrocytes scale linearly with genome size, including *X. longipes* (Fig 4.1A,B). However, in both early cleaving blastulae (stage 8), and neurula (stage 21), cell size does not scale with genome size. In fact, by stage 21, *X. longipes* cells are smaller than

Figure 4.1



B

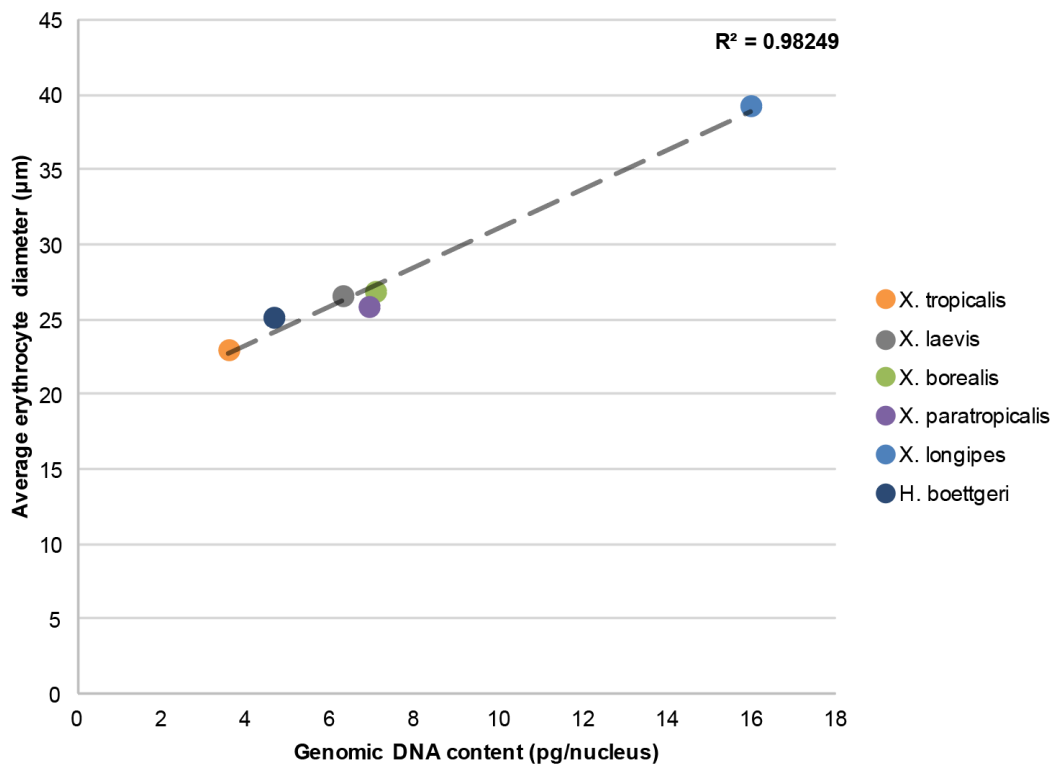
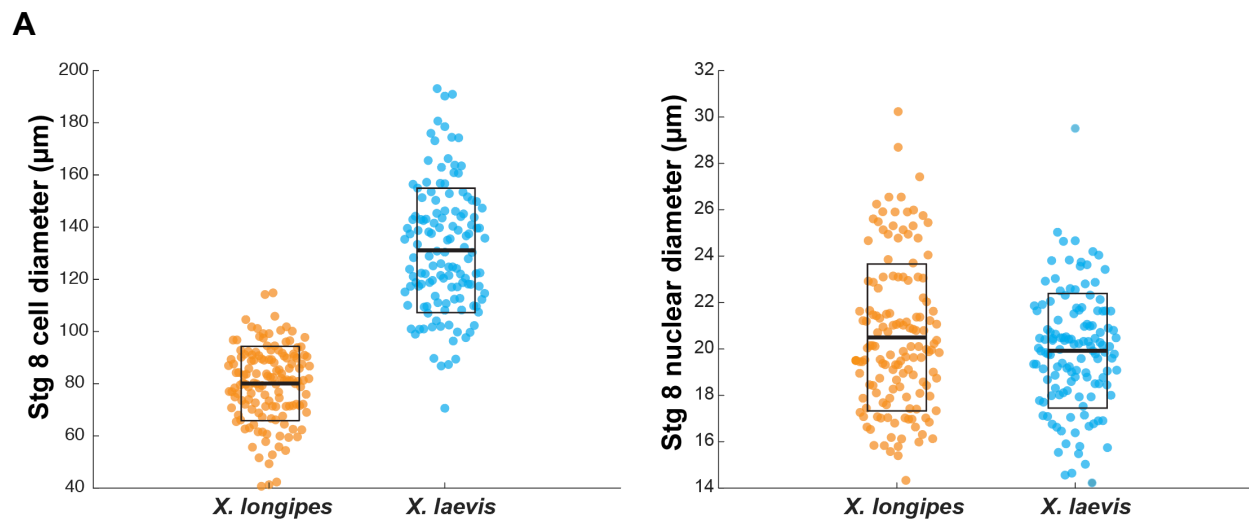
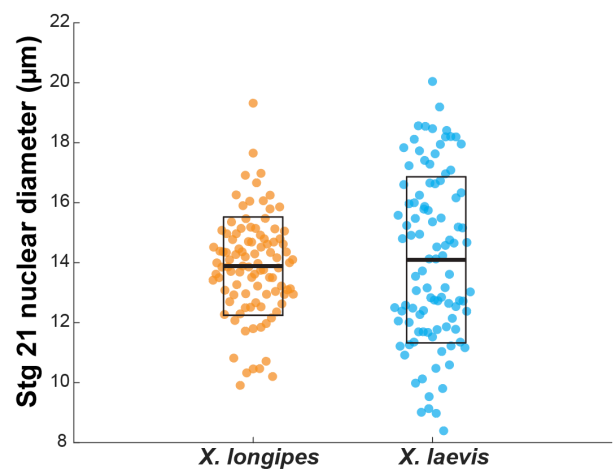
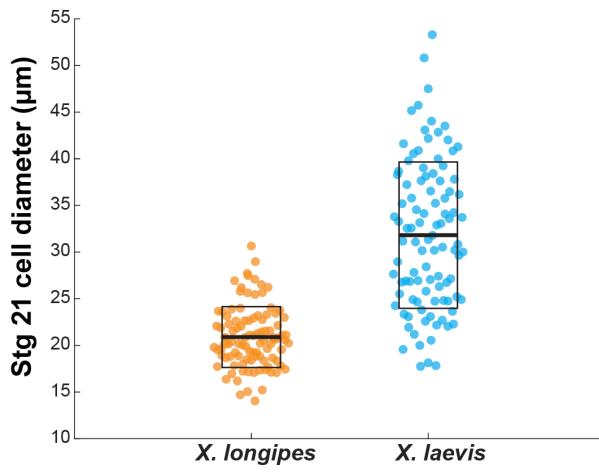
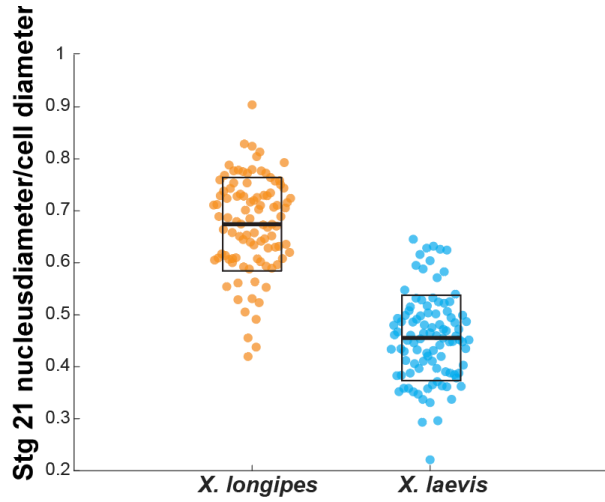
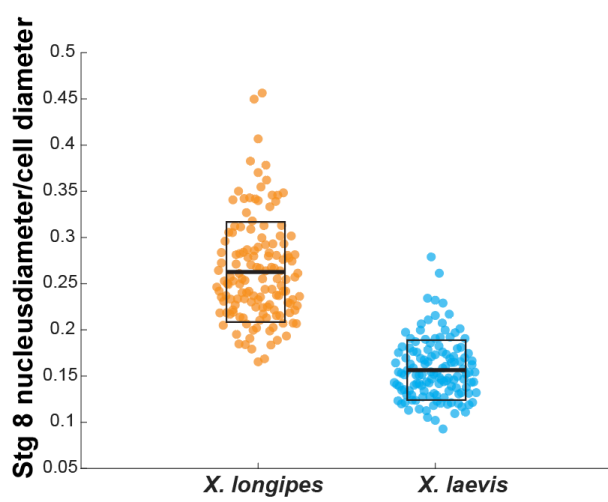


Figure 4.1: Measurement of erythrocytes in Pipid frogs. A. Representative images of Giemsa-stained erythrocytes from frog blood smears. Purple=DNA. **B.** Correlation between erythrocyte diameter and genomic DNA content in cells measured in (A). n=100 erythrocytes for each species.

X. laevis cells (Fig 4.2 A,B), even though *X. laevis* contains less than half the genome content at 3.2 pg DNA per haploid nucleus (Fig 2.1). Therefore the nuclear:cell size ratio is greater in *X. longipes* (Fig 4.2C). While these 2D measurements did not show that nuclear diameter was significantly different between the two species at either stage (Fig 4.2 A,B), we took measurements using Imaris software, which calculated the area and volume of nuclei in 3D and increased the sample size ~10fold. From this we found that by stage 21, nuclear area and volume in *X. longipes* is significantly larger than that in *X. laevis* (Fig 4.3 A,B). From these measurements, we can conclude that the ratio of nuclear size to cell size is significantly larger in *X. longipes* compared to *X. laevis*. We also found that by stage 21, nuclei in *X. longipes* were more irregularly shaped and less spherical than *X. laevis* (Fig 4.2D, 4.3C).

Figure 4.2



B**C**

Continued on next page

D

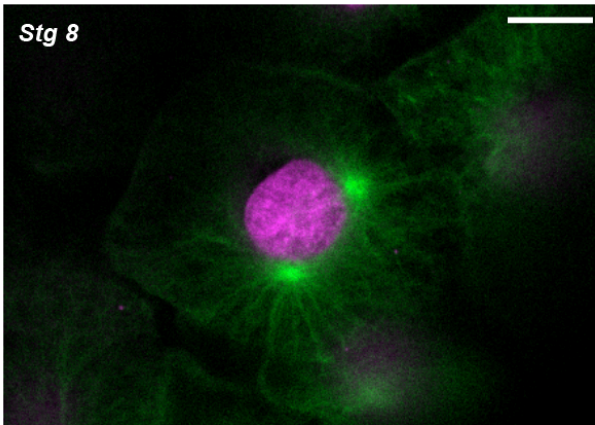
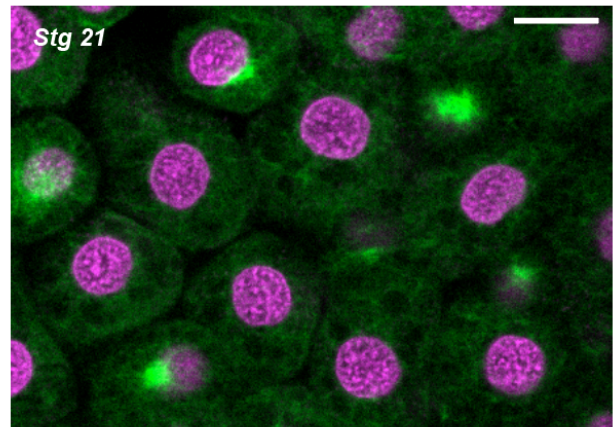
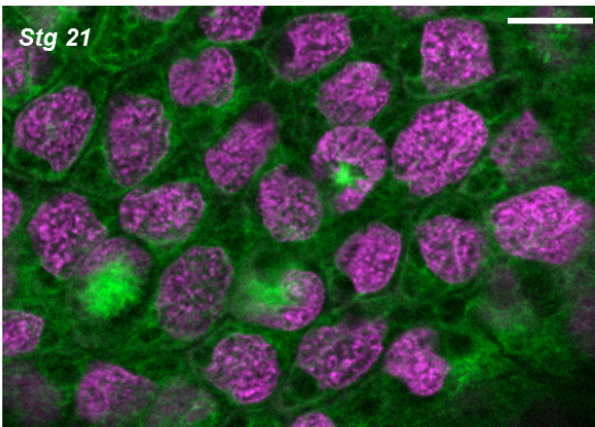
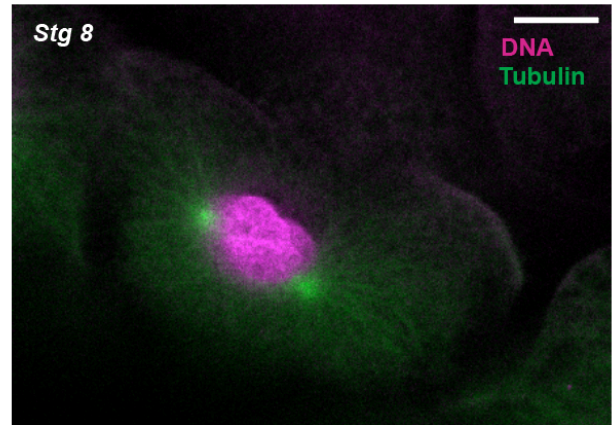
X. longipes*X. laevis*

Figure 4.2: Comparison of cell and nuclear size in *X. laevis* and *X. longipes* embryos. A. Diameter of stage 8 cells and nuclei. $p < 0.0001$ for cells, $p = 0.097$ for nuclei. **B.** Diameter of stage 21 cells and nuclei. $p < 0.0001$ for cells, $p = 0.516$ for nuclei. **C.** Ratio of nucleus diameter: cell diameter of cells measured in (A) and (B). **D.** Representative images of cells and nuclei from (A) and (B). $p < 0.0001$ for both stages. Scale bars = $20 \mu\text{m}$. For all box plots, thick line inside box = average length, upper and lower box boundaries = \pm SD. $n \geq 100$ cells or nuclei.

Figure 4.3

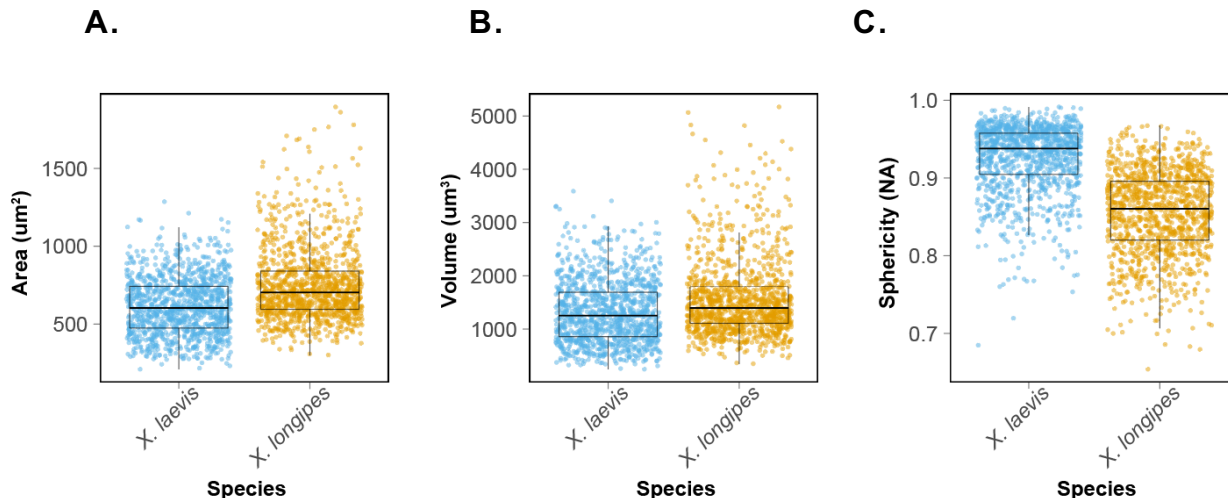


Figure 4.3: Comparison of area (A), volume (B), and sphericity (C) of nuclei in *X. laevis* and *X. longipes* embryos at stage 21. For all box plots, thick line inside box= mean, upper and lower box boundaries = \pm SD. Whiskers=minimum and maximum. $n \geq 1152$ nuclei from 2 separate clutches. $p \leq 0.001$ in A, B, and C.

*Adapted from C. Cadart

Interestingly, while early cleavages in *X. longipes* and *X. laevis* displayed similar timing at early stages, development in *X. longipes* appeared to proceed more slowly than that of *X. laevis* starting at around stage 13 (Fig 4.4, movies, K. Miller), with embryos showing reduced body lengthening and slower neural tube closure. By early tailbud stage (48 hpf), the *X. longipes* tadpoles were considerably smaller than *X. laevis* (Fig 4.5, 4.6). This size difference continues through the early tadpole stage before feeding. Timing to metamorphosis is also longer in *X. longipes* than in other *Xenopus* species[110].

Like the embryos and tadpoles, *X. longipes* eggs are significantly smaller than those of *X. laevis*. Meiotic spindles are also significantly smaller than the *X. laevis* meiotic spindle ($\sim 35 \mu\text{m}$, [75][66]) concomitant with egg size (Fig 4.7). By stage 21, morphological differences between *X. laevis* and *X. longipes* spindles can be observed, with the spindle appearing more rounded rather than oblong, perhaps in response to the increased amount of chromatin at the metaphase plate (Fig 4.8).

Figure 4.4

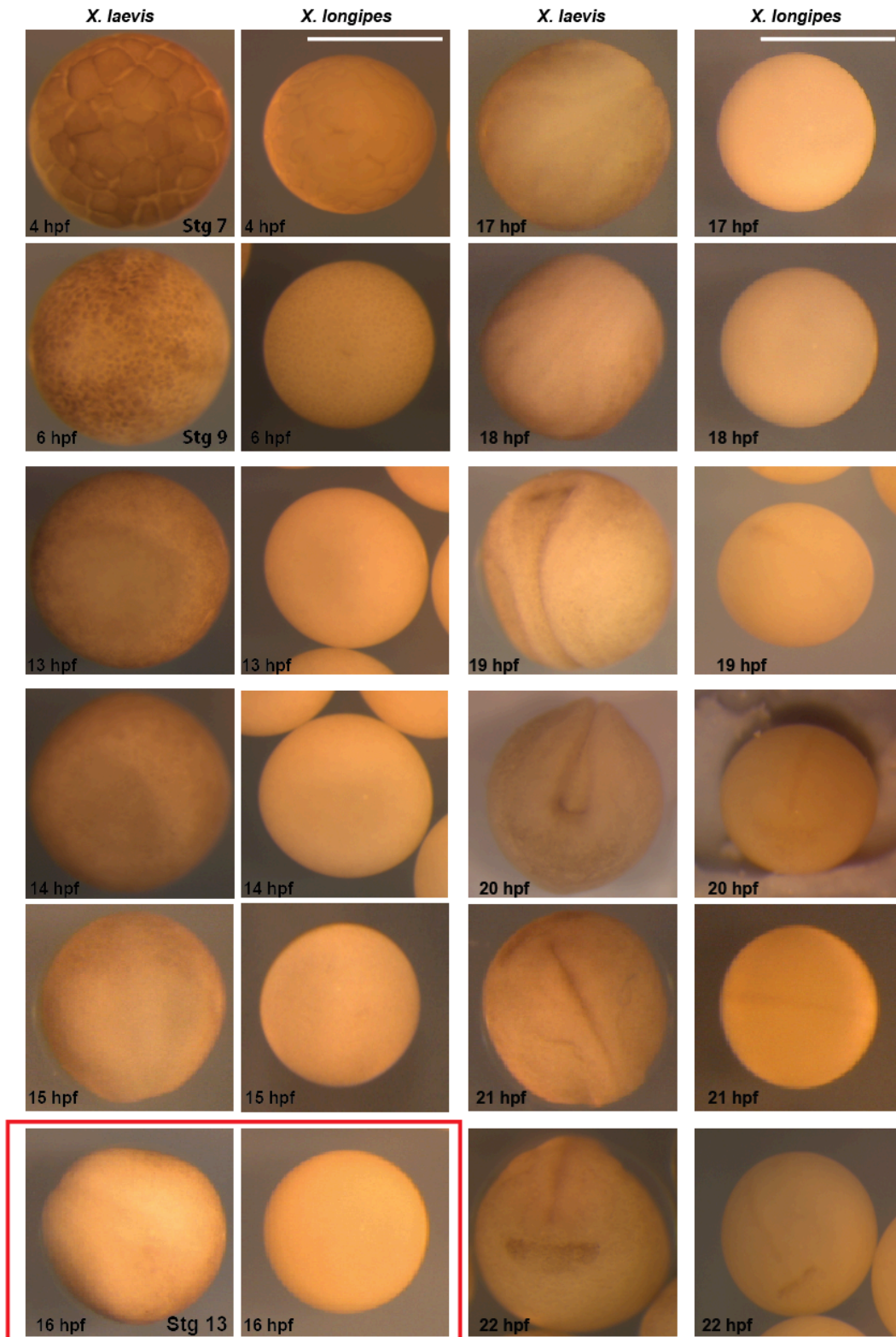


Figure 4.4: Comparison of development in *X. laevis* and *X. longipes* embryos through neurulation. *X. laevis* embryos are staged according to Nieuwkoop and

Faber. Red box indicates where *X. longipes* embryos appear to slow in development. Scale bars= 1mm.

Figure 4.5

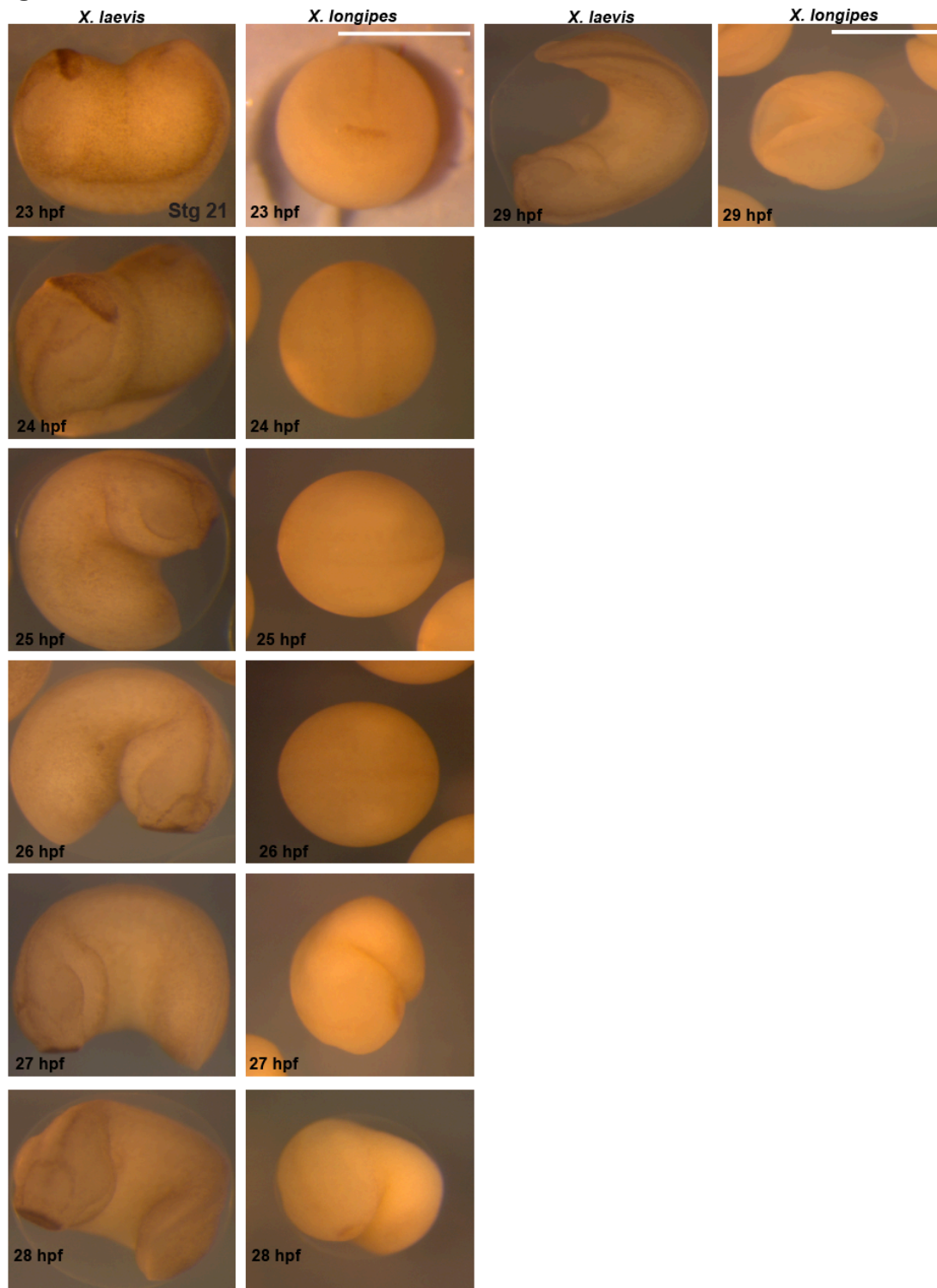


Figure 4.5: Comparison of development in *X. laevis* and *X. longipes* embryos through tadpole stage. *X. laevis* embryos are staged according to Nieuwkoop and Faber. hpf=hours post fertilization. Scale bars= 1mm.

Figure 4.6

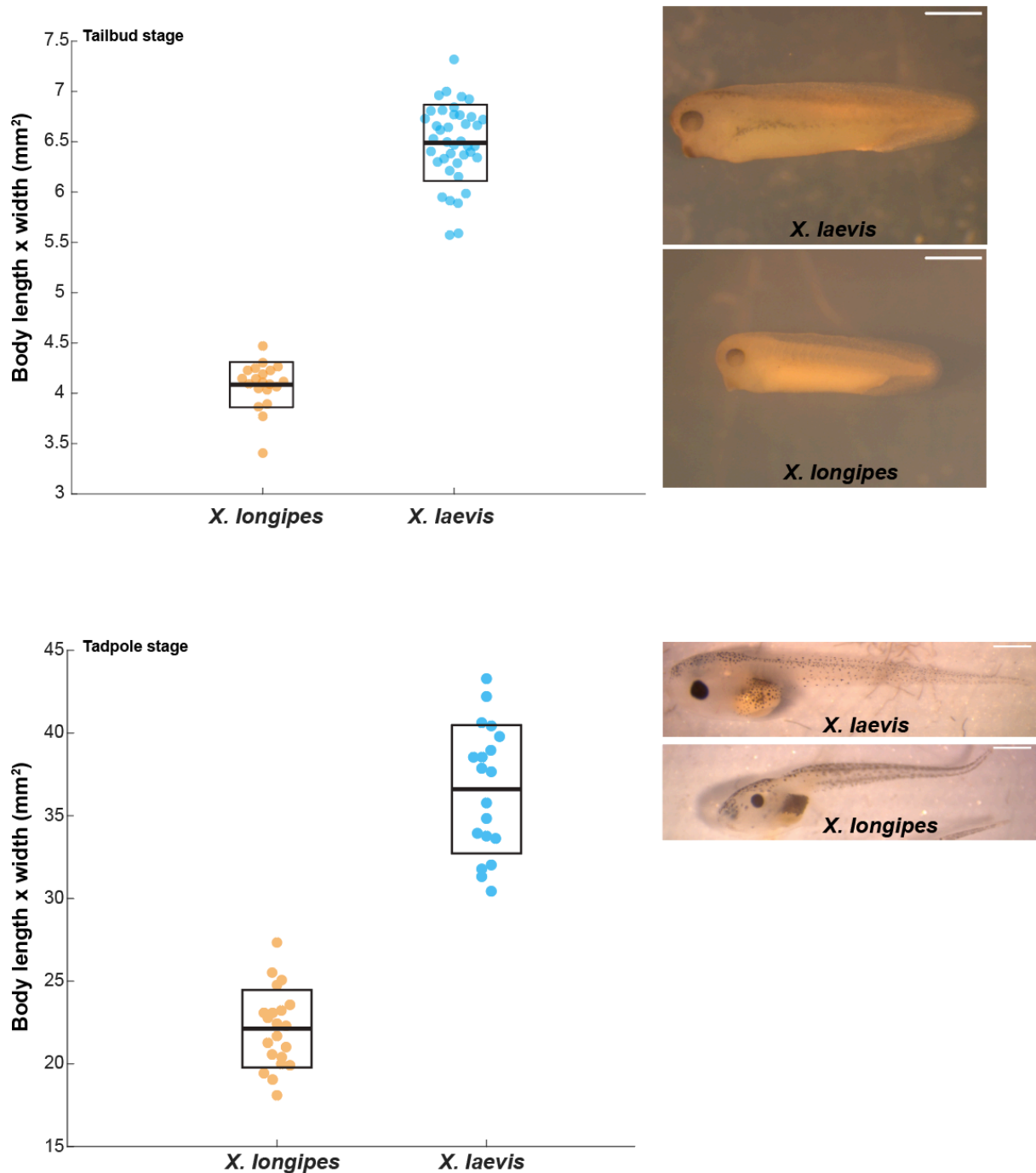


Figure 4.6: Body size in *X. laevis* and *X. longipes* tailbuds and tadpoles. Tailbuds are 45 hours post fertilization, swimming tadpoles are 7 days post fertilization. Scale

bars= 1mm. For box plots, thick line inside box = average length, upper and lower box boundaries = +/- SD. $p < 0.0001$ for both tailbud and tadpole stage. $n \geq 20$ individuals in each condition.

Figure 4.7

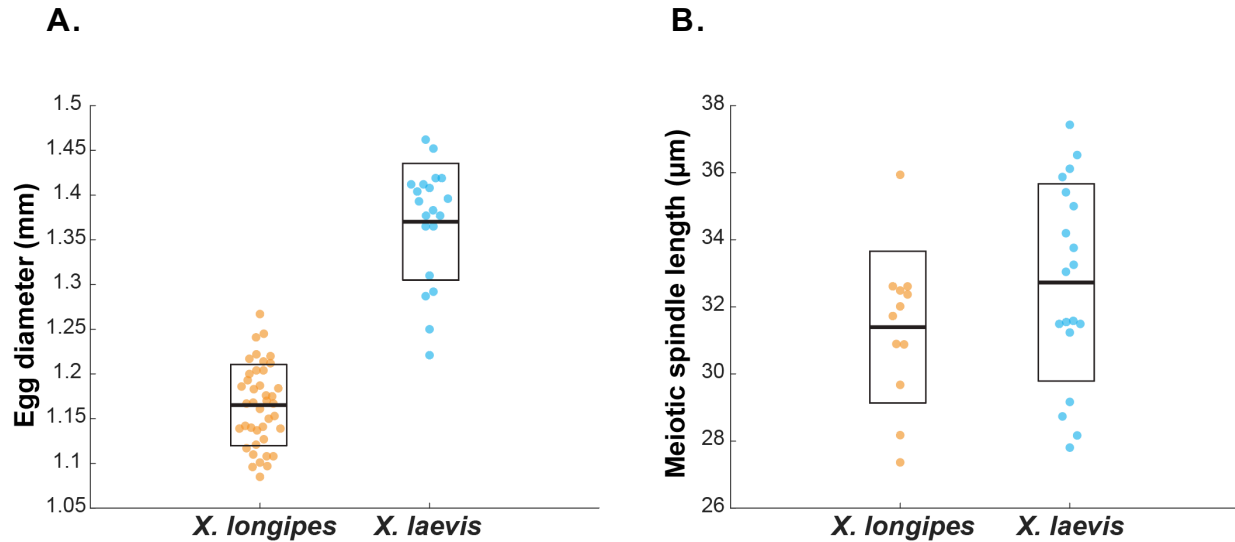


Figure 4.7: Egg and meiotic spindle size in *X. laevis* and *X. longipes*. A. Egg diameter quantification of each frog species. $n \geq 20$ eggs for each species. B. Meiotic spindle length in fixed eggs of each frog species. $n \geq 12$ spindles for each species. For box plots, thick line inside box = average length, upper and lower box boundaries = +/- SD. For egg diameters, $p < 0.0001$, for meiotic spindles $p = 0.016$.

Figure 4.8

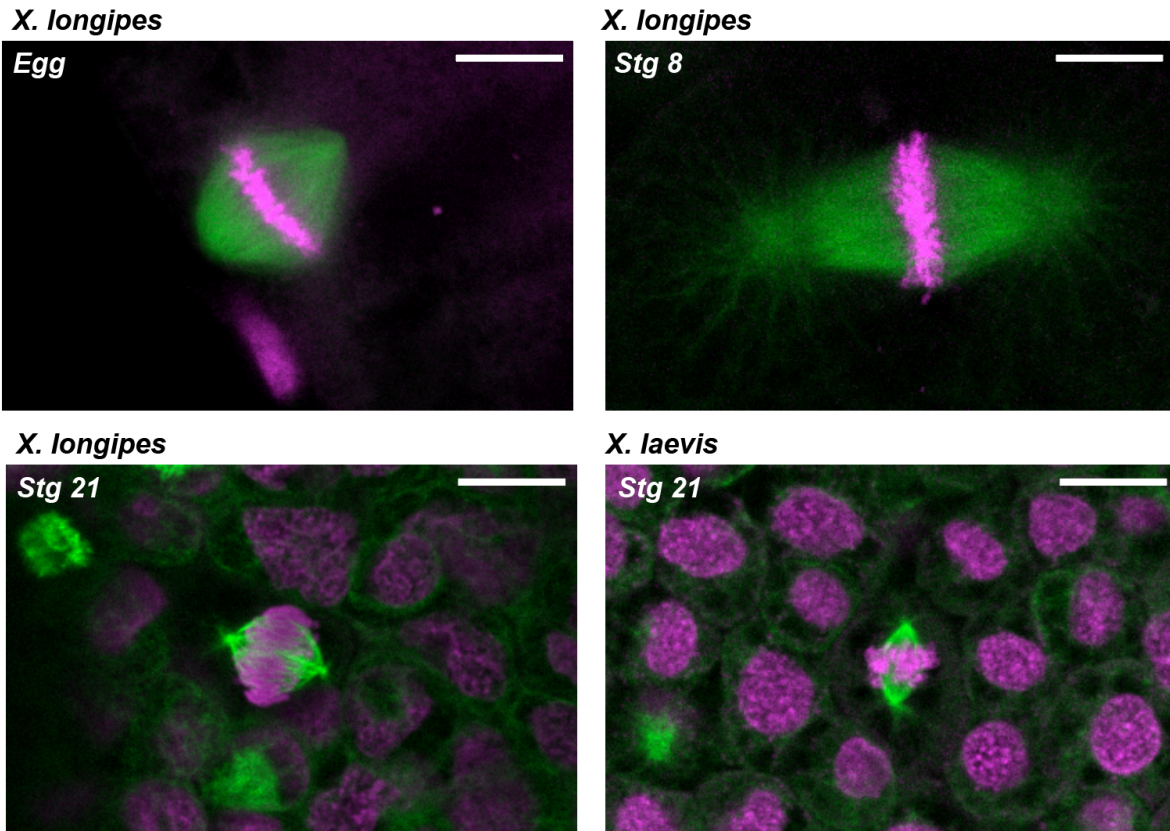


Figure 4.8: Meiotic and mitotic spindles in *X. longipes* and *X. laevis*. Purple=DNA, green=tubulin. Scale bars=20 μm .

4.3 Discussion

These basic observations bring up several questions for future mechanistic exploration. Firstly, although cell size correlates with genome size in somatic cells of many organisms including *Xenopus*, our findings demonstrate that this relationship does not apply in early development. This makes intuitive sense as cells of early embryos derive solely from maternal components and initially their size is determined by egg size. When then does cell size start to scale with genome size? Zygotic genome activation, which occurs at around stage 8-9 in *Xenopus*, does not appear relevant, as smaller cells persist in *X. longipes* stage 21 neurula, well after ZGA. Measuring *X. longipes* cells at later developmental stages such as swimming tadpole may be informative. Interestingly, *X. longipes* tadpoles eventually attain a larger size than *X. laevis* just before metamorphosis. Is this a consequence of slower

development and metabolism or a consequence of large somatic cell size? And what is the mechanism by which genome to cell size scaling occurs? Recent studies in unicellular organisms use resource allocation models to link biomass properties such as RNA, proteins, lipids, and ribosomes to cellular features, such as cell and genome size [112][113]. One possibility is that resource allocation varies depending on ploidy. This hypothesis can be tested by measuring the amount of raw materials such as RNA, proteins, lipids, and ribosomes in embryos of varying ploidies, either through interspecies comparisons or by altering ploidy within a single species, and using correlations between these and genome size to inform models for cell size. Whole-embryo metabolic rate at different cell sizes may be examined as well.

Another fascinating observation is the apparent developmental slowdown starting at neurulation in *X. longipes*. It is known that larger cells take longer to proliferate [114], which is thought to contribute to slower embryonic development in amphibians [115]. However, by stage 21, long after we observed the slowing, *X. longipes* cells are still smaller and do not scale with genome size. Could this phenomenon instead be a scaling issue- perhaps a consequence of the large nuclear size compared to cell size? The maintenance of a constant nuclear-to-cytoplasmic (N/C) volume ratio is a conserved cellular property [116–118]. However, this ratio changes during development in *Xenopus* [119]. Developmental consequences of this phenomenon are poorly understood, but one study observed that artificially increasing the size of the nucleus by microinjecting scaling factors such as importin proteins, lamins, and reticulons into cleaving *Xenopus* embryos resulted in a lengthening of cell cycle timing [120]. Future experiments will involve characterizing this developmental feature in *X. longipes*, starting with identifying whether development is indeed slower by examining the timing of zygotic genes known to turn on at precise developmental timepoints.

Another interesting follow up question regards the impact of large genome size on meiotic and mitotic spindle architecture. Does chromatin compaction proceed similarly to other *Xenopus* species? How is microtubule nucleation and organization impacted by the presence of a large amount of DNA within the spindle? We might anticipate for instance that chromatin-mediated microtubule nucleation may play a larger role in spindle assembly, which would influence spindle architecture. These questions may be addressed by taking similar approaches outlined in Chapter 1 and using *X. longipes* egg and embryo extracts to examine the architectural features of spindles.

4.4 Methods

Erythrocyte preparation and measurements

A small drop of blood was collected from the frog foot with a sterile needle, and the drop was smeared on a slide. The smear was then fixed with methanol and stained with Giemsa stain (Sigma GS). Cells were imaged in brightfield using micromanager software [109] with an Olympus BX51 microscope equipped with an ORCA-II camera (Hamamatsu Photonics, Hamamatsu city, Japan).

Natural mating of *X. longipes*

Male and female *X. longipes* were injected with a priming dose of 75 iu HCG (Sigma) 48 hours before the desired mating day, and kept separately to avoid premature amplexus. On the day of ovulation, males and females were injected with a boosting dose of 200 iu HCG. Amplexus began soon after injection with egg laying 6-8 hours later. Embryos were collected in batches for fixation and live imaging.

In vitro fertilization of *X. laevis*

X. laevis females were primed with 100 IU of pregnant mare serum gonadotropin (PMSG, National Hormone and Peptide Program, Torrance, CA) at least 48 h before use and boosted with 500 IU of HCG (Human Chorionic Gonadotropin CG10, Sigma) 14-16 hours before experiments. To obtain testes, males were euthanized by anesthesia through immersion in double-distilled (dd)H₂O containing 0.15% MS222 (tricaine) neutralized with 5 mM sodium bicarbonate before dissection. Testes were collected in 1X Modified Ringer (MR) (100 mM NaCl, 1.8 mM KCl, 1 mM MgCl₂, 5 mM HEPES-NaOH pH 7.6 in ddH₂O) and stored at 4°C until fertilization. To prepare the sperm solution, 1/3 testis was added to 1 mL of ddH₂O in a 1.5 mL microcentrifuge tube, and homogenized using scissors and a pestle. *X. laevis* females were squeezed gently to deposit eggs onto petri dishes coated with 1.5% agarose in 1/10X MMR. Any liquid in the petri dishes was removed and the eggs were fertilized with 1 mL of sperm solution per dish. Fertilized embryos were swirled in the solution to form a monolayer on the bottom of the petri dish and incubated for 10 min with the dish slanted to ensure submersion of eggs. Dishes were then flooded with 1/10X MMR, swirled and incubated for 10 min. To remove egg jelly coats, the 1/10X MMR was completely exchanged for freshly prepared Dejellying Solution (2% L-cysteine in ddH₂O-NaOH, pH 7.8). After dejellying, eggs were washed extensively (>4X) with 1/10X MMR before incubation at 23°C. At Nieuwkoop and Faber stage 2-3, fertilized embryos were sorted and placed in fresh 1/10X MMR in new petri dishes coated with 1.5% agarose in 1/10X MMR.

Maintenance of *X. laevis* and *X longipes* embryos

Embryos were raised side by side in 1.5% agarose in 1/10X MMR -coated petri dishes covered in 1/10X MMR in a 20 °C incubator. The MMR was changed and dead/lysed embryos removed frequently to prevent contamination.

Live imaging and measurement of egg diameters, developing embryos, and tadpoles

Eggs and embryos were placed in an agarose-coated imaging chamber filled with 1/10X MMR and imaged at 12x-31x magnification using a Wild Heerbrugg M7A StereoZoom microscope coupled to a Leica MC170HD camera and Leica LAS X software. Tadpoles were imaged by placing in a petri dish filled with a limited amount of water to prevent depth-biased measurements, at 6x magnification.

Embryo whole mount immunofluorescence

Embryos at the desired developmental stage were fixed for one hour using MAD fixative (2 parts methanol [Thermo Fisher Scientific, Waltham, MA], 2 parts acetone [Thermo Fisher Scientific, Waltham, MA]), 1 part DMSO [Sigma]). After fixation, embryos were dehydrated in methanol and stored at -20°C. Embryos were then processed as previously described [76] with modifications. Following gradual rehydration in 0.5X SSC (1X SSC: 150 mM NaCl, 15 mM Na citrate, pH 7.0), embryos were bleached with 1-2% H₂O₂ (Thermo Fisher Scientific, Waltham, MA) in 0.5X SSC containing 5% formamide (Sigma) for 2-3 h under light, then washed in PBT (137 mM NaCl, 2.7 mM KCl, 10 mM Na₂HPO₄, 0.1% Triton X-100 [Thermo Fisher Scientific, Waltham, MA]) and 2 mg/mL bovine serum albumin (BSA). Embryos were blocked in PBT supplemented with 10% goat serum (Gibco – Thermo Fisher Scientific, Waltham, MA) and 5% DMSO for 1-3 h and incubated overnight at 4°C in PBT supplemented with 10% goat serum and primary antibodies. The following antibodies were used to label tubulin and DNA, respectively: 1:250 mouse anti-beta tubulin (E7; Developmental Studies Hybridoma Bank, Iowa City, IA), and 1:250 rabbit anti-histone H3 (ab1791; Abcam, Cambridge, MA). Embryos were then washed 4× 2 h in PBT and incubated overnight in PBT supplemented with 1:500 goat anti-mouse or goat anti-rabbit secondary antibodies coupled either to Alexa Fluor 488 or 568 (Invitrogen – Thermo Fisher Scientific, Waltham, MA). Embryos were then washed 4× 2 h in PBT and gradually dehydrated in methanol. Embryos were cleared in Murray's clearing medium (2 parts of Benzyl Benzoate, 1 part of Benzyl Alcohol).

Confocal imaging and measurement of embryos, cells and nuclei after whole mount immunofluorescence

Embryos were placed in a chamber made using a flat nylon washer (Grainger, Lake Forest, IL) attached with nail polish (Sally Hansen, New York, NY) to a slide, filled with Murray's clearing medium, and covered by a coverslip (Beckman coulter, Brea, CA) for confocal microscopy. Confocal microscopy was performed on a Zeiss LSM 800 confocal running the Zeiss Zen Software. Embryos were imaged using a Plan-Apochromat 20x/1.0 air objective and laser power of 12%, on multiple 1024x1024 pixel plans spaced 0.68 μm apart in Z. Nuclear area was measured in Fiji using the ellipse tool. From this, we calculated the diameter of a circle of the same area, a value that we could directly compare the cell size determined through the measurement of the cell diameter at the nucleus central plane.

Chapter 5

Conclusions

Due to wide-ranging sizes differences at the organismal, genome, cell, and subcellular levels, combined with the ease of embryo and ploidy manipulation, Pipid frogs stand out as a unique vertebrate system particularly well-suited to study size relationships. Frog embryos have provided a platform for basic observations about the contribution of genome and cell size to organism physiology. These observations coupled with current molecular tools provide a powerful approach to the ongoing study of these topics. Frog egg and embryo extracts, both of *Xenopus* and other genera, recapitulate complex physiological processes in vitro and can be used in multiple capacities to identify precise physical and molecular mechanisms governing the size of organelles and subcellular structures.

Through this work, we have seen that molecular mechanisms of scaling are not conserved even at the level of the genus, with different mechanisms operating to construct conserved and fundamental structures like the meiotic spindle (Chapter 2). Why have *H. boettgeri* and *X. tropicalis* evolved different molecular mechanisms for generating similarly sized meiotic spindles? Do these changes provide a fitness advantage by optimizing spindle function? As we have seen, from the standpoint of spindle architecture, it is not surprising that differences in molecular components alter spindle morphology. One particularly exciting prospect would be to compare spindles in more frog species to try to make predictions about spindle size and morphology as it relates to frog phylogeny – a “phylogenetic spindle zoo”. Examining sequence and expression levels of known spindle size control factors across a diverse range of amphibian species-from *X. longipes* and beyond may reveal whether additional mechanisms have evolved together with changes in ploidy to influence spindle architecture and mediate scaling.

How does genome size contribute to the size of cells and subcellular structures? Our results indicate that genome size may not impact cell size as strongly during development as it does in somatic cells. In *Xenopus* egg extracts, increasing DNA content only results in a minimal increase in spindle size [48]. Furthermore, while we documented a robust correlation between genome size and erythrocyte size, we could not detect this in developing *Xenopus* embryos. By stage 21, nuclear and cell size scaling in *X. tropicalis* and *X. laevis* hybrids is not intermediate between the two species but more similar to that of haploid *X. laevis* embryos (18 chromosomes) at the same stage (Chapter 3). Therefore, it appears unlikely that bulk genome content alone is responsible for scaling, at least during embryogenesis. These results were similar in *X. longipes* at stage 21, with embryos having cells even smaller than those of *X. laevis*. *X. longipes* spindles are also smaller than those of *X. laevis* (Chapter 4). When precisely then does cell size begin to scale with genome size? Further experiments focusing on later developmental timepoints may be necessary to answer this question. A good timepoint to start with may be the early swimming tadpole stage before environmental factors introduce other variables such as feeding and housing density. As discussed in Chapter 4, correlations exist in animals between single-cell properties, such as genome or cell size [121,122], with metabolic rate and availability of resources such as RNA, proteins, lipids, and ribosomes within cells [121,123]. Precise measurements of these resources combined with the ease of ploidy manipulation in frogs may inform mathematical models of resource allocation to describe how genome size may be linked to biosynthetic mechanisms of size control at a systems level.

The apparent slowing of *X. longipes* development compared to *X. laevis* starting at neurulation was an intriguing observation. Could this developmental slowing be related to large genome size? One potential experiment would be to compare the developmental rates of frogs with experimentally induced changes in ploidy, such as viable *Xenopus* hybrids. Results of these experiments may help to explain other aspects of amphibian biology. It may be exciting, for example, to apply similar methods to other amphibians such as salamanders, as scaling phenomena may relate to their unique physiology. Future studies could shed new light on how extremely large genome sizes in salamanders correlate with large cell sizes, low metabolic rates, and decreased rates of growth and development [1,115]. These traits may allow them to retain juvenile or larval features in a neotenic state throughout their lifespan, and also enforce ecological constraints such as the need for some species to live in permanent aquatic habitats [124]. Salamanders additionally possess an incredible capacity for regeneration; the Mexican axolotl *Ambystoma mexicanum* regenerates entire lost limbs and large pieces of organs at any age, a feat impossible for most organisms including frogs, which lose

the ability to regrow limbs after metamorphosis [125–127]. Whether and how large genome and cell size may play a role in this unique trait is another fascinating question. The recent sequencing of the axolotl genome [128] will aid in the identification of molecular factors that govern size and development in these unique organisms. Thus, amphibian systems promise to continue revealing novel insights into biological size control.

References

1. Sessions, S.K., and Larson, A. (1987). Developmental Correlates of Genome Size in Plethodontid Salamanders and Their Implications for Genome Evolution. *Evolution* (N. Y). *41*, 1239.
2. Cavalier-Smith, T. (2005). Economy, speed and size matter: Evolutionary forces driving nuclear genome miniaturization and expansion. In *Annals of Botany*, pp. 147–175.
3. Gillooly, J.F., Hein, A., and Damiani, R. (2015). Nuclear DNA content varies with cell size across human cell types. *Cold Spring Harb. Perspect. Biol.* *7*, 1–27.
4. Bridges, C.B. (1925). Haploidy in *Drosophila melanogaster*. *Proc. Natl. Acad. Sci.* *11*, 706–710.
5. Bridges, C.B. (1921). Triploid intersexes in *Drosophila melanogaster*. *Science* (80-.). *54*, 252–254.
6. Müntzing, A. (1936). The Evolutionary Significance of Autopolyploidy. *Hereditas* *21*, 363–378.
7. Fankhauser, G. (1937). The production and development of haploid salamander larvae. *J. Hered.* *28*, 3–16.
8. Fankhauser, G., and Watson, R.C. (1942). Heat-Induced Triploidy in the Newt, *Triturus Viridescens*. *Proc. Natl. Acad. Sci.* *28*, 436–440.
9. Gurdon, J.B. (1959). Tetraploid frogs. *J. Exp. Zool.* *141*, 519–543.
10. Hamilton, L. (1963). An experimental analysis of the development of the haploid syndrome in embryos of *Xenopus laevis*. *J. Embryol. Exp. Morphol.* *11*, 267–78.
11. Fankhauser, G. (1945). Maintenance of normal structure in heteroploid salamander larvae, through compensation of changes in cell size by adjustment of cell number and cell shape. *J. Exp. Zool.* *100*, 445–455.
12. Winklbauer, R. (1989). Development of the lateral line system in *Xenopus*. *Prog. Neurobiol.* *32*, 181–206.
13. Olmo, O., and Morescalchi, A. (1975). Evolution of the genome and cell sizes in salamanders. *Experientia* *31*, 804–806.
14. Olmo, E., and Morescalchi, A. (1978). Genome and cell sizes in frogs: A comparison with salamanders. *Experientia*.
15. Mitsuru, K. (1981). Relationships between number, size and shape of red blood cells in amphibians. *Comp. Biochem. Physiol. -- Part A Physiol.* *69*, 771–775.
16. Olmo, E. (1983). Nucleotype and cell size in vertebrates: a review. *Basic Appl. Histochem.* *27*, 227–256.

17. Olmo, E., Capriglione, T., and Odierna, G. (1989). Genome size evolution in vertebrates: Trends and constraints. *Comp. Biochem. Physiol. -- Part B Biochem.* 92, 447–453.
18. Smith, H.M. (1925). Cell size and metabolic activity in amphibia. *Biol. Bull.* 48, 347–378.
19. Goniakowska, L. (1973). Metabolism, resistance to hypotonic solutions, and ultrastructure of erythrocytes of five amphibian species. *Acta Biol. Cracoviensia Ser. Zool.* 16, 114–134.
20. Monnickendam, M.A., and Balls, M. (1973). The relationship between cell sizes, respiration rates and survival of amphibian tissues in long-term organ cultures. *Comp. Biochem. Physiol. -- Part A Physiol.* 44, 871–880.
21. Gregory, T.R. (2003). Variation across amphibian species in the size of the nuclear genome supports a pluralistic, hierarchical approach to the C-value enigma. *Biol. J. Linn. Soc.* 79, 329–339.
22. Bonett, R.M., Trujano-Alvarez, A.L., Williams, M.J., and Timpe, E.K. (2013). Biogeography and body size shuffling of aquatic salamander communities on a shifting refuge. *Proc. R. Soc. B Biol. Sci.* 280.
23. Parra-Olea, G., Rovito, S.M., García-París, M., Maisano, J.A., Wake, D.B., and Hanken, J. (2016). Biology of tiny animals: Three new species of minute salamanders (Plethodontidae: Thorius) from Oaxaca, Mexico. *PeerJ* 2016.
24. Gregory, T.R., Nicol, J.A., Tamm, H., Kullman, B., Kullman, K., Leitch, I.J., Murray, B.G., Kapraun, D.F., Greilhuber, J., and Bennett, M.D. (2007). Eukaryotic genome size databases. *Nucleic Acids Res.* 35.
25. Bonett, R.M., Chippindale, P.T., Moler, P.E., van Devender, R.W., and Wake, D.B. (2009). Evolution of gigantism in amphiumid salamanders. *PLoS One* 4.
26. Björklund, M., Taipale, M., Varjosalo, M., Saharinen, J., Lahdenperä, J., and Taipale, J. (2006). Identification of pathways regulating cell size and cell-cycle progression by RNAi. *Nature* 439, 1009–1013.
27. Marguerat, S., and Bähler, J. (2012). Coordinating genome expression with cell size. *Trends Genet.* 28, 560–565.
28. Amodeo, A.A., and Skotheim, J.M. (2016). Cell-size control. *Cold Spring Harb. Perspect. Biol.* 8.
29. Lloyd, A.C. (2013). The regulation of cell size. *Cell* 154, 1194.
30. Vitt, L.J., and Caldwell, J.P. (2014). Chapter 17 - Frogs. In *Herpetology (Fourth Edition)*.
31. Rittmeyer, E.N., Allison, A., Gründler, M.C., Thompson, D.K., and Austin, C.C. (2012). Ecological guild evolution and the discovery of the world's smallest vertebrate. *PLoS One* 7.
32. Sabater-Pi, J. (1985). Contribution to the Biology of the Giant Frog (*Conraua goliath*, Boulenger). *Amphib. Reptil.* 6, 143–153.
33. Gregory, T.R. (2001). Coincidence, coevolution, or causation? DNA content, cell size, and the C-value enigma. *Biol. Rev. Camb. Philos. Soc.* 76, 65–101.
34. Thiébaud, C.H., and Fischberg, M. (1977). DNA content in the genus *Xenopus*. *Chromosoma* 59, 253–257.
35. Session, A.M., Uno, Y., Kwon, T., Chapman, J.A., Toyoda, A., Takahashi, S., Fukui, A., Hikosaka, A., Suzuki, A., Kondo, M., *et al.* (2016). Genome evolution in

- the allotetraploid frog *Xenopus laevis*. *Nature* 538, 336–343.
36. Roth, G., and Walkowiak, W. (2015). The influence of genome and cell size on brain morphology in amphibians. *Cold Spring Harb. Perspect. Biol.* 7.
 37. Catenazzi, A., and Lehr, E. (2009). The generic allocation of “*Hyla*” *antoniiochoai* de la riva & chaparro, 2005 (Anura), with description of its advertisement call and ecology. *Zootaxa*, 61–68.
 38. Murray, A.W., and Kirschner, M.W. (1989). Cyclin synthesis drives the early embryonic cell cycle. *Nature* 339, 275–280.
 39. Lohka, M.I., and Maller, J.L. (1985). Induction of nuclear envelope breakdown, chromosome condensation, and spindle formation in cell-free extracts. *J. Cell Biol.* 101, 518–523.
 40. Sawin, K.E., and Mitchison, T.J. (1991). Mitotic spindle assembly by two different pathways in vitro. *J. Cell Biol.* 112, 925–940.
 41. Lohka, M.J., and Masui, Y. (1983). Formation in vitro of sperm pronuclei and mitotic chromosomes induced by amphibian ooplasmic components. *Science* (80-). 220, 719–721.
 42. Blow, J.J., and Laskey, R.A. (1986). Initiation of DNA replication in nuclei and purified DNA by a cell-free extract of *Xenopus* eggs. *Cell* 47, 577–587.
 43. Hirano, T., and Mitchison, T.J. (1991). Cell cycle control of higher-order chromatin assembly around naked DNA in vitro. *J. Cell Biol.* 115, 1479–1489.
 44. Murray, A.W., Desai, A.B., and Salmon, E.D. (1996). Real time observation of anaphase in vitro. *Proc. Natl. Acad. Sci. U. S. A.*
 45. Shamu, C.E., and Murray, A.W. (1992). Sister chromatid separation in frog egg extracts requires DNA topoisomerase II activity during anaphase. *J. Cell Biol.* 117, 921–934.
 46. Desai, A., Maddox, P.S., Mitchison, T.J., and Salmon, E.D. (1998). Anaphase a chromosome movement and poleward spindle microtubule flux occur at similar rates in *Xenopus* extract spindles. *J. Cell Biol.*
 47. Wilbur, J.D., and Heald, R. (2013). Mitotic spindle scaling during *Xenopus* development by kif2a and importin α . *Elife* 2, e00290.
 48. Brown, K.S., Blower, M.D., Maresca, T.J., Grammer, T.C., Harland, R.M., and Heald, R. (2007). *Xenopus tropicalis* egg extracts provide insight into scaling of the mitotic spindle. *J. Cell Biol.* 176, 765–770.
 49. Neumann, F.R., and Nurse, P. (2007). Nuclear size control in fission yeast. *J. Cell Biol.* 179, 593–600.
 50. Goehring, N.W., and Hyman, A.A. (2012). Organelle growth control through limiting pools of cytoplasmic components. *Curr. Biol.* 22.
 51. Jorgensen, P., Edgington, N.P., Schneider, B.L., Rupeš, I., Tyers, M., and Fitcher, B. (2007). The size of the nucleus increases as yeast cells grow. *Mol. Biol. Cell* 18, 3523–3532.
 52. Good, M.C., Vahey, M.D., Skandarajah, A., Fletcher, D.A., and Heald, R. (2013). Cytoplasmic volume modulates spindle size during embryogenesis. *Science* (80-). 342, 856–860.
 53. Hazel, J., Krutkramelis, K., Mooney, P., Tomschik, M., Gerow, K., Oakey, J., and Gatlin, J.C. (2013). Changes in cytoplasmic volume are sufficient to drive spindle scaling. *Science* (80-). 342, 853–856.

54. Hara, Y., and Merten, C.A. (2015). Dynein-Based Accumulation of Membranes Regulates Nuclear Expansion in *Xenopus laevis* Egg Extracts. *Dev. Cell* 33, 562–575.
55. Levy, D.L., and Heald, R. (2010). Nuclear Size Is Regulated by Importin α and Ntf2 in *Xenopus*. *Cell* 143, 288–298. Available at: <http://dx.doi.org/10.1016/j.cell.2010.09.012>.
56. Chen, P., Tomschik, M., Nelson, K.M., Oakey, J., Gatlin, J.C., and Levy, D.L. (2019). Nucleoplasmin is a limiting component in the scaling of nuclear size with cytoplasmic volume. *J. Cell Biol.* 218, 4063–4078.
57. Brownlee, C., and Heald, R. (2019). Importin α Partitioning to the Plasma Membrane Regulates Intracellular Scaling. *Cell*.
58. Loughlin, R., Wilbur, J.D., McNally, F.J., Nédélec, F.J., and Heald, R. (2011). Katanin contributes to interspecies spindle length scaling in *xenopus*. *Cell* 147, 1397–1407.
59. Helmke, K.J., and Heald, R. (2014). TPX2 levels modulate meiotic spindle size and architecture in *Xenopus* egg extracts. *J. Cell Biol.* 206, 385–393.
60. Burbank, K.S., Mitchison, T.J., and Fisher, D.S. (2007). Slide-and-Cluster Models for Spindle Assembly. *Curr. Biol.* 17, 1373–1383.
61. Loughlin, R., Heald, R., and Nédélec, F. (2010). A computational model predicts *Xenopus* meiotic spindle organization. *J. Cell Biol.* 191, 1239–1249.
62. Buster, D., McNally, K., and McNally, F.J. (2002). Katanin inhibition prevents the redistribution of gamma-tubulin at mitosis. *J. Cell Sci.* 115, 1083–92.
63. Zhang, D., Grode, K.D., Stewman, S.F., Diaz-Valencia, J.D., Liebling, E., Rath, U., Riera, T., Currie, J.D., Buster, D.W., Asenjo, A.B., *et al.* (2011). *Drosophila* katanin is a microtubule depolymerase that regulates cortical-microtubule plus-end interactions and cell migration. *Nat. Cell Biol.* 13, 361–372.
64. Gruss, O.J., and Vernos, I. (2004). The mechanism of spindle assembly: functions of Ran and its target TPX2. *J. Cell Biol.* 166, 949–55.
65. Kitaoka, M., Heald, R., and Gibeaux, R. (2018). Spindle assembly in egg extracts of the Marsabit clawed frog, *Xenopus borealis*. *Cytoskeleton* 75, 244–257.
66. Miller, K.E., Session, A.M., and Heald, R. (2019). Kif2a Scales Meiotic Spindle Size in *Hymenochirus boettgeri*. *Curr. Biol.* 29, 3720–3727.e5. Available at: <https://linkinghub.elsevier.com/retrieve/pii/S0960982219311546>.
67. Loughlin, R., Wilbur, J.D., McNally, F.J., Nedelec, F.J., and Heald, R. (2011). Katanin contributes to interspecies spindle length scaling in *xenopus*. *Cell* 147, 1397–1407.
68. Session, A.M., Uno, Y., Kwon, T., Chapman, J.A., Toyoda, A., Takahashi, S., Fukui, A., Hikosaka, A., Suzuki, A., Kondo, M., *et al.* (2016). Genome evolution in the allotetraploid frog *Xenopus laevis*. *Nature* 538, 336–343.
69. Feng, Y.-J., Blackburn, D.C., Liang, D., Hillis, D.M., Wake, D.B., Cannatella, D.C., and Zhang, P. (2017). Phylogenomics reveals rapid, simultaneous diversification of three major clades of Gondwanan frogs at the Cretaceous–Paleogene boundary. *Proc. Natl. Acad. Sci.* 114, E5864–E5870.
70. Trofimova, D., Paydar, M., Zara, A., Talje, L., Kwok, B.H., and Allingham, J.S. (2018). Ternary complex of Kif2A-bound tandem tubulin heterodimers represents a kinesin-13-mediated microtubule depolymerization reaction intermediate. *Nat.*

- Commun. 9, <https://doi.org/10.1038/s41467-018-05025-7>.
71. Miyamoto, T., Hosoba, K., Ochiai, H., Royba, E., Izumi, H., Sakuma, T., Yamamoto, T., Dynlacht, B.D., and Matsuura, S. (2015). The Microtubule-Depolymerizing activity of a mitotic kinesin protein KIF2A drives primary cilia disassembly coupled with cell proliferation. *Cell Rep.* 10, 664–673.
 72. Jang, C.-Y., Coppinger, J. a, Seki, A., Yates, J.R., and Fang, G. (2009). Plk1 and Aurora A regulate the depolymerase activity and the cellular localization of Kif2a. *J. Cell Sci.* 122, 1334–1341.
 73. Reber, S.B., Baumgart, J., Widlund, P.O., Pozniakovsky, A., Howard, J., Hyman, A.A., and Jülicher, F. (2013). XMAP215 activity sets spindle length by controlling the total mass of spindle microtubules. *Nat. Cell Biol.* 15, 1116–1122.
 74. Goshima, G., and Scholey, J.M. (2010). Control of Mitotic Spindle Length. *Annu. Rev. Cell Dev. Biol.* 26, 21–57.
 75. Crowder, M.E., Strzelecka, M., Wilbur, J.D., Good, M.C., vonDassow, G., and Heald, R. (2015). A Comparative Analysis of Spindle Morphometrics across Metazoans. *Curr. Biol.* 25, 1542–1550. Available at: <http://dx.doi.org/10.1016/j.cub.2015.04.036>.
 76. Lee, C., Kieserman, E., Gray, R.S., Park, T.J., and Wallingford, J. (2008). Whole-mount fluorescence immunocytochemistry on *Xenopus* embryos. *CSH Protoc.* 2008, pdb.prot4957.
 77. Hannak, E., and Heald, R. (2006). Investigating mitotic spindle assembly and function in vitro using *Xenopus laevis* egg extracts. *Nat. Protoc.* 1, 2305–14. Available at: <http://www.ncbi.nlm.nih.gov/pubmed/17406472>.
 78. Minsuk, S.B., and Keller, R.E. (1996). Dorsal mesoderm has a dual origin and forms by a novel mechanism in *Hymenochirus*, a relative of *Xenopus*. *Dev. Biol.* 174, 92–103. Available at: <http://www.ncbi.nlm.nih.gov/pubmed/8626024>.
 79. Minsuk, S.B., and Keller, R.E. (1997). Surface mesoderm in *Xenopus*: A revision of the stage 10 fate map. *Dev. Genes Evol.* 207, 389–401.
 80. Schindelin, J., Arganda-Carreras, I., Frise, E., Kaynig, V., Longair, M., Pietzsch, T., Preibisch, S., Rueden, C., Saalfeld, S., Schmid, B., *et al.* (2012). Fiji: An open-source platform for biological-image analysis. *Nat. Methods* 9, 676–682.
 81. Gibeaux, R., Acker, R., Kitaoka, M., Georgiou, G., Van Kruijsbergen, I., Ford, B., Marcotte, E.M., Nomura, D.K., Kwon, T., Veenstra, G.J.C., *et al.* (2018). Paternal chromosome loss and metabolic crisis contribute to hybrid inviability in *Xenopus*. *Nature* 553, 337–341.
 82. Grabherr, M.G., Haas, B.J., Yassour, M., Levin, J.Z., Thompson, D.A., Amit, I., Adiconis, X., Fan, L., Raychowdhury, R., Zeng, Q., *et al.* (2011). Full-length transcriptome assembly from RNA-Seq data without a reference genome. *Nat. Biotechnol.* 29, 644–652.
 83. Camacho, C., Coulouris, G., Avagyan, V., Ma, N., Papadopoulos, J., Bealer, K., and Madden, T.L. (2009). BLAST+: Architecture and applications. *BMC Bioinformatics* 10.
 84. Subramanian, A.R., Kaufmann, M., and Morgenstern, B. (2008). DIALIGN-TX: Greedy and progressive approaches for segment-based multiple sequence alignment. *Algorithms Mol. Biol.* 3, doi:10.1186/1748-7188-3-6.
 85. Zerbino, D.R., Achuthan, P., Akanni, W., Amode, M.R., Barrell, D., Bhai, J., Billis,

- K., Cummins, C., Gall, A., Girón, C.G., *et al.* (2018). Ensembl 2018. *Nucleic Acids Res.* 46, D754–D761.
86. Sun, Y.-B., Xiong, Z.-J., Xiang, X.-Y., Liu, S.-P., Zhou, W.-W., Tu, X.-L., Zhong, L., Wang, L., Wu, D.-D., Zhang, B.-L., *et al.* (2015). Whole-genome sequence of the Tibetan frog *Nanorana parkeri* and the comparative evolution of tetrapod genomes. *Proc. Natl. Acad. Sci.* 112, E1257–E1262.
 87. Christenson, M.K., Trease, A.J., Potluri, L.-P., Jezewski, A.J., Davis, V.M., Knight, L.A., Kolok, A.S., and Davis, P.H. (2014). De novo Assembly and Analysis of the Northern Leopard Frog *Rana pipiens* Transcriptome. *J. Genomics* 2, 141–149.
 88. Hyman, A., Drechsel, D., Kellogg, D., Salser, S., Sawin, K., Steffen, P., Wordeman, L., and Mitchison, T. (1991). Preparation of modified tubulins. *Methods Enzymol.* 196, 478–485.
 89. McNally, F.J., and Thomas, S. (1998). Katanin is responsible for the M-phase microtubule-severing activity in *Xenopus* eggs. *Mol. Biol. Cell* 9, 1847–61.
 90. Hartman, J.J., Mahr, J., McNally, K., Okawa, K., Iwamatsu, A., Thomas, S., Cheesman, S., Heuser, J., Vale, R.D., and McNally, F.J. (1998). Katanin, a microtubule-severing protein, is a novel AAA ATPase that targets to the centrosome using a WD40-containing subunit. *Cell* 93, 277–287.
 91. Gibeaux, R., Miller, K., Acker, R., Kwon, T., and Heald, R. (2018). *Xenopus* hybrids provide insight into cell and organism size control. *Front. Physiol.* 9, 1758.
 92. Mirsky, A.E. (1951). THE DESOXYRIBONUCLEIC ACID CONTENT OF ANIMAL CELLS AND ITS EVOLUTIONARY SIGNIFICANCE. *J. Gen. Physiol.* 34, 451–462. Available at: <http://www.jgp.org/cgi/doi/10.1085/jgp.34.4.451>.
 93. Frawley, L.E., and Orr-Weaver, T.L. (2015). Polyploidy. *Curr. Biol.* 25, R353–R358.
 94. Lee, H.O., Davidson, J.M., and Duronio, R.J. (2009). Endoreplication: Polyploidy with purpose. *Genes Dev.* 23, 2461–2477.
 95. Galitski, T., Saldanha, A.J., Styles, C.A., Lander, E.S., and Fink, G.R. (1999). Ploidy regulation of gene expression. *Science* (80-). 285, 251–4. Available at: http://www.ncbi.nlm.nih.gov/entrez/query.fcgi?cmd=Retrieve&db=PubMed&dopt=Citation&list_uids=10398601.
 96. Taft, R.J., Pheasant, M., and Mattick, J.S. (2007). The relationship between non-protein-coding DNA and eukaryotic complexity. *BioEssays* 29, 288–299.
 97. Narbonne, P., Simpson, D.E., and Gurdon, J.B. (2011). Deficient induction response in a *Xenopus* nucleocytoplasmic hybrid. *PLoS Biol.* 9.
 98. Bürki, E. (1985). The expression of creatine kinase isozymes in *Xenopus tropicalis*, *Xenopus laevis laevis*, and their viable hybrid. *Biochem. Genet.* 23, 73–88.
 99. Lindsay, L.L., Peavy, T.R., Lejano, R.S., and Hedrick, J.L. (2003). Cross-fertilization and structural comparison of egg extracellular matrix glycoproteins from *Xenopus laevis* and *Xenopus tropicalis*. *Comp. Biochem. Physiol. A. Mol. Integr. Physiol.* 136, 343–52.
 100. Elurbe, D.M., Paranjpe, S.S., Georgiou, G., van Kruijsbergen, I., Bogdanovic, O., Gibeaux, R., Heald, R., Lister, R., Huynen, M.A., van Heeringen, S.J., *et al.* (2017). Regulatory remodeling in the allo-tetraploid frog *Xenopus laevis*. *Genome Biol.* 18, 198.

101. Nieuwkoop, P.D., and Faber, J. (1994). Normal table of *Xenopus laevis* (Daudin) (Garland Publishing).
102. Hamilton, L. (1957). Androgenic haploids of a toad, *Xenopus laevis*. *Nature* 179, 159.
103. James-Zorn, C., Ponferrada, V.G., Jarabek, C.J., Burns, K. a, Segerdell, E.J., Lee, J., Snyder, K., Bhattacharyya, B., Karpinka, J.B., Fortriede, J., *et al.* (2012). Xenbase: expansion and updates of the *Xenopus* model organism database. *Nucleic Acids Res.*, 1–6.
104. Karimi, K., Fortriede, J.D., Lotay, V.S., Burns, K.A., Wang, D.Z., Fisher, M.E., Pells, T.J., James-Zorn, C., Wang, Y., Ponferrada, V.G., *et al.* (2018). Xenbase: a genomic, epigenomic and transcriptomic model organism database. *Nucleic Acids Res.* 46, D861–D868.
105. Scerbo, P., Girardot, F., Vivien, C., Markov, G. V., Luxardi, G., Demeneix, B., Kodjabachian, L., and Coen, L. (2012). Ventx factors function as Nanog-like guardians of developmental potential in *Xenopus*. *PLoS One* 7.
106. Willet, C.E., Makara, M., Reppas, G., Tsoukalas, G., Malik, R., Haase, B., and Wade, C.M. (2015). Canine disorder mirrors human disease: Exonic deletion in HES7 causes autosomal recessive spondylocostal dysostosis in miniature schnauzer dogs. *PLoS One* 10.
107. Sparrow, D.B., Faqeih, E.A., Sallout, B., Alswaid, A., Ababneh, F., Al-Sayed, M., Rukban, H., Eyaid, W.M., Kageyama, R., Ellard, S., *et al.* (2013). Mutation of HES7 in a large extended family with spondylocostal dysostosis and dextrocardia with situs inversus. *Am. J. Med. Genet. Part A* 161, 2244–2249.
108. Schindelin, J., Arganda-Carreras, I., Frise, E., Kaynig, V., Longair, M., Pietzsch, T., Preibisch, S., Rueden, C., Saalfeld, S., Schmid, B., *et al.* (2012). Fiji: An open-source platform for biological-image analysis. *Nat. Methods* 9, 676–682.
109. Edelstein, A.D., Tsuchida, M. a, Amodaj, N., Pinkard, H., Vale, R.D., and Stuurman, N. (2014). Advanced methods of microscope control using μ Manager software. *J. Biol. Methods* 1, 10.
110. Michaels, C.J., Tapley, B., Harding, L., Bryant, Z., and Grant, S. (2015). Breeding and rearing the Critically Endangered Lake Oku Clawed Frog (*Xenopus longipes* Loumont and Kobel 1991). *Amphib. Reptile Conserv.* 9, 100–110.
111. Loumont, C., and Kobel, H.R. (1990). *Xenopus longipes* sp. nov., a new polyploid pipid from western Cameroon. *Rev. Suisse Zool.* 98, 731–738. Available at: <http://direct.biostor.org/reference/114997> [Accessed February 22, 2016].
112. Kempes, C.P., Dutkiewicz, S., and Follows, M.J. (2012). Growth, metabolic partitioning, and the size of microorganisms. *Proc. Natl. Acad. Sci. U. S. A.* 109, 495–500.
113. Metzli-Raz, E., Kafri, M., Yaakov, G., Soifer, I., Gurvich, Y., and Barkai, N. (2017). Principles of cellular resource allocation revealed by condition-dependent proteome profiling. *Elife* 6.
114. Vinogradov, A.E. (2005). Genome size and chromatin condensation in vertebrates. *Chromosoma* 113, 362–369.
115. Horner, H.A., and Macgregor, H.C. (1983). C value and cell volume: their significance in the evolution and development of amphibians. *J. Cell Sci.* 63, 135–146.

116. Jorgensen, P., Edgington, N.P., Schneider, B.L., Rupeš, I., Tyers, M., and Fitcher, B. (2007). The size of the nucleus increases as yeast cells grow. *Mol. Biol. Cell* 18, 3523–3532.
117. Conklin, E.G. (1912). Cell size and nuclear size. *J. Exp. Zool.* 12, 1–98.
118. Nurse, P. (2000). A long twentieth century of the cell cycle and beyond. *Cell* 100, 71–78.
119. Gerhart, J.C. (1980). Mechanisms Regulating Pattern Formation in the Amphibian Egg and Early Embryo. In *Biological Regulation and Development*, pp. 133–316.
120. Jevtić, P., and Levy, D.L. (2015). Nuclear size scaling during xenopus early development contributes to midblastula transition timing. *Curr. Biol.* 25, 45–52.
121. Scott, M., Gunderson, C.W., Mateescu, E.M., Zhang, Z., and Hwa, T. (2010). Interdependence of cell growth and gene expression: Origins and consequences. *Science* (80-). 330, 1099–1102.
122. Vinogradov, A.E., and Anatskaya, O. V. (2006). Genome size and metabolic intensity in tetrapods: A tale of two lines. *Proc. R. Soc. B Biol. Sci.* 273, 27–32.
123. Molenaar, D., Van Berlo, R., De Ridder, D., and Teusink, B. (2009). Shifts in growth strategies reflect tradeoffs in cellular economics. *Mol. Syst. Biol.* 5.
124. Lertzman-Lepofsky, G., Mooers, A., and Greenberg, D.A. (2019). Ecological constraints associated with genome size across salamander lineages. *Proc. R. Soc. B Biol. Sci.* 286.
125. Dent, J.N. (1962). Limb regeneration in larvae and metamorphosing individuals of the South African clawed toad. *J. Morphol.* 110, 61–77.
126. Roensch, K., Tazaki, A., Chara, O., and Tanaka, E.M. (2013). Progressive specification rather than intercalation of segments during limb regeneration. *Science* (80-). 342, 1375–1379.
127. Simon, A., and Tanaka, E.M. (2013). Limb regeneration. *Wiley Interdiscip. Rev. Dev. Biol.* 2, 291–300.
128. Nowoshilow, S., Schloissnig, S., Fei, J.F., Dahl, A., Pang, A.W.C., Pippel, M., Winkler, S., Hastie, A.R., Young, G., Roscito, J.G., *et al.* (2018). The axolotl genome and the evolution of key tissue formation regulators. *Nature* 554, 50–55.